

Nr. 226

RÜDIGER GENS

**Quality assessment  
of SAR interferometric data**

Referent: Prof. Dr. mult. G. Konecny  
Korreferenten: Prof. Dr. G. Seeber  
Prof. Dr. J.L. van Genderen

Tag der mündlichen Prüfung: 27. Mai 1998

**Schlagworte:**

quality assessment, SAR interferometry, satellite images

Qualitätsabschätzung, Radar-Interferometrie, Satellitenbilder

## ABSTRACT

---

Digital elevation models (DEMs) and the products derived from them are widely used for numerous applications within the geoscientific community. Radar interferometry is a new technique which can provide these digital elevation models. The increasing availability of digital elevation models has led to a growing need for assessing the quality of such models.

A common way to assess the quality of interferometrically derived DEMs is by comparison with a reference model. This is done assuming that the reference DEM is reliable and without any distortions. From the statistical point of view, the accuracy of the reference DEM should be at least one order better than the model to be tested. This study investigates the possibilities of assessing the quality of SAR interferometric data independent of any reference model.

After reviewing the technique of SAR interferometry, geometrical constraints and relevant parameters for the processing are identified. Potential applications of interferometrically derived DEMs and recent trends are also addressed. Factors influencing the quality of SAR interferometric data and the necessary steps for the processing of these data are then studied. The suitability of various data sets for SAR interferometry is investigated. Special attention is paid to the influence of each single processing step on the quality of the final interferometric product, and potential sources of error are identified. Technical details of available software packages for interferometric processing have been collected. Quality measures suitable for the assessment of DEMs are investigated focusing on the requirements of the end-product user. Some alternative techniques for the generation of digital elevation models are also described.

The key issue of this study is the development of an error propagation model as an alternative method for the quality assessment of SAR interferometric data. Results of the empirically implemented error propagation model and of the sensitivity study of the parameters used as input for the interferometric processing are evaluated. The sensitivity study emphasises the importance of good quality input data for obtaining results with the desired reliability. The empirical propagation model for the quality assessment of interferometric DEMs is applied to results from two test sites. The advantages and limitations of the empirical propagation model are pointed out and some useful recommendations for future studies are made. Finally it is concluded that the developed technique provides a useful tool for the quality assessment of SAR interferometric data.

# ZUSAMMENFASSUNG

---

Digitale Geländemodelle und von ihnen abgeleitete Produkte finden weitreichende Anwendung in zahlreichen Geowissenschaften. SAR-Interferometrie ist eine neue Technik, die diese Geländemodelle zur Verfügung stellen kann. Die steigende Zahl von verfügbaren Geländemodellen führt zu einem wachsendem Bedarf, die Qualität dieser Modelle abzuschätzen.

Eine gebräuchliche Methode der Qualitätsabschätzung von interferometrisch erstellten Geländemodellen ist der Vergleich mit einem Referenzmodell. Dieser Vergleich beruht auf der Annahme, daß das Referenzgeländemodell zuverlässig ist und keine Verzerrungen beinhaltet. Statistisch gesehen sollte die Genauigkeit der Referenzgeländemodelle mindestens eine Größenordnung besser sein als das zu testende Modell. In dieser Arbeit wird die Möglichkeit der Qualitätsabschätzung von SAR-interferometrischen Daten unabhängig von irgendwelchen Referenzmodellen untersucht.

Nach einem Rückblick auf die interferometrische Technik werden die geometrischen Einschränkungen und die für die Datenverarbeitung relevanten Parameter identifiziert. Die potentielle Anwendung interferometrisch erstellter Geländemodelle und die jüngsten Entwicklungen werden vorgestellt. Faktoren, die die Qualität von SAR-interferometrischen Daten beeinflussen, sowie die zur Berechnung dieser Daten notwendigen Schritte werden eingehend untersucht. Spezielles Augenmerk wird dabei sowohl auf den Einfluß jedes einzelnen Verarbeitungsschrittes als auch auf die Qualität des interferometrischen Endproduktes gelegt. Dabei werden potentielle Fehlerquellen identifiziert. Technische Details der verfügbaren Softwarepakete für die interferometrische Datenverarbeitung werden zusammengestellt. Qualitätsmerkmale, die für die Bewertung von Geländemodellen geeignet sind, werden erforscht im Hinblick auf die Anforderungen der Benutzer des Endproduktes. Einige alternative Techniken zur Generierung von Geländemodellen werden ebenfalls beschrieben.

Ein Kernstück dieser Arbeit ist die Entwicklung eines Fehlerfortpflanzungsmodells als eine alternative Methode zur Qualitätsabschätzung von SAR-interferometrischen Daten. Ergebnisse eines empirisch umgesetzten Fehlerfortpflanzungsmodells und einer Sensitivitätsstudie der Parameter, die als Input der interferometrischen Datenverarbeitung benutzt wurden, werden präsentiert. Die Sensitivitätsstudie unterstreicht die Bedeutung der hohen Qualität der Eingangsdaten, um die erwünschten, zuverlässigen Ergebnisse zu erhalten. Das empirische Fortpflanzungsmodell zur Qualitätsabschätzung interferometrischer Geländemodelle wird für die Ergebnisse von zwei Testgebieten angewendet. Die Vor- und Nachteile des empirischen Fehlerfortpflanzungsmodells werden aufgezeigt und einige hilfreiche Vorschläge für zukünftige Studien gemacht. Schließlich kann zusammenfassend festgestellt werden, daß die entwickelte Methode ein hilfreiches Werkzeug zur Qualitätsabschätzung SAR-interferometrischer Daten ist.

## ACKNOWLEDGEMENTS

---

Many individuals and organisations contributed in different ways to the successful completion of this thesis and I would like to take this opportunity to express my gratitude to them.

I am grateful to Prof. Gottfried Konecny who gave me the chance to carry out this research by being my promoter. He trusted my skills and gave me the freedom to work in a very independent way. I am thankful to Prof. John van Genderen for his excellent supervision. He helped me in organising my work very efficiently, knew the secret of motivating me whenever it was needed, and provided me with an encouraging working environment. From him I learnt much more than just working in a scientific way. I would also like to thank Prof. Günther Seeber for being available as second reviewer at such a short notice and for his flexibility in handling this task.

This research was carried out within the European Scientific Research Network ‘Synergy of Remotely Sensed Data’ which is part of CEC’s Human Capital and Mobility Programme of the European Community. I appreciate the useful discussions I had with the network members during the workshops which gave me a broader perspective of the applications of SAR interferometry and helped me in developing my research ideas. I especially thank Manfred Wiggenghagen for his patience while introducing me to the field of radar and his help in defining the topic of this research, the colleagues from CO.RI.S.T.A. and IPG Freiburg for providing data sets and for their hospitality during my visits and Thomas Schneider for the information about the MOMS system. Phisan Santitamnont provided me with the data sets and the reference DEM of the Lower Saxony area which he used for his PhD thesis.

This research was carried out with the support of the European Union which funded the ‘Synergy’ network, of the European Space Agency (ESA) which provided data sets and of the Delft Institute for Earth-Oriented Space Research (DEOS) which provided precise orbit information.

Bernie Armour, William Bayer, Jim Ehrisman and Marco van der Kooij from Atlantis Inc. supported me by solving various problems with the InSAR software and answered all my technical questions, collaborating in a direct and uncomplicated way.

I gained a lot from the meetings of the Dutch Interferometry group (DIG). I thank all its members for sharing their expertise in SAR interferometry and for the collaboration during the BCRS project. Special thanks go to Ramon Hanssen and Stefania Usai for the valuable discussions and technical support.

I would like to thank all the scientists who provided me with information about interferometric software packages.

ITC with its international atmosphere was always an inspiring working environment. During my research I had the chance to meet people from different countries, cultures and background. I am glad that I could gain this experience. The people from the coalfire

group, in particular, created an environment which was pleasant to work in. Some of them became more than just colleagues.

A special thank you to Wim Bakker, Wan Bakx and Gerard Reinink from the Remote Sensing and Geoinformatics Laboratory (for me it will always remain the IPL) for their technical support in solving problems regarding system, data and software and in answering all my questions; to Marga Koelen, Lydia Franken, Carla Gerritsen and Hilde Hulsman from the library who were always helpful in finding and collecting references I needed; to Theo Bouloucos for his advice in the field of error propagation and to the facility management and service departments for their support. I will not forget all my PhD colleagues. It was a good feeling to have them around and to know that there are people with similar ideas and problems. I wish them all success.

I would like to thank all the other ITC staff members not mentioned here by name who contributed in their way to the successful completion of this thesis.

I am grateful to Zoltán for his critical comments, the hints for the layout and his cordial way of supporting me. A special thanks to Marcsi for all the cake.

I am very thankful to Craig for proof reading this thesis and for his positive influence on my English. He showed me the beauty of the Scottish Highlands and became a real friend over the years.

I had many fruitful discussions about radar and interferometry with Gerrit. He made valuable remarks on the contents of this thesis. I will remember the enjoyable time I had working with him.

I would also like to thank my friends for their moral support. They believed in me and my skills and were there whenever I needed somebody to talk to.

Finally, I would like to express my sincere gratitude to my parents for all their support. They gave me the freedom to find my own way and constantly supported all my decisions. Danke!

Last but not least, I give my special thanks to Anu for her tremendous support and her never-ending encouragement. She did not tire of reading the thesis again and again. It is just wonderful to know that somebody believes in you and is always there for you. धन्यवाद!

# CONTENTS

---

Abstract .....	i
Zusammenfassung .....	ii
Acknowledgements .....	iii
List of Acronyms and Abbreviations .....	ix
List of Figures .....	xi
List of Tables .....	xv
<b>1 INTRODUCTION .....</b>	<b>1</b>
1.1 PROBLEM IDENTIFICATION .....	1
1.2 OBJECTIVES AND RESEARCH METHODS .....	2
1.3 STRUCTURE OF THE THESIS .....	3
<b>2 REVIEW OF SAR INTERFEROMETRY .....</b>	<b>5</b>
2.1 HISTORY .....	5
2.2 RELEVANT RADAR AND INTERFEROMETRY PARAMETERS .....	7
2.2.1 Some relevant terms .....	7
2.2.2 Geometry of SAR interferometry .....	8
2.2.3 Interferometric baseline .....	10
2.3 TECHNIQUES .....	12
2.3.1 Across-track interferometry .....	12
2.3.2 Along-track interferometry .....	13
2.3.3 Repeat-pass interferometry .....	14
2.3.4 Differential interferometry .....	15
2.4 INTERFEROMETRIC PRODUCTS .....	15
2.5 APPLICATIONS .....	18
2.5.1 Topographic mapping .....	19
2.5.2 Digital elevation modelling .....	19
2.5.3 Surface movements .....	20
2.5.4 Other applications .....	21
2.6 TRENDS .....	22
2.7 FACTORS INFLUENCING THE DATA QUALITY .....	23
2.7.1 Orbits .....	23
2.7.2 Atmosphere .....	24
2.7.3 Temporal decorrelation .....	24
2.7.4 Baseline decorrelation .....	24
2.7.5 Processing .....	24



<b>3</b>	<b>INTERFEROMETRIC PROCESSING</b> .....	27
3.1	DATA SETS .....	27
3.2	CO-REGISTRATION .....	30
3.3	INTERFEROGRAM GENERATION .....	32
3.4	PHASE UNWRAPPING .....	32
3.5	CONVERSION FROM PHASE TO HEIGHT INFORMATION .....	34
3.6	GEOCODING OF THE DIGITAL ELEVATION MODEL .....	35
3.7	SOFTWARE PACKAGES .....	36
<b>4</b>	<b>QUALITY ASSESSMENT OF DIGITAL ELEVATION MODELS</b> .....	39
4.1	TECHNIQUES FOR CREATING DIGITAL ELEVATION MODELS .....	39
4.1.1	Contour lines .....	40
4.1.2	Aerial photogrammetry .....	41
4.1.3	Radar techniques .....	42
4.1.4	Stereoscopy with optical satellite imagery .....	43
4.1.5	Laser scanning .....	45
4.2	TECHNIQUES FOR QUALITY CONTROL .....	47
4.2.1	Theoretical background .....	47
4.2.2	Quality measures .....	48
4.2.3	Ground control points .....	49
4.2.4	Reference DEMs .....	50
4.2.5	User requirements .....	50
4.3	PROPOSED METHOD .....	53
<b>5</b>	<b>FACTORS INFLUENCING THE INTERFEROMETRIC PROCESSING</b> .....	55
5.1	CHOICE OF DATA SETS .....	55
5.2	SENSITIVITY OF INPUT PARAMETERS .....	56
5.2.1	Input parameters .....	58
5.2.2	Sensitivity study .....	59
5.2.3	Combination of input parameters .....	72
5.3	PROCESSING ALGORITHMS .....	73
5.3.1	Co-registration .....	73
5.3.2	Filtering .....	75
5.3.3	Phase unwrapping .....	75
<b>6</b>	<b>ERROR PROPAGATION MODEL</b> .....	77
6.1	BACKGROUND OF ERROR PROPAGATION .....	77
6.2	EMPIRICAL APPROACH .....	78
6.3	ESTIMATION OF THE DEM ACCURACY .....	79
6.3.1	Results from the Ningxia area, China .....	81
6.3.2	Results from the Lower Saxony area, Germany .....	84
6.4	LIMITATIONS .....	89
6.5	ADVANTAGES .....	90

<b>7 CONCLUSIONS AND RECOMMENDATIONS</b> .....	91
<b>REFERENCES</b> .....	95
Index.....	109
Glossary.....	113
Appendices	
Appendix A - Interferometric software .....	121
Appendix B - Curriculum vitae .....	139
Appendix C - Publications .....	141

## LIST OF ACRONYMS AND ABBREVIATIONS

---

AIRSAR	Airborne SAR
AODA	Attitude and Orbit Determination Avionics
ASF	Alaska SAR Facility
CCD	Charge-coupled Device (solid-state detector)
CCRS	Canada Center for Remote Sensing
CEC	Commission of the European Communities (Brussels)
CEOS	Committee on Earth Observation Satellites
CIS	Conventional Inertial System
CNES	Centre National D'Etudes Spatiales
CORISTA	Consorzio di Ricerca su Sistemi di Telesensori Avanzati
CPRF	Central Processing Reference Facility
CSR	Center of Space Research (Austin)
CTS	Conventional Terrestrial System
D-PAF	German Processing and Archiving Facility
DARA	Deutsche Agentur für Raumfahrtangelegenheiten (German Space Agency)
DASA	Deutsche Aerospace AG
DEM	Digital Elevation Model
DEOS	Delft Institute for Earth-Oriented Space Research
DLR	Deutsches Zentrum für Luft - und Raumfahrt (German Aerospace Research Establishment)
DOSAR	Dornier SAR
DTM	Digital Terrain Model
E-SAR	Experimental SAR
ERS-1	First European Remote Sensing Satellite
ERS-2	Second European Remote Sensing Satellite
ESA	European Space Agency
ESRIN	European Space Research Institute
GCP	Ground Control Point
GIS	Geographical Information System
GPS	Global Positioning System
I-PAF	Italian Processing and Archiving Facility
ICA	International Cartographic Association
INS	Inertial Navigation System
InSAR	Interferometric SAR
IRS-1C	Indian Remote Sensing Satellite
ITC	International Institute for Aerospace Survey and Earth Sciences
JERS-1	First Japanese Earth Resources Satellite
JPL	Jet Propulsion Laboratory
JRC	Joint Research Centre
LASER	Light Amplification by Stimulated Emission of Radiation
LIDAR	Light Detection And Ranging
MDA	MacDonald Dettwiler & Associates
MOMS	Modular Optoelectronic Multispectral Scanner
NASA	National Aeronautics and Space Administration (USA)

NASDA	National Space Development Agency (Japan)
NDCDB	National Digital Cartographic Data Base
NIMA	National Image and Mapping Agency (USA)
PAF	Processing and Archiving Facility
PRARE	Precise Range and Range Rate Equipment
PRF	Pulse Repetition Frequency
RADAR	Radio Detection and Ranging
rms	root mean square
RSL	Remote Sensing Laboratories
SAR	Synthetic Aperture Radar
SIR-C	Shuttle Imaging Radar (C-mission)
SLC	Single Look Complex
SNR	Signal-to-Noise Ratio
SPOT	Satellite Pour l'Observation de la Terre
SRTM	Shuttle Radar Topography Mission
TIN	Triangulated Irregular Network
TOPSAR	Interferometric Radar Topographic Mapping Instrument
UK-PAF	British Processing and Archiving Facility
USGS	United States Geological Survey
WGS84	World Geodetic System from 1984
X-SAR	SAR in X-band

## LIST OF FIGURES

---

<b>Figure 2-1</b> : Influence of the wavelength on backscatter behaviour.....	7
<b>Figure 2-2</b> : General geometry of SAR interferometry .....	9
<b>Figure 2-3</b> : Possible baseline representations .....	10
<b>Figure 2-4</b> : Geometry of across-track interferometry .....	12
<b>Figure 2-5</b> : Geometry of along-track interferometry .....	13
<b>Figure 2-6</b> : Geometry of repeat-pass interferometry.....	14
<b>Figure 2-7</b> : Example of an interferogram (Ningxia, China).....	16
<b>Figure 2-8</b> : Example of a coherence image (Groningen, the Netherlands).....	17
<b>Figure 2-9</b> : Example of a digital elevation model (Lower Saxony, Germany) .....	18
<b>Figure 2-10</b> : Potential applications of SAR interferometry .....	18
<b>Figure 2-11</b> : Interferometric processing chain.....	25
<b>Figure 3-1</b> : The three reference surfaces - topography, geoid and ellipsoid.....	34
<b>Figure 4-1</b> : Digitised contour lines.....	40
<b>Figure 4-2</b> : Geometry of block adjustment in aerial photogrammetry .....	41
<b>Figure 4-3</b> : Stereoscopic viewing geometry of the SPOT satellite .....	44
<b>Figure 4-4</b> : Along-track stereoscopic viewing geometry of the MOMS sensor .....	45
<b>Figure 4-5</b> : Data acquisition of a laser scanning system.....	46
<b>Figure 5-1</b> : Interferograms calculated with non-precise (left) and precise orbit state vectors (right).....	55
<b>Figure 5-2</b> : Difference interferogram .....	56
<b>Figure 5-3</b> : Processing scheme of the sensitivity study .....	57
<b>Figure 5-4</b> : Location of the 16 points used for the sensitivity study on the coherence image .....	58
<b>Figure 5-5</b> : Original interferogram.....	59
<b>Figure 5-6</b> : Original coherence image .....	59
<b>Figure 5-7</b> : Original interferogram (left) and interferogram with a change of -0.01 Hz in the pulse repetition frequency (right).....	60
<b>Figure 5-8</b> : Difference image (PRF changed by -0.01 Hz minus original) .....	60

<b>Figure 5-9 :</b>	Graph showing the relation between a change in the pulse repetition frequency and the change in the resulting interferogram.....	61
<b>Figure 5-10:</b>	Original interferogram (left) and interferogram with a change of 0.1 Hz in the range sampling rate (right) .....	62
<b>Figure 5-11:</b>	Difference image (Range sampling rate changed by 0.1 Hz minus original) .....	62
<b>Figure 5-12:</b>	Graph showing the relation between a change in the range sampling rate and the change in the resulting interferogram.....	63
<b>Figure 5-13:</b>	Original interferogram (left) and interferogram with a change of 0.005 MHz in the range bandwidth (right) .....	64
<b>Figure 5-14:</b>	Difference image (Range bandwidth changed by 0.005 MHz minus original) .....	64
<b>Figure 5-15:</b>	Graph showing the relation between a change in the range bandwidth and the change in the resulting interferogram.....	65
<b>Figure 5-16:</b>	Original interferogram (left) and interferogram with a change of 0.01 Hz in the azimuth bandwidth (right) .....	66
<b>Figure 5-17:</b>	Difference image (Azimuth bandwidth changed by 0.01 Hz minus original) .....	66
<b>Figure 5-18:</b>	Graph showing the relation between a change in the azimuth bandwidth and the change in the resulting interferogram.....	67
<b>Figure 5-19:</b>	Original interferogram (left) and interferogram with a change of -0.1 Hz in the Doppler centroid frequency (right).....	68
<b>Figure 5-20:</b>	Difference image (Doppler centroid frequency changed by -0.1 Hz minus original) .....	68
<b>Figure 5-21:</b>	Graph showing the relation between a change in the Doppler centroid frequency and the change in the resulting interferogram.....	69
<b>Figure 5-22:</b>	Original interferogram (left) and interferogram with a change of 0.01 m in the state vector position in x (right) .....	70
<b>Figure 5-23:</b>	Difference image (state vector position in x changed by 0.01 m minus original) .....	70
<b>Figure 5-24:</b>	Graph showing the relation between a change in the state vector position in the x direction and the change in the resulting interferogram.....	71
<b>Figure 5-25:</b>	Change in interferogram caused by a combination of changed input parameters .....	72
<b>Figure 5-26:</b>	Intensity images of the Groningen area.....	74
<b>Figure 5-27:</b>	Result of the auto-matching algorithm.....	74
<b>Figure 5-28:</b>	Result of the manual tie pointing .....	74

---

<b>Figure 6-1</b> :	Schematic representation of the error propagation model .....	78
<b>Figure 6-2</b> :	Map of the test site in Ningxia, China .....	79
<b>Figure 6-3</b> :	Map of the test site in Lower Saxony, Germany .....	80
<b>Figure 6-4</b> :	Coherence image of the Ningxia area.....	81
<b>Figure 6-5</b> :	Interferogram of the Ningxia area.....	82
<b>Figure 6-6</b> :	Digital elevation model (Ningxia, China) .....	83
<b>Figure 6-7</b> :	Error map of the Ningxia DEM (artefacts caused by phase discontinuities masked out in black) .....	84
<b>Figure 6-8</b> :	Interferogram of the Lower Saxony area .....	84
<b>Figure 6-9</b> :	Coherence image of the Lower Saxony area .....	85
<b>Figure 6-10</b> :	Digital elevation model of the Lower Saxony area .....	85
<b>Figure 6-11</b> :	Perspective view of the interferometrically derived digital elevation model of the Lower Saxony area overlaid on the corresponding interferogram .....	86
<b>Figure 6-12</b> :	Error map of the Lower Saxony DEM.....	87
<b>Figure 6-13</b> :	Difference image (Pulse repetition frequency changed by 0.03 Hz minus original digital elevation model).....	87
<b>Figure 6-14</b> :	Reference DEM of the Lower Saxony area.....	88
<b>Figure 6-15</b> :	Difference between the interferometrically derived and the reference DEM of the Lower Saxony area.....	89

## LIST OF TABLES

---

<b>Table 2-1:</b>	Potential applications for SAR interferometry for the ERS-1 satellite .....	11
<b>Table 3-1:</b>	Interferometric data sets supported by available software packages .....	27
<b>Table 3-2:</b>	Acquisition statistics of ERS tandem data.....	28
<b>Table 3-3:</b>	Influence of different parameters on the co-registration .....	31
<b>Table 3-4:</b>	Interferometric products supported by the available software packages .....	37
<b>Table 4-1:</b>	Products derived from digital elevation models, their applications and usage .....	51
<b>Table 5-1:</b>	Data sets used for the sensitivity study .....	57
<b>Table 6-1:</b>	Input parameters used for interferometric processing of ERS satellite data ..	79
<b>Table 6-2:</b>	Data sets used for the study of the Ningxia test site .....	80
<b>Table 6-3:</b>	Data sets used for the study of the Lower Saxony test site.....	81
<b>Table 6-4:</b>	Calculation scheme for the empirical error propagation model.....	82



# 1 INTRODUCTION

---

Digital elevation models (DEMs) are one of the most demanded products in the remote sensing community. Radar interferometry is a new technique for producing these digital elevation models. The increasing number of available DEMs stresses the importance of the quality assessment of these digital elevation models. First, the problems related to this assessment are identified. In this introductory chapter, the objectives of the research are defined and suitable research methods are proposed. Finally, the structure of the thesis is sketched out.

## 1.1 PROBLEM IDENTIFICATION

Radar interferometry is a technique for providing information about three-dimensional objects of the Earth's surface by using the phase content of the complex radar signal. The theoretical aspects of this technique are well studied and understood. With the availability of suitable data sets, especially after the launch of ERS-1 satellite, the potential of interferometric synthetic aperture radar (InSAR) for various geoscientific applications was investigated. Recent research mainly focuses on the limiting factors of this technique.

Radar interferometry is at the stage of becoming operational. In order to reach an operational level, there is an increasing need for quality measures for interferometric products since the user wants to know whether these products are suitable and reliable for his application. The focus of this study is on the quality assessment of digital elevation models because these are the most demanded interferometric product. DEMs are widely used within the geoscientific community e.g. for mapping purposes, geomorphological studies based on slope and aspect maps, and as a layer in geographical information systems (GIS) for combining relief data with thematic information. There is also a growing interest in the field of telecommunication. Therefore, DEMs have become key products on the market.

According to a study carried out by SPOT IMAGE (Guerre *et al.*, 1996), there is an increasing demand for high accuracy DEMs which cannot be satisfied by optical imagery. The problem of cloud coverage, especially in tropical areas, limits the suitability of optical images for the production of DEMs in some parts of the world. Radar interferometry could be the technique to fill this gap. Radar satellites such as JERS-1 and RADARSAT with their all-weather capabilities can provide nearly global coverage using on-board tape recording.

As mentioned before, DEMs are used in a wide range of applications. Despite this fact, there is still a lack of quality control. A standard procedure for this kind of assessment as well as generally accepted specifications about the accuracy of DEMs, e.g. in relation to the type of terrain or to the grid size, does not exist (Ackermann, 1996b). Research dealing with the problem of data quality is carried out in various fields. Recently, the United States Geological Survey (USGS) proposed standards for the collection, processing and quality control of DEM data for the entry into the National Digital Cartographic Data Base (USGS, 1997). The International Cartographic Association (ICA) established a commission on spatial data quality which defined seven elements to describe

the quality of data used in a GIS (Guptill and Morrison, 1995). Despite these efforts, quite a number of unsolved problems on how to treat the quality of spatial data still remain.

One of the common procedures for the quality assessment of a DEM, for example, is the comparison with a reference DEM (Lin *et al.*, 1994). This is done assuming that the reference DEM is correct and any differences are due to errors in the digital data (e.g. Giles and Franklin, 1996). Any distortions in the reference DEM remain undetected. Another critical aspect of this method is that, from the statistical point of view, the reference DEM should be one order better than the DEM to be evaluated. For an interferometrically derived DEM based on satellite data, which has on average a standard deviation of about five metres in the vertical direction (Zebker *et al.*, 1994b), a reference DEM with an accuracy of 50 centimetres is required.

## 1.2 OBJECTIVES AND RESEARCH METHODS

The work presented in this thesis was initiated by the CEC's Human Capital and Mobility Programme of the European Community entitled 'Synergy of Remotely Sensed Data'. The European Scientific Research Network also funded this research. Most of the network members are working in the field of geology or forestry where they combine different data sets in a synergistic way. Within this group there is a growing interest in SAR interferometric products as a complimentary data source. However, before combining these product with other data sources, the reliability of these data sets needs to be estimated.

The aim of this research is to develop a procedure for the quality assessment of SAR interferometric data. This procedure has to fulfil a number of requirements. Because suitable reference data sets are not always available, the quality control should exclude the comparison to any kind of reference, neither using a reference DEM nor ground control points (GCPs). Hence, the approach developed during this research had to be based on the quality estimation of the input parameters for the processing and also on the performance of the processing.

The focus of this research was on the quality assessment of SAR interferometric satellite data for several reasons. First of all, a large number of data sets acquired by the ERS satellites are available which are suitable for interferometric purposes and could be used for this investigation. Furthermore, the data sets have a certain level of quality, which is frequently controlled by ESA, and are processed to a CEOS standard format. The satellite systems have a configuration comparable to the airborne systems even though the latter are more complex in terms of equipment and performance (e.g. motion compensation). Thus, experience from this research could serve as a base for future studies on airborne systems. Finally, all the software packages commercially available are developed primarily to handle data sets from various satellite systems.

In this study a detailed review of the techniques used in SAR interferometry has been done. This served to identify the necessary input parameters involved in the processing. It also helped in understanding the role of different processing steps and possible sources of error. A sensitivity study was considered important as it provides information about the influence of each single input parameter on the performance of the interferometric

processing. The quality of the final output of the interferometric processing has been estimated by means of error propagation for two test sites.

In order to find suitable quality measures for SAR interferometric products, these products are defined precisely. It has to be clear which accuracy level is required in order to use an interferometric product for a certain application. The user requirements were studied to be able to provide the user with a quality measure which supports his decision on whether an interferometrically derived DEM is suitable for his application.

### **1.3 STRUCTURE OF THE THESIS**

After this introductory chapter, the basics of SAR interferometry are reviewed in chapter 2. This includes a brief look at the InSAR history, a description of the techniques, the potential applications and the trends as well as the identification of the factors influencing the data quality.

The available data sets and interferometric processing steps such as co-registration, interferogram generation, phase unwrapping, conversion from phase to height information and geocoding of the digital elevation model are the subject of chapter 3. Each single processing step is described with emphasis on the quality aspect. Details of the available software packages are also discussed.

In chapter 4 the various alternative techniques for creating digital elevation models such as from contour lines, aerial photogrammetry, adapted radar techniques, stereoscopy using optical images and laser scanning are reviewed. The techniques for quality control are evaluated.

The factors influencing the interferometric processing such as the choice of data sets, the sensitivity of the input parameters and the processing algorithms are studied in chapter 5.

The theoretical background of error propagation and the implementation of the proposed method is developed in chapter 6. This includes the presentation of the results and a critical analysis of the advantages and limitations of this technique.

Chapter 7 concludes this thesis with final remarks and recommendations.

## 2 REVIEW OF SAR INTERFEROMETRY

---

After a brief review of the history of SAR interferometry, relevant terms and the ways of acquiring SAR interferometric data are described. The development in the potential applications and recent trends are discussed. Finally, the factors influencing the quality of SAR interferometric data are addressed.

### 2.1 HISTORY

Imaging radar systems can be separated into two different categories: real aperture radars and synthetic aperture radars. The real aperture radar (RAR), also referred to as brute force system or non-coherent radar, requires a long antenna and a high power output in order to achieve an acceptable resolution and dynamic range since the resolution is proportional to the length of the antenna but inversely proportional to the range. The synthetic aperture radar (SAR), also known as coherent radar, overcomes the limitation of the antenna size by synthesising an antenna which receives a series of reflected waves and electronically combines them with reference wavelengths. The resolution of a SAR effectively remains the same over all ranges. A short introduction to these imaging radar systems is given by Trevett, 1986.

SAR interferometric data can provide information on three-dimensional objects. These data are derived from the phase content of the complex radar signal. The use of SAR interferometry can be traced back to the 1960s when the American military used an airborne system for mapping the Darien province in Panama at a scale of 1:250000 by means of radar interferometry. The first published results using this information source for the observation of the surface of Venus and the Moon are given by Rogers and Ingalls, 1969.

The interferometric principle was also applied to underwater sonar in order to generate a three-dimensional model of the sea-floor terrain (Kolouch, 1983). Using ultrasonic techniques with frequencies of about 20 KHz, a side-scan-sonar senses underwater objects from two different positions. Although the basic principle of sonar interferometry and SAR interferometry is the same, it differs quite substantially in terms of frequency, signal processing, the medium as well as the range from the sensor to the target.

Graham (1974) introduced this synthetic aperture radar (SAR) technique for topographic mapping. He showed that SAR interferometry, with side-looking airborne or spaceborne geometry, can be used to create topographic maps for two reasons. The resolution of some SAR data is adequate to identify various features and objects of the terrain. In addition to this, a sufficient number of points can be measured using the interferometric geometry to describe a terrain surface in detail.

After this theoretical study it was not until 1986 before the first practical studies, carried out at the Jet Propulsion Laboratory (JPL) in Pasadena, California, were published by Zebker and Goldstein. Two SAR antennas were mounted on an aircraft. One antenna transmitted a radar signal and the backscattered signal was received by both antennas simultaneously. A correction for the aircraft roll was not applied due to the lack of suitable

data on the aircraft attitude. Therefore, the achieved accuracy was still quite limited. Nevertheless, it showed what the limitations of the interferometric technique are and how the performance could be improved.

Gabriel and Goldstein (1988) extended the interferometric technique by adapting the existing technique to crossed orbits using interferometric repeat-pass data from the SIR-B mission inclined by an angle of 1.2 degrees. The angle between the orbits leads to a more complex processing. Besides a Doppler refocusing for the SAR azimuth correlation, the two images could not be overlaid without resampling in range direction. In addition to that, the crossed orbits caused small altitude variations appearing as small shifts in the azimuth direction.

The technique of differential interferometry was introduced by Gabriel *et al.* (1989). With two interferograms derived from three different SEASAT observations a double-difference interferogram was calculated. The change shown in the differential interferogram were due to swelling of water-absorbing clays in the scene. It was assumed that differential interferometry can detect small elevation changes in the order of 1 cm or even less (Gabriel *et al.*, 1989). That meant that the technique could provide accurate measurements of geophysical phenomena, residual from seismic events, for motions from prevolcanic swelling and other such events.

A multibaseline study by Li and Goldstein (1990) presented an error model for topographic mapping. They demonstrated that interferometric data regularly acquired by a spaceborne SAR can provide extremely useful topographic information. This study also showed that the sensitivity of the height measurements increases with the length of the baseline. At the same time the phase error also increases.

Since the launch of ERS-1 in July 1991, a large number of interferometric data sets acquired in C-band have become available. The ERS-1 satellite was the first operational spaceborne system which acquired radar data suitable for SAR interferometry on a routine basis. With these data sets it was possible to investigate the potentials and limitations of SAR interferometry. With the availability of data sets from ERS-2 launched in April 1995, the European Space Agency (ESA) could set up the tandem mission which combined data sets from ERS-1 and ERS-2 acquired only one day apart. An initial testing of ERS tandem data quality for InSAR applications was performed by Solaas *et al.* (1996). The tandem data sets enabled more detailed investigations on the optimal performance of spaceborne systems in terms of temporal decorrelation and atmospheric effects. All these efforts led to an increasing number of publications in various fields. At the ESA Fringe'96 workshop in Zurich, Switzerland, for example, about seventy papers were presented on results based on ERS satellite data.

For more information about the research activities in the various research groups the reader is referred to the review paper of Gens and van Genderen (1996b).

## **2.2 RELEVANT RADAR AND INTERFEROMETRY PARAMETERS**

Before introducing the techniques of SAR interferometry, some relevant terms concerning radar and SAR interferometry, the geometry of SAR interferometry and the interferometric baseline are explained.

### 2.2.1 Some relevant terms

A synthetic aperture radar is an active sensor transmitting and receiving microwave signals, i.e. measuring distances between the sensor and the point on the Earth's surface, where the signal is backscattered, perpendicular to the flight direction. This distance is defined as *slant range* which can be projected on the ground representing the *ground range*.

The flight direction is also referred to as *along-track* or *azimuth direction*, whereas the direction perpendicular to the flight path is defined as *across-track* or *range direction*. The angle between the direction the antenna is pointing and the nadir is called *look angle*. The angle between the radar beam centre and the normal to the local topography is referred to as *incidence angle*. Both angles are sometimes used synonymously which is only valid if the InSAR geometry is simplified neglecting the Earth's curvature and the local topography. The look angle of the sensor is one of the main parameters determining the viewing geometry and the incidence angle of the backscattered signal. It significantly affects the backscatter behaviour of the terrain. Depending on the characteristics of the illuminated terrain, areas of layover and shadow occur in the imagery.

Most of the energy between the transmission and reception of the radar signal is lost due to the long distances to be measured. Therefore, the received signal needs to be amplified to form the image. This amplification of the signal and effects from the system itself such as delays in the electronics etc. cause *system noise*, also referred to as thermal noise.

The *wavelength* of the sensor determines the penetration depth of the transmitted signal into the vegetation layer of the terrain surface. As shown in Figure 2-1, the longer the wavelength, the deeper the penetration layer. The energy of an X-band sensor is mainly reflected at the top layer of the canopies whereas most of the L-band signal penetrates through the upper vegetation layer and is reflected at the ground surface. The backscatter behaviour of C-band is less predictable. Due to volume scattering effects, the layer of backscattering is less determined and does not correspond directly to a terrain surface, neither the vegetation surface nor the ground surface.

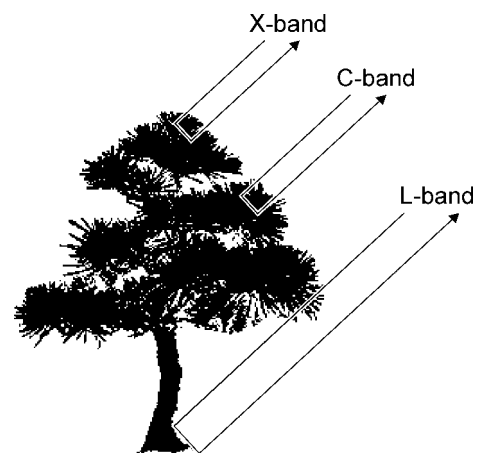


**Figure 2-1:** Influence of the wavelength on backscatter behaviour

The *spatial resolution* of the radar sensor defines the minimum separation between the measurements the sensor is able to discriminate and determines the amount of speckle introduced into the system. Speckle is a scattering phenomenon which arises because the spatial resolution of the sensor is not sufficient to resolve individual scatterers. The higher the spatial resolution of the sensor the more objects on the ground can be discriminated. The term 'spatial resolution' is often confused with the pixel size, which is actually the spacing of the pixels in the azimuth and ground range direction.

The *polarisation* of the signal influences the backscattering behaviour of the surface which is described in the scattering matrix. This matrix provides more information about the physics of the scattering and is determined by measurements with different polarisations. Signals with a vertical polarisation, for example, have a stronger response to rough surfaces than signals with horizontal polarisation.

The *bandwidth* with which a signal is processed has to be carefully chosen since it controls the phase aliasing and the amount of ambiguities introduced into the signal. In other words, the bandwidth determines the focusing of the signal.

As mentioned above, SAR interferometry is a technique for extracting information about three-dimensional objects from complex radar signals. The real (Re) and imaginary (Im) part of the complex values contain information about the *amplitude*  $a$ , as well as the *phase*  $\varphi$ . This information can be extracted from the complex values by

$$\begin{aligned}\varphi &= \arctan \frac{\text{Im}}{\text{Re}} , \\ a &= \sqrt{\text{Im}^2 + \text{Re}^2} .\end{aligned}\tag{2.1}$$

The phase information of two complex radar images is combined using SAR interferometric techniques. The phase difference of the two images is calculated for an interferogram where *fringes* represent the whole range of the phase from 0 to  $2\pi$  in a full colour cycle. The correlation of the phase information of two corresponding pixels is measured as *coherence* in the range from 0 to 1. The phase coherence can be decorrelated due to thermal noise introduced by the system, changes in the geometry affecting the baseline or temporal changes between the data acquisition.

### 2.2.2 Geometry of SAR interferometry

The general InSAR geometry, simplified by neglecting the Earth's curvature, is illustrated in Figure 2-2.

Two antennas  $O_1$  and  $O_2$  on ideally parallel flight paths are separated by a baseline  $B$ . From both antennas the slant ranges  $r_1$  and  $r_2$  to the same surface element are measured. With the look angle  $\theta$  and the flying height  $H$  the geometry is fixed.

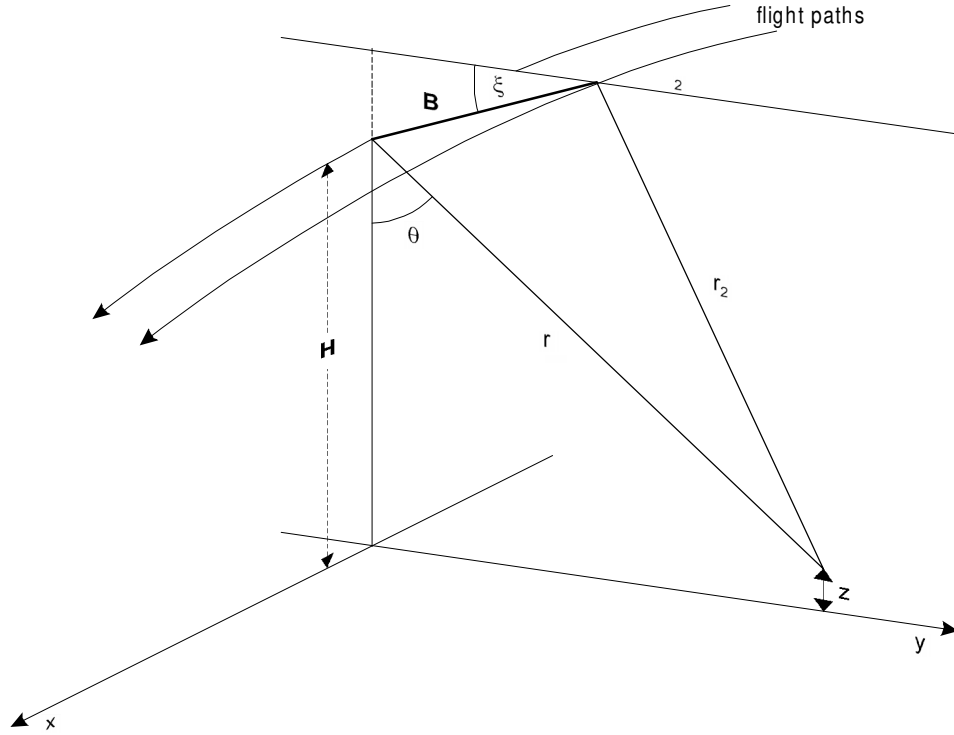


**Figure 2-2:** General geometry of SAR interferometry

The height of the point  $z(x,y)$  can be determined by

$$\begin{aligned}
 z(x,y) &= H - r_1 (\cos \xi \sqrt{1 - \sin^2(\theta - \xi)} - \sin \xi \sin(\theta - \xi)) \\
 &= H - r_1 (\cos \xi \cos(\theta - \xi) - \sin \xi \sin(\theta - \xi)) \\
 &= H - r_1 \cos(\xi + \theta - \xi) = H - r_1 \cos \theta
 \end{aligned} \tag{2.2}$$

Instead of the look angle, the baseline tilt angle  $\xi$  can be used for the calculation. In that case, the term  $\sin(\theta - \xi)$  can be derived from the interferometric range difference and the baseline.

Apart from the intensity value indicating how much backscattered energy is received by the radar antenna, the data sets used for the InSAR technique also provide phase information which is an ambiguous representation of the range. The phase difference  $\varphi$  between the two radar signals received from the same surface element at the two antenna positions is

$$\varphi = \frac{4\pi}{\lambda} (r_2 - r_1) = \frac{4\pi}{\lambda} (B_y \sin \theta - B_z \cos \theta). \tag{2.3}$$

Here the wavelength  $\lambda$  and the ranges  $r_1$  and  $r_2$  can also be described in terms of the baseline components  $b_y$  and  $b_z$  and the look angle  $\theta$ . This formula is valid for the satellite and the airborne configuration, addressed in the following paragraphs, under the assumption that in the airborne approach both antennas transmit and receive their own signals. This approach effectively doubles the physical baseline.



### 2.2.3 Interferometric baseline

The key element of this interferometric geometry is the baseline. The baseline, defined as the separation between two antenna positions either mounted on an aircraft or realised by two ideally parallel satellite orbits, can be represented in three different ways, as shown in Figure 2-3.

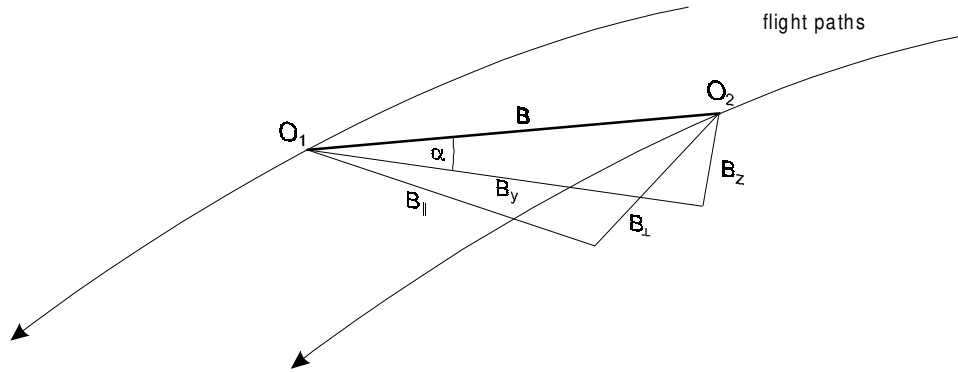


**Figure 2-3:** Possible baseline representations

The baseline can be described by its length  $B$  and the orientation angle  $\alpha$  or by dividing the baseline in two components, either in the horizontal ( $B_y$ ) and the vertical ( $B_z$ ) component or the components ( $B_{\parallel}$ ) and ( $B_{\perp}$ ) of the baseline, which are parallel and perpendicular to the range direction, respectively. All three representations can be found in the literature.

According to Small *et al.* (1996), there are several ways for estimating the InSAR baseline. Within flat areas the normal baseline component can be derived from the local fringe frequency. Furthermore, the baseline can be calculated using an orbit to orbit approach for each point in the reference orbit. This is based on a closest approach criterion or zero tangential component. Small *et al.* (1993) described an iterative non-linear least squares fit using tie points and the unwrapped phase in order to adjust the baseline model as well as the phase constant. A triangulation of the slant ranges to a point on a reference ellipsoid making use of the range image offset was developed by Pasquali (1995). Baselines for all points on a coarse grid distributed over the scene were calculated by Schwäbisch (1995) using image simulation based on precise orbits and a reference ellipsoid.

The length of the baseline determines the suitability of the data set for a particular application as is shown in Table 2-1 for the ERS-1 satellite (Solaas, 1994). The sensitivity of the baseline to height changes increases with decreasing length of the baseline. For the creation of digital elevation models from ERS-1 data, baselines in the order of 300 metres are most suitable.

Applications	Baseline
Practical InSAR limit	$< B_{\text{perp}} < 600 \text{ m}$
Digital Terrain Models	$150 \text{ m} < B_{\text{perp}} < 300 \text{ m}$
Surface Change Detection	$30 \text{ m} < B_{\text{perp}} < 70 \text{ m}$
Surface Feature Movement	$< B_{\text{perp}} < 5 \text{ m}$

**Table 2-1:** Potential applications for SAR interferometry for the ERS-1 satellite (Solaas, 1994)

With an increasing length of the baseline the phase noise leads to a decorrelation and a lower level of coherence. The coherence is lost completely if the baseline reaches its critical length. This critical baseline  $B_c$  calculated as

$$B_c = \frac{\lambda r}{2 R_y \cos^2 \theta} \quad (2.4)$$

depends on the wavelength  $\lambda$ , the range  $r$ , the resolution in range  $R_y$  and the look angle  $\theta$ . An optimal baseline as such does not exist. The dependency on the above mentioned system parameters leads to a trade off between the level of noise introduced in the data sets and the sensitivity of the phase to height changes.

Ferretti *et al.* (1996) proposed a multibaseline technique for improving the quality of interferometric results. They showed that the combination of more than two SAR images provides a robust technique for detecting and reducing atmospheric effects. Artefacts occurring in single interferograms are reduced by averaging the uncorrelated atmospheric contributions. This combination also provides an “atmospheric” noise map for each interferogram and an averaged coherence image that gives a measure of the signal-to-noise ratio (SNR) on a fine spatial resolution (Ferretti *et al.*, 1996).

An analysis by Zebker *et al.* (1994b) about the accuracy of topographic maps derived from ERS-1 data indicated that the baseline length is one of the potential error sources. Precise knowledge of the baseline geometry is needed because an error in the baseline angle cannot be distinguished from a slope on the terrain surface.

## 2.3 TECHNIQUES

The three main ways of acquiring SAR interferometric data are across-track, along-track and repeat-pass interferometry. These techniques are described in the following paragraphs.

### 2.3.1 Across-track interferometry

The across-track method requires two SAR antennas mounted on the same platform for simultaneous data acquisition. This technique is only employed on airborne systems, although studies for the implementation by means of a tethered satellite system, in which two vertically spaced physical antennas are connected by a tether and are carried along parallel paths by a deployer and a sub-satellite, have been carried out. The theoretical background is described by Moccia and Vetrella (1992), who also developed a mathematical model for this approach (Moccia *et al.*, 1995).

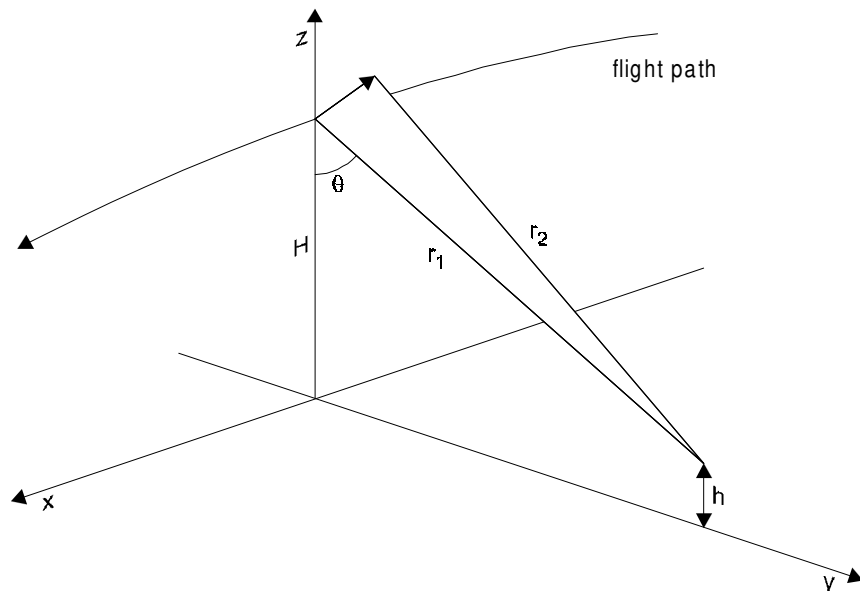


**Figure 2-4:** Geometry of across-track interferometry

As shown in Figure 2-4, the position of the two antennas mounted on the aircraft is perpendicular to the flight direction. The terrain height  $h$  can be calculated by equation 2.2. The ground range  $y$  is then derived by

$$y = r_1 \sin \theta . \quad (2.5)$$

Once the phase unwrapping (described in section 3.4) has successfully been performed, the elevation map can be derived. The main problem with this geometry in the airborne configuration is the fact that errors caused by the aircraft roll cannot be distinguished from the influence of the terrain slope. Since a satellite track is more stable than an airborne flight path, this problem is less critical in the spaceborne case.

### 2.3.2 Along-track interferometry

At present, the along-track approach is only applicable to airborne SAR systems, as it requires two antennas on the same platform.

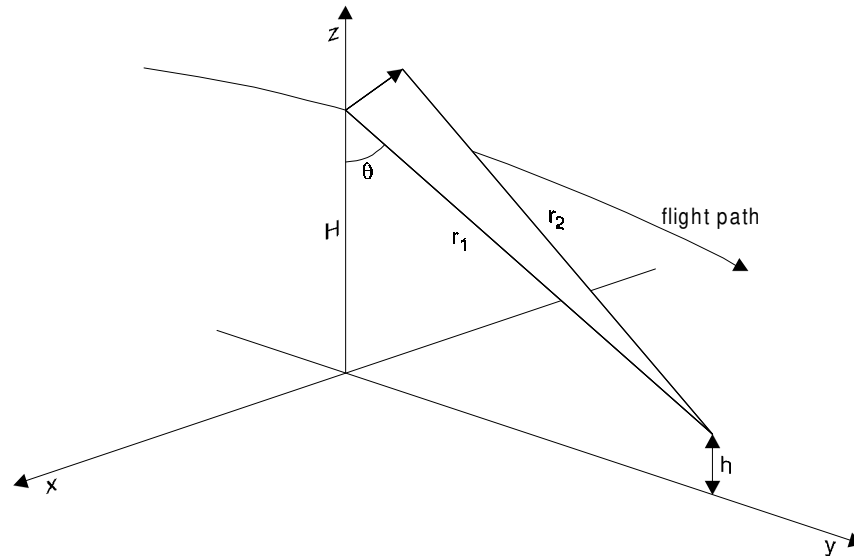


**Figure 2-5:** Geometry of along-track interferometry

The geometry of along-track interferometry, illustrated in Figure 2-5, does not differ significantly from the geometry of across-track interferometry. Only the x- and the y-axes are changed. Therefore, the phase difference  $\varphi$  between the corresponding signals is caused by the movement of the measured object, e.g. water currents. The moving surface leads to a Doppler shift according to the phase velocity of the water waves. All stationary targets are not visible whereas the moving ones can be seen in the radar imagery.

The velocity of an object  $u$  is related to the phase difference  $\varphi$  by

$$\varphi = \frac{4\pi}{\lambda} \frac{u}{V} B_x, \quad (2.6)$$

with the wavelength  $\lambda$ , aircraft velocity  $V$  and the baseline component  $B_x$ . For absolute velocity measurements, the phase difference needs to be calibrated due to baseline components in the y- and z-direction caused by aircraft movements (yaw and pitch).

This configuration is suitable mainly for the mapping of water currents, the detection of moving objects and the measurement of directional wave spectra (e.g. Orwig and Held, 1992; Goldstein *et al.*, 1989).

### 2.3.3 Repeat-pass interferometry

The repeat-pass method, illustrated in Figure 2-6, requires only one antenna that acquires data sets by passing the same area twice, covering it with a slightly different viewing geometry. This approach is based on the precise knowledge of the flight paths and hence is most suited to spaceborne systems.

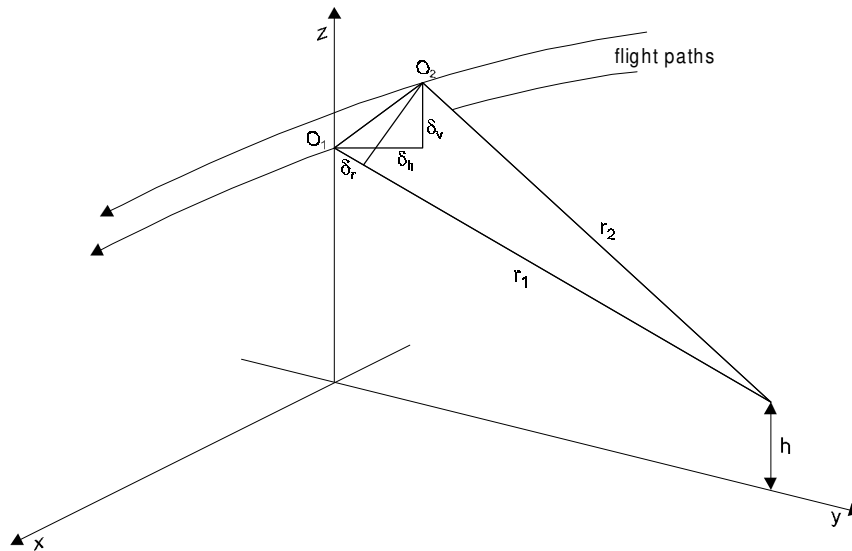


**Figure 2-6:** Geometry of repeat-pass interferometry

The observation points  $O_1$  and  $O_2$  are points on the motion compensation reference paths. The interferometric baseline can be described either by the horizontal  $\delta_h$  and vertical  $\delta_v$  components with reference to the motion compensation paths or by the path difference  $\delta_r$  between the slant ranges  $r_1$  and  $r_2$ :

$$\delta_r = r_1 - r_2 . \quad (2.7)$$

The phase difference  $\varphi$  can be estimated from the path difference  $\delta_r$  by

$$\varphi = \frac{-4\pi}{\lambda} \delta_r . \quad (2.8)$$

The repeat-pass approach for airborne SAR was studied by Gray and Farris-Manning (1993). The suitability of interferometric airborne data sets depends on a non-changing terrain backscatter, a stable viewing geometry and phase-preserved information of the motion compensated signal. The compensation of non-linear motions of the two antennas is essential for achieving accurate interferometric results from airborne data. Stevens *et al.* (1995) have given an overview of the work done in this field. Optimal motion compensation requires a precise knowledge of the relative geometry of the radar and each illuminated target. It is usually assumed that the terrain is flat at a certain reference level.

This assumption leads to phase errors, defocusing and peak misplacement (Stevens *et al.*, 1995). The motion compensation can be implemented in two different ways. In the single reference track approach the compensation is performed to the same reference track (Gray *et al.*, 1992). The advantage of this method is that errors in the estimation of the terrain elevation cannot occur because errors in phase are used as expected differential phase signals. Alternatively, the motion compensation can be applied for each antenna separately through definition of two reference tracks. Madsen *et al.* (1993) estimated the two antenna positions performing a resampling in the motion compensation stage using measurements from a digital avionics data system, a global positioning system (GPS) and an inertial navigation system (INS).

### 2.3.4 Differential interferometry

Differential interferometry, described in more detail by Gabriel *et al.* (1989), provides relative measures in the order of a few centimetres or even less for movements in the vertical direction, e.g. for change detection. Due to the viewing geometry, differential InSAR is able to measure only the displacement in the range direction. The differential interferogram can be calculated using three images or more. Alternatively, one of the interferograms can be simulated by registering an existing DEM to the geometry of another image pair. In this case the quality of the DEM has a significant impact on the result. For small-scale changes such as land subsidences, it is not possible to use digital elevation models as data source at all. Massonnet *et al.* (1993), for example, used this approach for the investigation of the Landers earthquake of 1992. Zebker *et al.* (1994a) carried out a study on the accuracies that can be achieved and the various limitations.

As the phase discontinuities in the two interferograms do not occur at the same position, each interferogram must be unwrapped. The sensitivity of this technique depends on the baseline geometry and can be increased by averaging over pixels at the expense of spatial resolution. With a decreasing baseline length the system noise can be reduced and hence higher accuracies of the detected height differences can be achieved. The wavelength of the sensor influences the resolution of the derived phase information. One colour cycle in an interferogram corresponds to a change of half the wavelength. According to Werner *et al.* (1992), the choice of the shorter wavelength of the ERS-1 satellite (C-band) compared to SEASAT (L-band) improves the height sensitivity significantly, by a factor of 4.25.

## 2.4 INTERFEROMETRIC PRODUCTS

The *interferogram*, shown in Figure 2-7, is defined as the product of the complex SAR values of a slave image and the complex conjugate of a master image. The amplitudes of the corresponding pixels are averaged and the difference of the phase values are calculated for each point in the image. The phase difference, given modulo  $2\pi$ , is colour encoded in the fringes.



**Figure 2-7:** Example of an interferogram (Ningxia, China). The interferogram contains the phase difference of the two complex images which is encoded in colour. A full colour cycle represents a phase cycle, also called fringe, covering the range between  $-\pi$  and  $\pi$ . The number of fringes of a certain distance determines the fringe rate which can be used for the flat earth removal.

The determination of the range is achieved by the additional use of the phase information of the complex radar signal. In the interferometric viewing geometry the phase difference is proportional to the range difference. This is the case as long as the signals have a fixed relation in phase, i.e. the signals are coherent. The *coherence* is a measure for the correlation of the phase information of two corresponding signals and varies in the range of 0 to 1, as shown in Figure 2-8.

The degree of coherence can be used as a quality measure because it significantly influences the accuracy of phase differences and height measurements. There are several factors decreasing the coherence. A list of these factors is given by Schwäbisch and Winter (1995):

- thermal noise,
- phase errors due to the processing,
- slightly different viewing positions (spaceborne systems),
- changes in the object phase between the data acquisition (spaceborne systems), and
- different atmospheric conditions during the data acquisition (spaceborne systems).

All these factors can even lead to a complete loss of coherence. This also occurs if the baseline exceeds its critical length.



**Figure 2-8:** Example of a coherence image (Groningen, the Netherlands). Bright parts show a high level of coherence, whereas dark areas indicate a loss of coherence. The loss of coherence in the agricultural fields is mainly caused by temporal decorrelation as the two data sets are acquired in August which is the harvest time in an agricultural area such as Groningen.

The phase information in the interferogram is directly related to the topography. Unfortunately, this information is given modulo  $2\pi$ . In order to calculate the elevation of each point, it is necessary to solve this ambiguity, i.e. the correct integer number of phase cycles needs to be added to each phase measurement to obtain the correct slant range distance. This ambiguity solution, referred to as phase unwrapping, is further described in section 3.4. The result of this procedure is the *unwrapped phase*.

The unwrapped phase containing the topographic information is converted to a *digital elevation model* (Figure 2-9).

A *differential interferogram* is generated by the difference of two interferograms and contains information about small-scale displacements that occur between the data acquisitions. The differential interferogram can be produced in two different ways. Based on two phase-unwrapped interferograms, the difference of these interferograms can be calculated. Alternatively, an existing digital elevation model can be registered to the viewing geometry of a calculated interferogram. The result of this approach is a *simulated interferogram*. The difference of the original and simulated interferogram is the required differential interferogram.

As a final step, all relevant interferometric products can be projected to a common reference system to obtain *geocoded products* in order to combine the interferometric results with information from other sources.

More details about the interferometric processing are discussed in chapter 3.



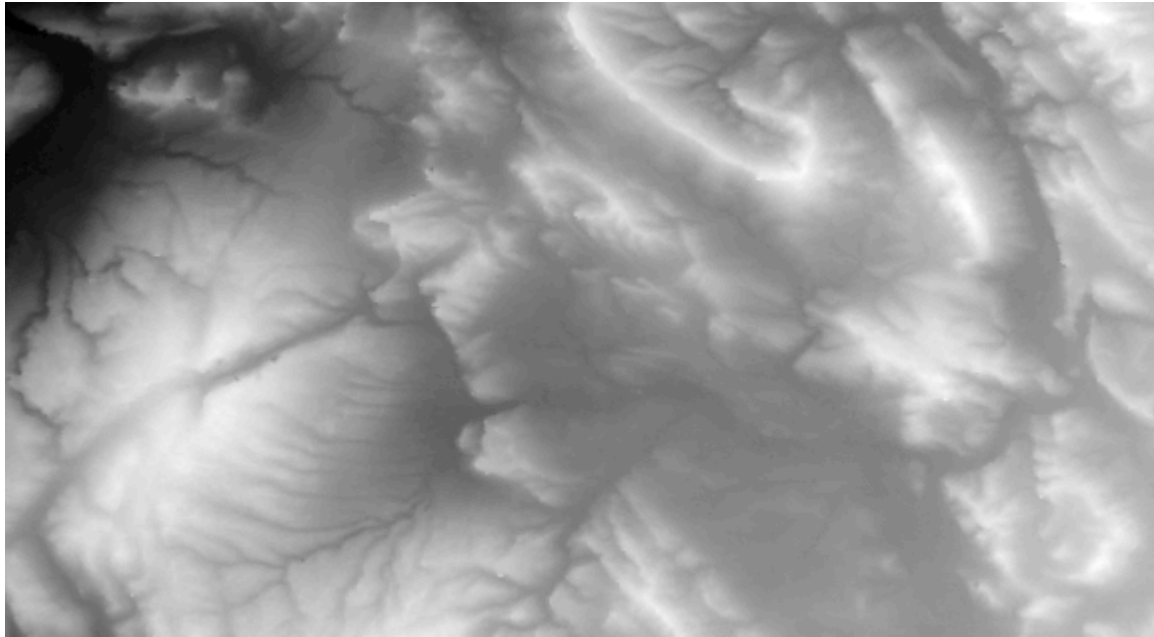


**Figure 2-9:** Example of a digital elevation model (Lower Saxony, Germany). The area shows a large variety of land forms. There are some relatively flat and homogeneous areas which are mostly agricultural fields. In other parts a hilly terrain structure (covered by forest) can be identified.

## 2.5 APPLICATIONS

After the technical background of SAR interferometry had been studied and basically understood, the focus of research changed to the limitations and potentials of the technique. After data sets from the ERS-1 satellite became available in particular, numerous studies were carried out on suitable applications (Figure 2-10).

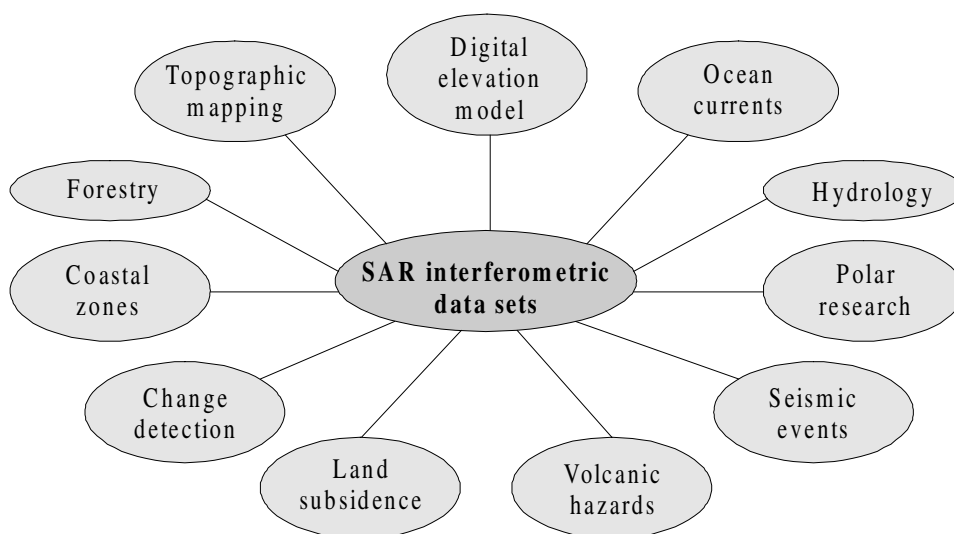


**Figure 2-10:** Potential applications of SAR interferometry

However, it is important to know that the InSAR technique was originally developed for topographic mapping. Generating digital elevation models still remains the most important applications of SAR interferometry.

### 2.5.1 Topographic mapping

One of the main reasons why the technique of interferometry was adapted to radar imagery, was the idea to use SAR interferometric data for topographic mapping (Graham, 1974). New processing techniques for the motion compensation of airborne interferometric data were developed by Madsen *et al.* (1993) in order to improve the accuracy of topographic mapping. By introducing GPS and INS measurements, it is possible to determine the aircraft motions more accurately and to generate significantly better topographic maps. Hagberg and Ulander (1993) estimated the optimal baseline for topographic mapping by spaceborne systems. They simulated the altitude error caused by the radar system or by the topography. With the increasing steepness of the terrain slope, phase aliasing leads to layover and shadow effects. The effects of speckle and thermal noise were reduced by averaging before the phase unwrapping was performed. Zebker *et al.* (1994b) estimated the accuracy of topographic maps derived from ERS-1 imagery. The analysis indicated two main errors: the height estimation error, which is a function of the error in phase estimation, and the error in the knowledge of the baseline length. Precise knowledge of the baseline geometry is needed because an error in the baseline angle cannot be distinguished from a slope on the terrain surface (Zebker *et al.*, 1994b). According to De Fazio and Vinelli (1993), topographic mapping based on ERS-1 data requires the use of tie points in order to perform the phase unwrapping properly.

### 2.5.2 Digital elevation modelling

Several theoretical studies about generating digital elevation models by SAR interferometry have been carried out. Due to the lack of suitable reference DEMs, the quantitative evaluation of the result is often difficult. Contour maps were often used for the comparison with the interferometric data sets (Zebker and Goldstein, 1986; Prati and Rocca, 1990). The main problem of this approach is the identification of ground features in both sources. Cumming and Hawkins (1990) assembled a list of possible error sources in the estimation of terrain elevation. Lin *et al.* (1994) compared a DEM derived from SEASAT with a USGS DEM. They assumed that geometrical distortion was due to the flight and stated that rms error between InSAR DEM and reference DEM is a function of the relative orientation angle, the offsets and scaling factors in azimuth and range direction as well as the baseline length (Lin *et al.*, 1994). Lanari *et al.* (1996) generated a digital elevation model derived from multifrequency shuttle mission data. The algorithm combined unwrapped phase patterns from L-, C- and X-band information. The fusion consisted of a bias removal in C- and X-band performed by a Kalman filter, followed by a weighting of the coherence and the wavelength. The final step in this approach was the summation of the three phase information. Ferretti *et al.* (1997) proposed a multibaseline approach for the automatic generation of high quality DEM. The resolution of the coherence image can be substantially improved and the combination of uncorrelated phase artefacts due to atmospheric effects significantly reduces their impact on the DEM accuracy.

### 2.5.3 Surface movements

The phase difference in the along-track geometry is caused by the motion of a surface and is used for monitoring, for example, *ocean currents*. This technique was first implemented by Goldstein and Zebker of JPL in 1987. Measurements from an inertial navigation system are used to correct phase shifts in the data caused by aircraft roll (Goldstein *et al.*, 1989). Another way of estimating the aircraft attitude is the inclusion of a small area of land in the scene (Goldstein and Zebker, 1987). After the correction for aircraft motion the remaining phase difference is assigned to geophysical sources such as wind effects, tidal currents, wave orbital velocities, internal waves and other currents (e.g. Shemer *et al.*, 1993; Thompson and Jensen, 1993). Carande (1994) estimated the coherence time of the ocean surface using a dual-baseline interferometric SAR. Ainsworth *et al.* (1995) demonstrated that under some conditions even absolute velocities can be determined. Bao *et al.* (1997) investigated the ocean wave imaging mechanism and derived a velocity bunching model.

In *polar research*, the InSAR based measurements provide information about flow velocities and tidal displacements as well as grounding line positions. The fringe patterns contain the effects of ice flow motion and tidal action between the times of data acquisition. Various studies were carried out in the Antarctic peninsula (e.g. Goldstein *et al.*, 1993; Hartl *et al.*, 1994) and in Greenland (e.g. Joughin *et al.*, 1996b; Rignot, 1996). Joughin *et al.* (1995) stated that InSAR has its potential for the observation of small-scale and regional velocity fields of ice sheets as well as for the detection of changes in ice flow patterns. Kwok and Fahnestock (1996) pointed out that due to the limited number of available data sets for polar regions, only observations of motions along the line of sight of the radar are possible so far. By combining data sets from ascending and descending orbits, an assumption of ice flow direction could be replaced by the more precise estimation using two velocity vectors.

Most of the papers published about the use of SAR interferometric data for monitoring *seismic events* deal with earthquakes that occurred in California in the first half of the 1990s. Studies on the Landers earthquake of 1992 (Massonnet *et al.*, 1993 and 1994; Feigl *et al.*, 1995) validated the potential of SAR interferometry for determining coseismic displacements. Results were also reported from the Eureka Valley earthquake in 1993 (Massonnet and Feigl, 1995; Peltzer and Rosen, 1995) and from the Northridge earthquake in 1994 (Massonnet *et al.*, 1996; Murakami *et al.*, 1996). Most of these results agreed well with the conventional measurements. Besides the coseismic displacements, the interferometric data sets provided more insight into the modelling of the earthquake motion, e.g. earthquake rupture processes and fault segmentation (Peltzer *et al.*, 1994) and focal mechanism (Massonnet and Feigl, 1995). The interferograms contain all the coseismic and some of the postseismic deformations. A rupture map and surface offset measurements at the faults lead to an elastic dislocation model which is able to explain most of the fringes in the far and intermediate fields. For the investigation of small-scale features in the interferogram, Peltzer *et al.* (1994) simulated three simple distortions - a rotation about the horizontal and the vertical axis as well as a distributed simple shear. From the orientation of the resulting fringes the direction of the local displacement gradient can be calculated. Zebker *et al.* (1994a) pointed out one important limitation of the studies previously carried out: the phenomena observed in the interferometric measurements had the same scale as the distortions contained in the reference data such as digital elevation models, GPS measurements etc.

SAR interferometric data have been used in the field of *volcanic hazards* for monitoring and mapping of lava flows. First results were achieved by observations from TOPSAR airborne data. Evans *et al.* (1992) assessed the damage caused by pyroclastic flows and lahars, and the intercomparison of volcano morphology. ERS satellite data were successfully used for the monitoring of small surface changes due to volcanic inflation and of magma movements due to volcanic deflation (Massonnet *et al.*, 1995; Wadge *et al.*, 1997). Briole *et al.* (1997) detected flank deformation due to lava emplacement. InSAR data were used for topographic mapping of volcanoes (Mouginis-Mark and Garbeil, 1993) and the mapping of lava flows (Zebker *et al.*, 1996). Stevens *et al.* (1997) stated that SAR interferometric data are suitable for the two approaches generally used for mapping lava. Planimetric mapping of the lava volume is calculated by multiplying the lava area by an estimated mean thickness, whereas the more precise topographic mapping of the volume and morphology of the lava is based on a comparison of changes between the pre- and post-emplacement topography. Because several of the most volcanically active areas of the world are not covered by the ERS satellite data, the use of these satellites for volcanic monitoring is limited. This is due to a lack of on-board data storage capabilities and due to a lack of ground receiving stations covering these areas (Stevens *et al.*, 1997). These problems can be overcome by using data sets from satellites such as RADARSAT and JERS-1 which have a tape recording facility.

The suitability of SAR interferometry for the field of *change detection* was first proved by a blind experiment carried out by the University of Stuttgart and the Politecnico di Milano (Hartl *et al.*, 1992; Prati *et al.*, 1992). The height of two corner reflectors deployed in a calibrated test site was changed between two ERS-1 data acquisitions and these small changes were detected with millimetre accuracy. Hartl and Thiel (1993) estimated the extract in a gravel quarrying area based on two cuts in perpendicular directions. Polidori *et al.* (1994) evaluated the capabilities of airborne SAR interferometry for change detection by comparing it with other change detection techniques (multitemporal radiometric analysis and differential radargrammetry). They concluded that under good imaging conditions differential interferometry is suitable for mapping small changes such as land subsidence, landslides or soil erosion.

#### 2.5.4 Other applications

Various studies have been carried out to derive additional information from InSAR data for areas covered by *forestry*. Early results based on ERS-1 repeat-pass imagery indicated that the coherence level in scenes covering forested areas was not sufficient for the derivation of additional information. Askne *et al.* (1997) concluded that the coherence is mainly determined by temporal decorrelation, the volume scattering layer width and the area fill factor. They developed a model to define a relation between the interferometric observations and basic forest properties. Coherence properties can be used to distinguish between forested and non-forested areas. Furthermore, the interferometric effective forest height was estimated by comparing it with an existing digital elevation model (Askne *et al.*, 1997). According to Hagberg *et al.* (1995), the coherence was found to be sensitive to temperature changes around zero degrees but insensitive to wind speed. Wegmüller and Werner (1995) were even able to distinguish a number of different forest types. Finally, Wegmüller and Werner (1997) studied the derivation of vegetation parameters. This was also extensively investigated by Treuhaft *et al.* (1996).

Wegmüller (1996) analysed the potential of SAR interferometric data for *hydrology*, i.e. the monitoring of soil moisture. He was able to identify areas with sparse or no vegetation cover. Furthermore, he could separate changes due to surface roughness from soil moisture.

The *coastline* delineation was performed by Schwäbisch *et al.* (1997) based on a sufficient coherence level. They concluded that the coherence contains suitable information for defining the sea/land boundary and monitoring coastal morphodynamics.

The problem of *land subsidence* due to gas exploration has been the subject of several studies in the Netherlands (van der Kooij *et al.*, 1995; van Halsema *et al.*, 1995). The main problem with these kind of land subsidences is that the amount of change over a year is that small that it is difficult to separate it from atmospheric effects. Compared to the land subsidence in the Netherlands, the changes due to oil exploration in California, investigated by Fielding *et al.* (1997), were much larger.

## 2.6 TRENDS

The InSAR technique is now well on the way to becoming operational. The focus of current interferometric research is shifting to operational constraints such as data availability, quality assessment and future system specifications. More and more interferometric software packages, described in more detail in section 3.7, are becoming commercially available.

The success of the ERS satellites inspired the European Space Agency to continue with the launching of other satellites. The ENVISAT satellite, planned for a December 1998 launch, carries an advanced SAR (ASAR) instrument which has characteristics similar to the ERS satellites. This satellite operates in the C-band and has a spatial resolution of 30 metres. In addition to that, the ASAR sensor offers a dual polarisation and an incidence angle range of 15-45 degrees. An on-board tape recording facility provides global coverage. More technical details about the ENVISAT mission can be found in Bruzzi *et al.* (1995) and Kramer (1994).

One complex and spectacular project planned for September 1999 (Werner, 1997) is the shuttle radar topography mission (SRTM). This co-operative project by the National Aeronautics and Space Administration (NASA), the National Image and Mapping Agency (NIMA) and the German Space Agency (DARA) is based on the experience gained during the two flights of the second SIR-C/X-SAR repeat-pass mission in April and October 1994. The SRTM project is supposed to generate a consistent interferometric data set acquired during a ten day single-pass shuttle mission covering 80 percent of the global land surface. The C-band radar will allow continuous coverage through its scanSAR facility, whereas the X-SAR will operate in a high resolution mode with a swath width of approximately 50 kilometres. The single-pass approach will be realised by one antenna placed in the cargo bay of the shuttle and a second antenna system mounted on a 60 metre long deployable boom structure. In order to achieve the required accuracies, the baseline needs to be known within an accuracy of 3 millimetres (Werner, 1997). An attitude and orbit determination avionics (AODA) system will ensure a continuous observation of the baseline performance. Two GPS receivers on each antenna will provide relative and absolute position measurements. Electronic distance measurements can be performed in

case of any system failures. The system will be calibrated over the ocean areas and by using corner reflectors as ground control points. The successful completion of this mission will prove itself that the InSAR technique is truly operational.

## 2.7 FACTORS INFLUENCING THE DATA QUALITY

The quality of SAR interferometric data is influenced by several factors. As mentioned before, the radar sensor acquiring the data sets is characterised by system parameters such as look angle, system noise, spatial resolution, wavelength, polarisation and bandwidth. The satellite orbits provide essential information for describing the viewing geometry during the data acquisition. Atmospheric effects are assumed to be the most limiting factor for the quality of spaceborne interferometric data. Decorrelation due to differences in the two data takes and due to the baseline geometry also have to be considered. Finally the performance of the data processing needs to be investigated.

### 2.7.1 Orbits

For spaceborne systems the motion of a satellite along the flight path is described by its orbit. The actual position and velocity of the satellite at a particular time is given by means of orbit state vectors. The user is usually provided with five state vectors in the leader file attached to the complex radar image file. Based on additional observations more precise orbit information can be obtained which, is available at ESA and other institutions such as the Delft Institute for Earth-Oriented Space Research (DEOS).

The motion of a satellite,  $\vec{r}$ , can be described by the basic equation for Keplerian motion given by

$$\ddot{\vec{r}} = -\frac{GM}{r^3} \vec{r} , \quad (2.9)$$

with the universal gravitation constant  $G$ , the mass of the Earth  $M$ , the geocentric distance to the satellite  $r$  and the geocentric position vector of the satellite  $\vec{r}$ .

For the precise orbit determination, a number of additional forces have to be considered (Fernandes, 1993; Seeber, 1993). Besides the Earth's gravitational field, the motion of the satellite is also affected by the sun, the moon and the planets. In this respect, the moon has the most significant influence. Although the sun is more massive, its effect is relatively smaller as the distance between the sun and the Earth is very large. An atmospheric drag is caused by the friction between the satellite surface and the surrounding atmosphere. The solar radiation produces a pressure on the satellite most of which comes directly from the sun but part of it also comes from the reflection from the Earth (albedo). The solid Earth and oceanic tides change the gravitational potential of the Earth and are therefore indirectly a gravitational effect of the sun and the moon.

### 2.7.2 Atmosphere

Atmospheric effects are assumed to be one of the most limiting factors of differential interferometry. A homogeneous atmosphere affects the entire image and depends on the incidence angle as well as on the baseline whose effect on the atmosphere is negligible. These atmospheric effects can be removed by adequate processing. The refraction, for example, causes pixel misregistration and artefacts in the phase difference (Tarayre and Massonnet, 1994 and 1996). The heterogeneous atmospheric effects appear locally and are difficult to detect. These effects are caused by tropospheric turbulences and by time and space variations of the water vapour content (Goldstein, 1995; Zebker *et al.*, 1997). One proposed method for the reduction of the effect of atmospheric noise is the averaging of interferometric measurements from independent image pairs (Zebker *et al.*, 1997). Tarayre and Massonnet (1996) stated that with SAR interferometric measurements ionospheric phenomena could be detected more precisely than with GPS. InSAR is a new remote sensing tool for the investigation of tropospheric turbulences and ionospheric phenomena.

### 2.7.3 Temporal decorrelation

Temporal decorrelation is one of the major constraints of repeat-pass interferometry. It is caused by all the physical changes occurring at the terrain surface between two data acquisitions. These changes are measurable as variations in the dielectric constant of the vegetation surface and covering soil layer. Zebker and Villasenor (1992) studied changes over time for various terrain types. The correlation of a desert area remained unchanged whereas forested terrain showed a significant loss of coherence with time.

### 2.7.4 Baseline decorrelation

Baseline decorrelation is a factor of the viewing geometry which is determined by the orbits chosen for the data acquisition. With an increasing length of the baseline the noise level rises which leads to a decorrelation of the radar signals. The baseline decorrelation is always in the system and cannot be avoided (Zebker *et al.*, 1996). It can be reduced to a certain extent at the expense of image resolution (Gatelli *et al.*, 1994). Franceschetti *et al.* (1996) developed a general and compact formulation of the baseline decorrelation coefficient.

### 2.7.5 Processing

The performance of the interferometric processing is another important factor influencing the quality of the final products. The processing steps shown in Figure 2-11 are well studied and different procedures for the implementation have been proposed. Due to the limitations in terms of processing speed, InSAR processing is a trade off between accuracy and processing time. A standard procedure therefore does not exist. For the quality of the final products, accurate co-registration of the two input images is a prerequisite. Based on a good image registration, ideally up to 1/10 of a pixel, reliable quality for interferometric products can be achieved. Due to its complex nature, phase unwrapping remains the most

critical issue in the interferometric processing. There is still some research effort needed in order to optimise the processing steps. These are described in more detail in chapter 3.

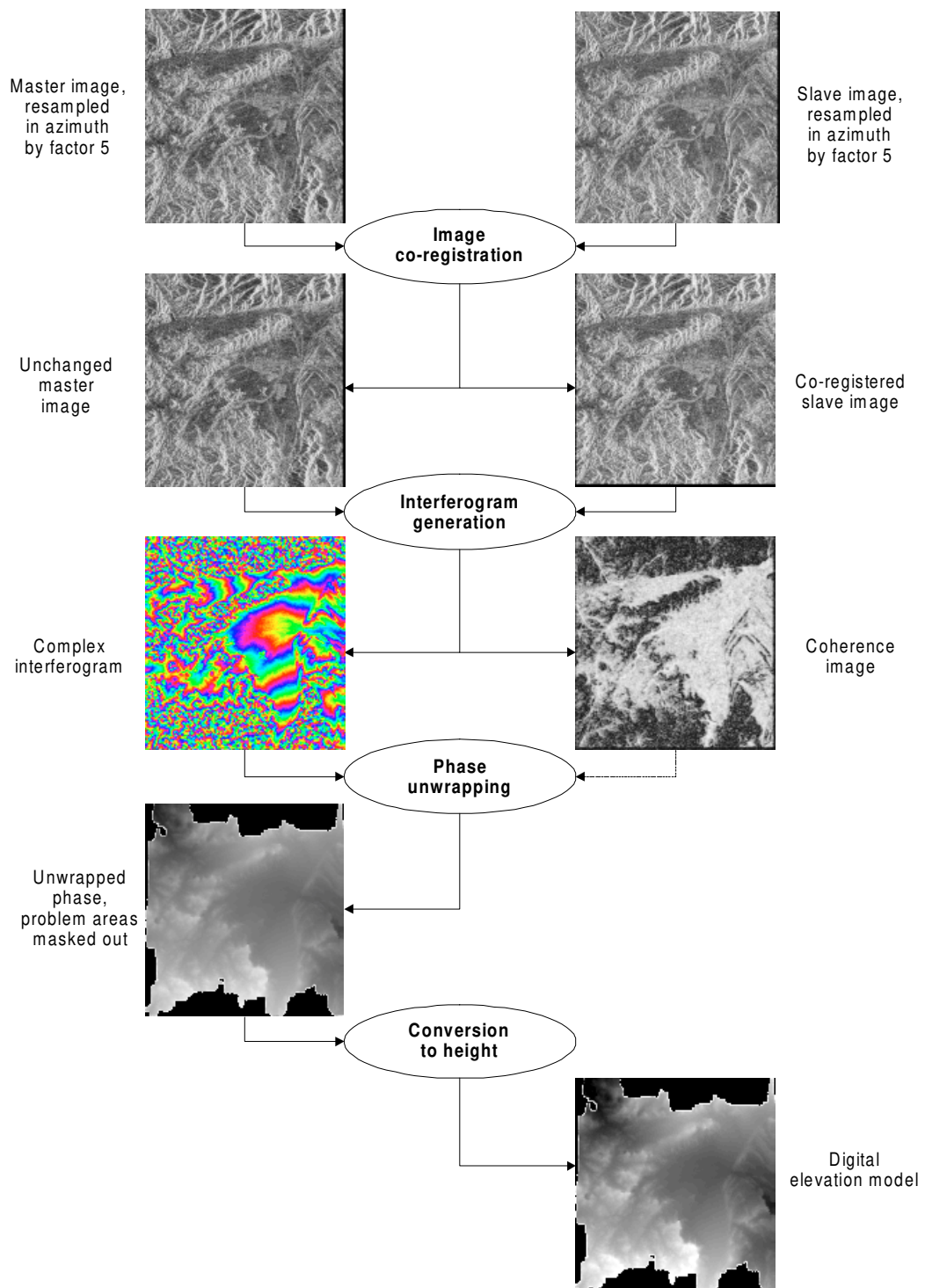


**Figure 2-11:** *Interferometric processing chain*



### 3 INTERFEROMETRIC PROCESSING

The processing of SAR interferometric data is a complex issue. Based on the quality of the data sets, the performance of each single processing step has its influence on the final product. With the increasing availability of more powerful hardware, the performance of the software packages can still be improved in terms of accuracy, flexibility and processing speed.

#### 3.1 DATA SETS

Successful data processing is possible only if the quality of the input data is suitable. For the interferometric processing complex radar imagery is required, i.e. the radar signal needs to contain an intensity information as well as a phase value. A convenient representation of the complex signal, as it consists of a real and an imaginary part, is a vector whose length represents the amplitude and whose orientation refers to the phase. This vector is the resultant of all scattering objects within the resolution cell and is, in radar terminology, referred to as phasor. For the interferometric processing either raw data or single look complex (SLC) data can be used. In case of SLC data, it is a prerequisite that the phase information contained in the raw data is preserved during the SAR processing.

	ASF	Atlantis *	CNES	CORISTA	DLR	Gamma *	INS	ISTAR	IRECE-CNR	JPL	Joanneum/ERDAS *	JRC	PCI *	POLIMI Quicklook	POLIMI InSAR	RSL	UBC	University Stanford
<b>Supported sensors</b>																		
ERS-1 / ERS-2	•	•	•	•	•	•	•	•	•	•	•	•	•	•	•	•	•	•
JERS-1		•				•				•								•
SIR-C / X-SAR			•	•	•	•	•		•	•	•					•		•
RADARSAT		•	•			•		•		•	•						•	•
TOPSAR				•					•	•								•
E-SAR									•									•
DOSAR						•												•
ERIM Lear jet																		•
SRTM										•								
<b>Supported formats</b>																		
RAW	•	•	•	•	•	•		•	•	•				•	•	•		•
SLC	•	•	•	•	•	•	•	•	•	•	•	•	•			•	•	•

**Table 3-1:** Interferometric data sets supported by available software packages<sup>1</sup>. \* Commercially available

<sup>1</sup> Besides these, there are other software packages such as from Intermap (Canada), NPA (United Kingdom) etc. for which no detailed information was available

The sensors supported by the available software packages are given in Table 3-1.

As mentioned before, the ERS-1 satellite was the first operational spaceborne system which acquired radar data theoretically suitable for SAR interferometry. Coulson (1993) reported about the first interferometric experiments based on ERS-1 data sets. He concluded that ERS-1 satellite meets all the requirements for interferometric applications. From the theoretical point of view, the InSAR technique is assumed to generate digital elevation models with an accuracy in the order of a few metres (Coulson, 1993). The results are even more remarkable, when one considers that the ERS-1 satellite was designed for the observation of the sea surface, and not specifically for SAR interferometry over land.

With the launch of the ERS-2 satellite, the acquisition of data sets from both ERS satellites on two consecutive days was possible decreasing the effect of temporal decorrelation by reducing the repeat cycle from 35 days to one day. This combined data acquisition is referred to as tandem mission. A first testing of the ERS tandem data quality was performed by Solaas *et al.* (1996). A large number of interferometric data sets acquired one day apart are available covering large parts of the Earth's surface, as shown in Table 3-2. The range of the baselines indicates that these data sets can be used for most of the interferometric applications.

Baseline	Number of frame pairs	Percentage of total
$B_{\text{perp}} < 50 \text{ m}$	22181	20
$50 \text{ m} < B_{\text{perp}} < 300 \text{ m}$	81619	73
$300 \text{ m} < B_{\text{perp}} < 600 \text{ m}$	6221	6
$600 \text{ m} < B_{\text{perp}}$	1028	1

**Table 3-2:** Acquisition statistics of ERS tandem data (Solaas, 1996)

The combination of ERS-1 data sets from ascending and descending orbits was used to improve the accuracy of an interferometrically derived DEM (Schwäbisch, 1995; Carrasco *et al.*, 1997). Carrasco *et al.* (1997) generated digital elevation models, one from an ascending image pair and one from a descending image pair, and combined both elevation maps using coherence based height averaging. This approach led to a significant improvement in the overall DEM accuracy. The effects caused by layover and shadow can also be reduced (Schwäbisch, 1995). The most critical step of this method is the exact superimposition of one DEM over the other. The elevation models should not contain propagated errors from the phase unwrapping in order to allow an accurate matching of both DEMs.

ERS data are acquired and processed by several processing and archiving facilities (PAFs). It is in the user's interest to perform SAR interferometric processing without having to take into account which PAF actually produced the data sets. A number of tests are defined in the product specifications of SLC data to ensure the data quality e.g. the already mentioned phase preservation during the processing. The cross-compatibility of the

images, i.e. the overall performance of the processors including the combination of data sets processed by different PAFs, are not covered by these tests. For these reasons, Barmettler *et al.* (1996) carried out a study comparing data sets from the central (CPRF), the German (D-PAF) and the Italian (I-PAF) processing and archiving facility. They concluded that, apart from problems with the time-referencing and minor disagreements in the CEOS header format, SLC data can be used for interferometric processing without a loss of overall quality.

Rossi *et al.* (1996) evaluated the interferometric potential of JERS-1. The only operational spaceborne L-band system has a repeat cycle of 44 days. This leads to temporal decorrelation but this loss of coherence is limited in time because the wavelength is relatively insensitive to changing vegetation. The geometrical constraints and the coherence loss due to baseline decorrelation are partly compensated by the relatively large look angles in the range of 32-38 degrees. With this stability in time, JERS-1 data sets are suitable for the monitoring of surface displacements. Besides this, the on-board tape recording facility on board the JERS-1 satellite provides nearly global coverage.

The capabilities of RADARSAT were evaluated by Vachon *et al.* (1995). They extended the ERS-1 case and performed a theoretical, comparative study. The fine-resolution mode of RADARSAT with large look angles has a more favourable geometry than ERS satellites. It is expected that high quality interferometric data sets can be acquired especially over dry regions with little vegetation. The on-board tape recording of RADARSAT also allows global coverage. Besides these advantages, it appears that RADARSAT's interferometric capabilities also have some limitations. A repeat cycle of 24 days leads to temporal decorrelation. The tracking of the RADARSAT satellite is less precise compared to ERS satellites. Overall, the RADARSAT system is assumed to have a lack of robustness to generate DEMs in an operational way (Gens and van Genderen, 1996b). For a final evaluation more experimental results are required.

The potential of X-SAR for SAR interferometry was demonstrated by Moreira *et al.* (1995). The operational use of the X-SAR sensor on the shuttle platform was limited due to the squint instability of the shuttle. On the other hand, the short wavelength enables a short baseline for a given height resolution if the sensor is used in the across-track mode. The system in a single-pass SIR-C/X-SAR configuration on the shuttle, as suggested for a third SIR-C mission, is only limited by the system noise.

The TOPSAR system, a multifrequency (P-, L- and C-band) and multipolarisation airborne system, is operated by NASA/JPL (Zebker *et al.*, 1992). The existing AIRSAR system was modified to optimise the performance in the topographic mapping mode. Madsen *et al.* (1995) analysed and evaluated the TOPSAR system concerning its interferometric capabilities. They stated that the evaluation of InSAR systems in relation to topographic mapping should be split into two separate problems. Effects directly related to system parameters should be dealt with separately from target effects such as volume scattering etc. For the optimisation of the performance a calibration of the InSAR system is essential. This needs to be carefully planned and executed. Further research on appropriate calibration procedures is required.

Faller and Meier (1995) presented first results from the DOSAR system, an airborne interferometer using C-band. The results achieved agree well with known airborne InSAR characteristics. The advantage of single-pass interferometry in terms of temporal

decorrelation leads to a high coherence in difficult areas e.g. forested areas. The platform motion has a critical influence on the interferometric height but the effect of the roll angle can be eliminated by precise motion compensation techniques. The phase noise caused by the small airborne baseline can be compensated by multilook processing. Goblirsch *et al.* (1995) investigated the influence of filtering in the process of DEM generation. They suggested to minimise the filtering of the height values due to the sensitivity of the phase information.

### 3.2 CO-REGISTRATION

One of the key issues of the whole interferometric processing is the co-registration. The quality of the co-registration significantly influences the final quality of any SAR interferometric product. No reliable results can be achieved if the initial co-registration is not sufficient. The co-registration invokes the challenging trade off between the processing time and the quality of the applied method, especially because it is one of the most critical and time consuming processing steps. Therefore, special care should be taken during this important processing step.

During co-registration, one image called the slave image is aligned to a reference image called the master image. The co-registration consists of two steps: the change of the location of each pixel in the slave image with respect to the master image, and the recalculation of the amplitude and phase information of the phasor by interpolation for each pixel of the slave image. Due to a fractional shift of a pixel during the co-registration, the phasor will now contain different scatterers. Therefore, the resultant of the phasor will be slightly different. Practically, the first part of the process of co-registration, the alignment of master and slave image, can be further split up into two separate steps, the *coarse co-registration* and the *fine co-registration*.

The coarse co-registration can be realised in different ways. The most preferred and generally used approach makes use of the information on satellite orbits. Theoretically, the satellite orbits could also be used for the fine co-registration but the accuracy of the satellite orbits and the moments of acquisition is not sufficient for this purpose. Based on the orbital state vectors, the moments and the centres of the image, the coarse co-registration of master and slave image is carried out. According to Small *et al.* (1993), an accuracy of  $\pm 2$  pixels in range direction and  $\pm 10$  pixels in azimuth direction have been achieved in this study. Alternatively, the master and slave image can be co-registered manually by using tie points that need to be selected in both images (Kwoh *et al.*, 1994). Finally, a multiresolution approach for the matching of two images was proposed by Lemmens (1992) which could also be used for the coarse co-registration of complex radar data. It basically uses techniques for the fine co-registration but with the data sets in lower resolution to save significant processing time.

For the fine co-registration several methods have been proposed and implemented.

The coherence co-registration estimates the optimal shift of the slave image for a maximal coherence between master and slave image. This approach was used by many scientists (Prati and Rocca, 1990; Hartl and Xia, 1993; Carrasco *et al.*, 1995).

The signal-to-noise ratio (SNR) co-registration (Gabriel and Goldstein, 1988) achieves the optimal shift of the slave image by calculating the noise of the interferogram in the frequency domain using the full complex values for the co-registration.

The average fluctuation co-registration (Lin *et al.*, 1992) calculates the level of noise directly in the interferogram, i.e. based only on phase information, assuming that the fluctuation of the phase represents the noise. The optimal shift of the slave image is achieved when the average fluctuation function reaches a minimum.

A detailed study on the different co-registration techniques was carried out by Samson (1996).

The co-registration depends on a number of parameters, given in Table 3-3. For a sufficient approximation of some of these effects higher-order polynomials are required.

Co-registration parameters	Causes	Order of polynomial
<b>Shift</b>		
in range direction	- distance between orbits (Small <i>et al.</i> , 1993), different orientation of the antenna	0
in azimuth direction	- different occasions of start acquisition (Small <i>et al.</i> , 1993)	0
<b>Scale</b>		
in range direction	- different time difference between the first and last echo of pulse emission	1
in azimuth direction	- different satellite velocity during acquisition, different orientation of the antenna	1
<b>Rotation</b>	- non-parallel satellite orbits (Gabriel and Goldstein, 1988)	1
<b>Skewness</b>	- different satellite velocity during acquisition - different earth rotation velocity	1
<b>Non-linear parameter</b>	- different vantage points cause different overlay - deformations with component perpendicular to slant range vector between two acquisition - different atmospheric conditions (degree of refraction, delay of radar signals) - malfunctioning of the antenna	>1

**Table 3-3:** Influence of different parameters on the co-registration (modified from Samson, 1996)

The requirements in terms of quality of the co-registration process are related to the expected phase error caused by any misregistration. Just and Bamler (1994) showed in a study that a misregistration does not lead to a shift of the interferometric phase but to a variance in phase. According to this study, no significant reduction of the phase error can be expected if the co-registration is carried out with an accuracy better than  $\frac{1}{8}$  of a pixel.

The interpolation method used during the co-registration process has a significant impact on the quality of SAR interferometric products. Geudtner (1995) investigated the influence of the interpretation method used for the resampling of the slave image. He compared the processing results of data sets based on bilinear interpolation with the resampling using cubic splines and achieved an improvement of ten percent in terms of coherence in the correlation between master and slave image.

### 3.3 INTERFEROGRAM GENERATION

As mentioned before, the interferogram is defined as the product of the complex SAR values of a slave image and the complex conjugate of a master image, i.e. the amplitudes of the corresponding pixels are averaged and the difference of the phase values for each point in the image is calculated. The generation of the interferogram results in a reduction in size of the data set. The pixel size in the calculated interferogram is generally adapted to the pixel size in ground range. Since the ERS data sets, for example, are given with a pixel spacing of 20 metres in range direction and 4 metres in azimuth direction, respectively, the amount of data can be reduced by factor 5. Multilook processing can further reduce the amount of data and the noise at the expense of a loss in spatial resolution. For the multilook processing the range and azimuth bandwidths are divided into sub-bands focusing each sub-band to an individual image (look). The summation of the spectrally not overlapping and therefore uncorrelated sub-bands leads to a speckle reduced image.

The complex multiplication of the two images in the spatial domain corresponds to a convolution of both spectra in the frequency domain. The bandwidth of the product is, therefore, the sum of the bandwidths of the original data sets. Since the sampling rate of the originals do not exceed twice the Nyquist frequency, phase aliasing effects, a folding of the spectra in azimuth direction which shows up as ambiguities, occur. These phase aliasing effects can be eliminated by oversampling. For two-dimensional complex data sets, this is realised by zero-padding, i.e. the spectral values are set to zero by limiting the bandwidth (Schwäbisch, 1995).

### 3.4 PHASE UNWRAPPING

An interferogram contains a phase information which is directly related to the topography. Since this information is given modulo  $2\pi$ , there is an ambiguity problem in calculating the correct integer number of phase cycles that needs to be added to each phase measurement in order to obtain the correct slant range distance. This ambiguity solution is referred to as phase unwrapping.

The problem of phase unwrapping has been the focus of InSAR research for several years. Numerous methods were proposed and implemented for this most complex issue of the interferometric processing chain. No satisfying solution to this problem has been found so

far. Also an overall comparison of the existing techniques, e.g. on a simulated data set under controlled conditions, is missing. A complete description as well as an evaluation of all existing techniques is beyond the scope of this study. Therefore, only the basic techniques, the main developments and trends of phase unwrapping are discussed here.

The first method developed for the unwrapping of the interferometric phase was developed by Goldstein *et al.* (1988). This so called *branch cuts* approach is based on the identification of residues, local errors in the measured phase caused by signal noise or by actual discontinuities, and the definition of suitable branch cuts to prevent any integration path crossing these cuts. The estimated neighbouring pixel differences of unwrapped phase are integrated along paths avoiding the branch cuts where these estimated differences are inconsistent. The problems of this approach are the definition of suitable branch cuts and the time consuming computations.

The *fringe detection* method from Lin *et al.* (1992) tries to find the location of fringe lines in the phase difference image which might be interrupted. Using edge detection techniques the image is enhanced by filtering and a threshold is applied to the image. The phase is unwrapped by adding a multiple of  $2\pi$  each time the integration path crosses a fringe line. The multiple is determined by the number of fringe lines between the pixel and a reference pixel. Practically, this method can only be applied in interferograms where fringes are greatly separated and the signal-to-noise ratio (SNR) is high (Hartl and Wu, 1993; Schwäbisch, 1995).

The *least squares* approach is based on studies of Fried (1977) and Hudgin (1977) on optical imagery. The mean square deviation between the estimated and the unknown neighbouring pixel differences of the unwrapped phase is minimised. The computational efficiency can be significantly improved by fast Fourier transform techniques (Takajo and Takahashi, 1988; Ghiglia and Romero, 1994). The least squares approach tends to spread the errors occurring instead of concentrating them on a limited set of points. To overcome this accuracy problem, least squares algorithms weighting the wrapped phase were proposed (Ghiglia and Romero, 1994; Pritt, 1996). The resulting accuracy depends on the weighting mask used and the computational efficiency decreases compared to the unweighted approach.

A very promising new technique has recently been proposed by Constantini (1996). He formulated the phase unwrapping as a *minimum cost network flow* problem. This new approach appears to be relatively accurate and efficient (Constantini, 1996). The development of solutions of minimum cost network flow problems itself is a very active research field and there are a reasonable number of implemented algorithms available. An exhaustive review of these algorithms is given by Ahuja *et al.* (1993).

### 3.5 CONVERSION FROM PHASE TO HEIGHT INFORMATION

For the derivation of the terrain height from interferometric phase information, several approaches have been developed. The method described by Small *et al.* (1993) requires a refinement of the baseline and imaging geometry, which can later also be used for the geocoding (section 3.6) of the digital elevation model. With a suitable number of well distributed reference points, the spatial position and orientation of the baseline is determined. This method requires the knowledge of precise orbit parameters as well as a number of reference points which are sometimes difficult to identify. Schwäbisch (1995) proposed an alternative approach for the conversion from phase to height using only one reference point. This method is based on the measurement of the absolute interferometric phase in a regular grid and the solution of an equation system to convert the phase into height information by least squares adjustment.

The most critical step of this procedure, that is often underestimated, is the transformation of the height information from the satellite geometry, given in the conventional terrestrial system (CTS), to a reference system suitable for topographic mapping. The CTS is an earth-fixed reference system established through the conventional direction to the mean orientation of the polar axis (conventional terrestrial pole) and a zero longitude on the equator (Greenwich mean observatory)(Seeber, 1993). For the conversion between the different height systems three surfaces, illustrated in Figure 3-1, are to be considered.

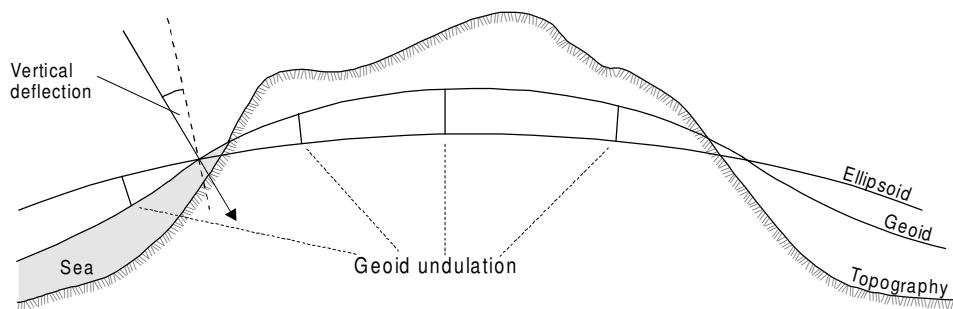


**Figure 3-1:** The three reference surfaces - topography, geoid and ellipsoid

The *topography* represents the physical surface of the Earth. The *geoid* is defined as that level surface of the gravity field with the best fit to the mean sea level which may extend inside the solid body of the Earth (Torge, 1991). The *ellipsoid* defines a mathematical surface approximating the physical reality while simplifying the geometry for computations. The geoid undulation, the vertical separation between the geoid and a reference ellipsoid, can reach values up to 100 metres on a global scale (Seeber, 1993). The vertical deflection is defined as the angle between the directions of the ellipsoidal normal and of the plumb line.

A comprehensive introduction to the different height systems is given by Heiskanen and Moritz (1990). The different height systems can be related to each other by means of the geopotential number  $C$  which is defined as



$$C = W_0 - W = \int_{\text{geoid}}^{\text{point}} g \, dn , \quad (3.1)$$

where  $W$  and  $W_0$  are the potentials of gravity of a point and the geoid, respectively. Alternatively, it is expressed in terms of the gravity  $g$ , and the levelling increment  $dn$ . The different heights are then calculated by dividing the geopotential number by a gravity value. For the *dynamic height* a constant normal gravity  $\gamma_0$  for an arbitrary standard latitude, usually 45 degrees, is used. As it has no geometrical meaning, the dynamic height has a limited practical sense. The *orthometric height* is the natural “height above sea level” and measured along the current plumb line from the foot point on the geoid and the point on the Earth’s surface. As the gravity value the mean gravity  $\bar{g}$  is taken. The *normal height* represents the vertical distance from the terrain surface to the quasigeoid, i.e. the ellipsoidal height reduced by the height anomaly  $\zeta$ , measured along the ellipsoidal normal. In this case, the gravity value for the calculation of the height is the mean normal gravity  $\bar{\gamma}$  along the plumb line (Heiskanen and Moritz, 1990). Extending the normal heights downward from the Earth’s surface yields the quasigeoid as reference surface for heights (Torge, 1991).

The height derived from SAR interferometric data sets are basically calculated based on a viewing geometry determined by means of orbital parameters. The satellite orbits are given in the CTS system. Therefore, the heights calculated in this system refer to a reference ellipsoid. The ellipsoid is a convenient reference frame, as it is a mathematical figure, and also provides a good approximation to the geoid. According to Frei *et al.* (1993), there are mainly two reasons to give a preference to the geoid as a reference system rather than an ellipsoid. The reference to the mean sea level allows to use tide gauges placed around the coastline as height reference points. The second point is the physical significance of orthometric heights. The geoid ensures a horizontal representation of water surfaces such as lakes and seas. This is why the heights used in topographic maps have the geoid as reference whereas the horizontal information refers to a position on an ellipsoid. If the DEM is used as an input for further calculations, the user might need to combine this height information with his own measurements which are usually in geoid related reference system. In this case it is more user friendly to provide the required information in the same reference system as the measurements.

### 3.6 GEOCODING OF THE DIGITAL ELEVATION MODEL

The geocoding of SAR interferometric products makes these products useful for a number of applications. According to Small *et al.* (1995), geocoded products can be used for

- validation of InSAR derived height maps,
- investigation of class dependent coherences (Small *et al.*, 1994),
- investigation of ascending versus descending coherences (Small *et al.*, 1994),
- normalisation for radiometric effects of topography (Holecz *et al.*, 1994) and
- differential interferometry (Massonnet *et al.*, 1993).

The geocoding defines the transformation between a local coordinate system and global Cartesian coordinates. It can be performed in two different ways depending on the availability of a reference DEM. If a reference DEM is available, the Doppler frequency

can be calculated based on the DEM positions and the satellite orbit. Knowing the Doppler centroid, which determines the position of the sensor for any backscatter element, the frequency shift is iteratively calculated. The sensor position is moved until the Doppler frequency is equal to the Doppler centroid, providing the azimuth coordinate. The range coordinate is given by the difference of the slant ranges of determined pixel and first near range pixel divided by the pixel spacing in range. The final step is the resampling in a standard map projection. This approach was described in more detail by Meier *et al.* (1993).

The geocoding can also be performed without a reference DEM (Small *et al.*, 1995). For the approach the refinement of the baseline and imaging geometry is a prerequisite. The geocoding is then done by calculating the look vector corresponding to each azimuth pixel and adding it to the orbital position. This procedure leads to an irregularly gridded set of points which can be resampled to a regular grid using e.g. a Delauney triangulation. Other interpolation methods such as nearest neighbour etc. are less time consuming but also less accurate.

### 3.7 SOFTWARE PACKAGES

Over the past few years, numerous software packages for SAR interferometric processing have been developed. Most of them were designed by the research institutes that started working in the field of SAR interferometry, due to a lack of commercially available software. Therefore, most of the software packages are for internal use and generally consist of standalone modules created for the various interferometric processing steps. Their main purpose is to support the research carried out at these institutes and, hence, the aspects of user friendliness (e.g. user interface, standards, documentation, user manuals, etc.) is of minor importance. In the meantime, a few commercial software packages, based mainly on the mentioned “research” packages, have become available in the market. The interferometry module distributed by PCI was developed by the Institute of Navigation in Stuttgart. The Gamma software was programmed by scientists of the RSL in Zurich and JPL in Pasadena. The Atlantis Scientific Inc., the provider of the third commercially available packet, recently entered into an agreement with PCI and the future releases will be integrated into the existing PCI software package. Finally, the software developed from the Joanneum in Graz has now been integrated into the Erdas IMAGINE package.

The information about the different software packages presented in Table 3-4 is the result of a questionnaire sent to the institutes asking for the technical specifications of their system (for more details on each software package see Appendix A). The specifications about the commercial packages are taken from the user manuals, the websites of the companies and by means of personal communication.

The questionnaire aimed at gathering general information about the software packages such as system specifications, supported sensors and formats, and calculated products. More detailed information about algorithms, processing time etc. were out of the scope of this investigation. Therefore, a general comparison of the packages is not possible. For a detailed study about the performance, capabilities and limitations of the software packages, more specific information about the implemented algorithms is required. Furthermore, an artificial data set could simulate different scenarios checking the performance of the systems in terms of processing speed, accuracy of the implemented algorithms, noise and

influences of terrain such as slope gradient and aspect, type of landscape etc. within a controlled environment. Another point to be considered is that products such as a differential interferogram can be produced without having included an automatic procedure in the InSAR package. Often modules developed for different purposes were adapted for the use in SAR interferometry. It is difficult to take these considerations into account for an objective evaluation of software performance.

	ASF	Atlantis *	CNES	CORISTA	DLR	Gamma *	INS	ISTAR	IRECE-CNR	JPL	Joanneum/ERDAS *	JRC	PCI *	POLIMI Quicklook	POLIMI InSAR	RSL	UBC	University Stanford
<b>Calculated products</b>																		
Interferogram	•	•	•	•	•	•	•	•	•	•	•	•	•	•	•	•	•	•
Coherence image	•	•	•	•	•	•	•	•	•	•	•	•	•	•	•	•	•	•
Unwrapped phase	•	•	•	•	•	•	•	•	•	•	•	•	•	•	•	•	•	•
Digital elevation model	•	•	•	•	•	•	•	•	•	•	•	•	•	•	•	•	•	•
Differential interferogram	•	•	•	•	•	•	•	•	•	•	•	•	•	•	•	•	•	•
Simulated interferogram	•	•	•	•	•	•	•	•	•	•	•	•	•	•	•	•	•	•
Geocoded products	•	•	•	•	•	•	•	•	•	•	•	•	•	•	•	•	•	•
<b>Quality control</b>																		
Ground control points	•	•	•	•	•	•	•	•	•	•	•	•	•	•	•	•	•	•
Reference DEM	•	•	•	•	•	•	•	•	•	•	•	•	•	•	•	•	•	•

**Table 3-4:** Interferometric products supported by the available software packages <sup>2</sup>.

\* Commercially available

For this study two commercially available software packages, one from Atlantis Scientific Inc. (EarthView InSAR, Versions 1.0.5 and 1.1.0) and the other from PCI (PACE IFSAR Interferometric SAR, Version 6.1 Beta) were used. With the Atlantis package, running on a SUN Ultra workstation, the research on the sensitivity study and the error propagation was carried out. The PCI software, a PC version running under Windows '95, only served as reference for the comparison of results obtained from the Atlantis software package. Since each single processing step needs to be started separately with changing parameter files, the system has but limited practical use for a study of error propagation, whereas the Atlantis package allows the performance of a tailored processing scheme.

<sup>2</sup> Besides these, there are other software packages such as from Intermap (Canada), NPA (United Kingdom) etc. for which no detailed information was available

## 4 QUALITY ASSESSMENT OF DIGITAL ELEVATION MODELS

---

In the literature the terms digital elevation model (DEM) and digital terrain model (DTM) are often used synonymously. Burrough (1986) defines a DEM as “any digital representation of the continuous variation of relief over space”. He states that the term digital terrain model “often implies attributes of a landscape other than the altitude of the landscape”. Considering that a high quality DEM contains information not only about the height but also about all morphological features such as breaklines or height spots, these terms can be used in a synonymous way.

There are two main aspects concerning the quality assessment of digital elevation models which are of particular interest for this study. For the estimation of the potential of SAR interferometry in terms of providing high quality height information, it is useful to compare the InSAR technique with other existing techniques used for creating DEMs. Besides that, the procedures for assessing the quality of these digital elevation models indicate which quality measures could be used for the error propagation approach.

### 4.1 TECHNIQUES FOR CREATING DIGITAL ELEVATION MODELS

A wide range of techniques has been developed for creating digital elevation models. The classical approach of deriving DEMs from contour lines on topographic maps is still a commonly used technique. Aerial photogrammetry has been used for many years and the geometry was adapted to the field of airborne radar. With the availability of optical satellite sensors it was possible to acquire DEMs from spaceborne imagery in a stereoscopic way. The improvement in the development of kinematic GPS and inertial navigation systems (INS) improved the performance of aerial photogrammetry and enabled the implementation of laser scanning systems. All these techniques are described in further detail later in this section.

Digital elevation models can be stored in several ways depending on the techniques used to acquire the elevation information. According to Carrara *et al.* (1997), these methods can be grouped into four basic approaches. *Contour lines* are mostly used as relief representation in topographic maps. Stereo aerial photographs provide height information in form of *profiles*. The most common approach to represent three-dimensional data is to use a regular *raster* grid. In order to store the morphological information in an optimal way, *triangulated irregular networks* (TINs) were developed. TIN structures are not aiming at an efficient interpolation technique. They represent a straight forward possibility to derive terrain characteristics. Therefore, the distribution of points used as nodes in the TIN structure should represent the actual morphology in an optimal way.

### 4.1.1 Contour lines

Contours are still the main source for creating DEMs since they provide necessary morphological details, such as breaklines and spot heights, to represent the terrain surface in a suitable form as shown in Figure 4-1. In general, they are derived from existing topographic maps. Additionally, selected point or profile measurements are sometimes necessary to describe the terrain surface in more detail.

Contour lines need to be interpolated in order to determine the height of the intervening points. A large number of interpolation algorithms has been proposed or developed. Some of these algorithms consider that the measured elevations are a group of randomly distributed point observations. The interpolation is performed using weighted moving averages, bicubic splines, finite elements etc. Other techniques were specifically developed for contours exploiting the specific topological and morphological characteristics of the contour lines. These methods are discussed in more detail by Clarke *et al.* (1982).

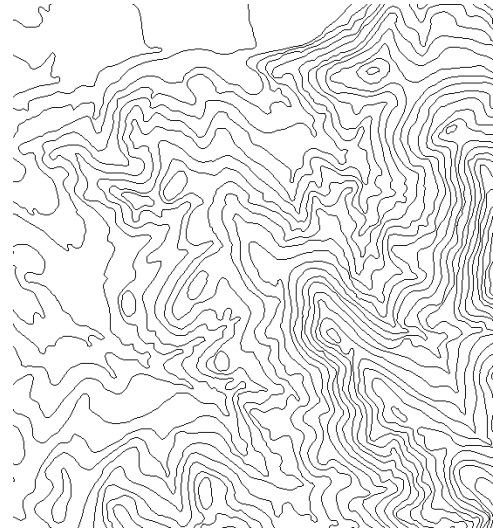


**Figure 4-1:** Digitised contour lines

According to Carrara *et al.* (1997), the accuracy of the contours mainly depends on the quality and scale of the aerial photographs, on the characteristics of the photogrammetric device as well as on the skills of the operator. Regardless of the efficiency of the selected DEM generator, the original data are degraded by any kind of processing. According to Finsterwalder (1952), the error of contour lines  $m_h$  derived from photogrammetry can be estimated by

$$m_h = a + b \cdot \tan \alpha, \quad (4-1)$$

with the height error  $a$ , the error in position  $b$  and slope of the terrain  $\alpha$ . This equation was first given by Koppe in 1902.

In North America the so called  $c$ -factor is used to determine the smallest contour interval which can be achieved with different photogrammetric instruments (Konecny and Lehmann, 1984). The  $c$ -factor is defined as the ratio of the flying height and the contour interval and varies with the instruments.

Wood and Fisher (1993) evaluated the interpolation methods such as inverse distance weighting, contour flood filling, simultaneous over-relaxation and one-dimensional spline fitting, and concluded that the interpolation using profile convexity detects the artefacts produced by the interpolation process most effectively. For this assessment they visualised the discrepancy between the measurements and the reference model by superimposition. The suitability of this approach lies in its flexibility in the visual interpretation and its significance for showing the data uncertainty e.g. to GIS users. Wood and Fisher (1993) stated that the root mean square (rms) error indicates the frequency distribution of the

differences between the measured heights and the true elevation and, hence, a more precise measure than the maximum discrepancy. That does not solve the problem to extract the meaning of a single global measure for the description of a spatially varying elevation surface.

#### 4.1.2 Aerial photogrammetry

Aerial photogrammetry using block adjustment (Figure 4-2) is the classical technique for the creation of elevation models and has been used for a very long time. It is based on the basic principle of aerial triangulation which determines the coordinates of a point on the ground in three dimensions. The early developments of block adjustment methods (Schermerhorn, 1960) with analogue instruments were replaced by programs for the adjustment of triangulation strips on analytical plotters (Ackermann, 1961). The introduction of additional parameters for systematic image distortions led to an improved accuracy (Bauer and Müller, 1972). This was the first step in the development of advanced bundle block adjustment programs (e.g. Jacobsen, 1982). For a summary of the developments in the field of aerial photogrammetry, the reader is referred to Konecny and Lehmann (1984).

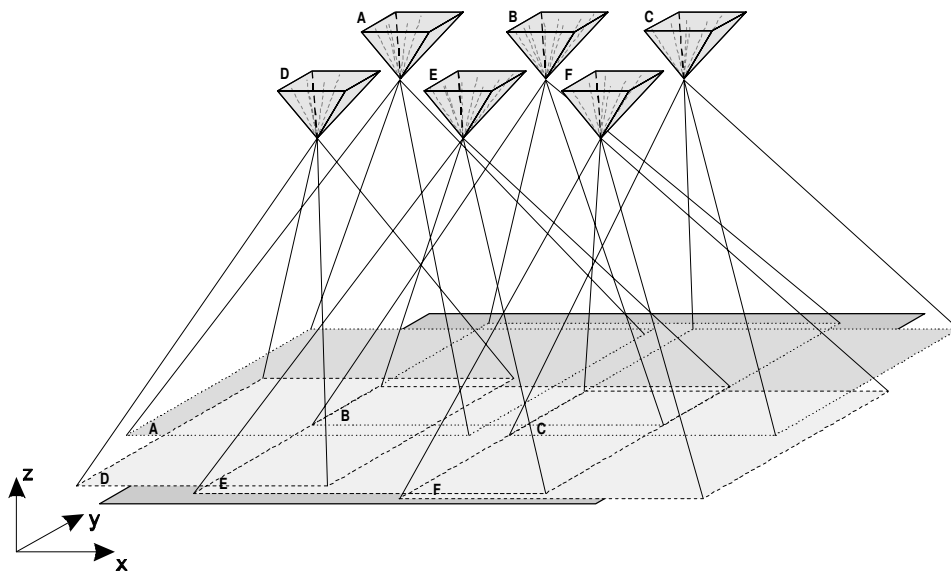


**Figure 4-2:** *Geometry of block adjustment in aerial photogrammetry*

The development of the global positioning system (Kaplan, 1996; Seeber, 1993) had a large impact on the requirements for aerial photogrammetry in the production of elevation models. GPS data and conventional photogrammetric aerial triangulation observations can be merged into a combined block adjustment. With the introduction of GPS measurements in aerial photogrammetry, the number of ground control points required for the block adjustment could be significantly reduced (Ackermann, 1992).

According to Ackermann (1996c), GPS positioning is applied in aerial photogrammetry in different ways. The first application of GPS for photogrammetry is the determination of

ground control points by standard GPS ground survey methods. Secondly, GPS is regularly used for flight navigation based on real-time positioning by pseudo-range observations. Furthermore, the camera position for aerial triangulation is measured using relative kinematic GPS positioning by differential carrier phase observations.

Since the GPS measurements are given in the WGS84 reference system, the GPS coordinates need to be transformed into local coordinates. The relation between a local ellipsoid and a global reference system, called datum, is defined by at least five parameters: the semi-major axis of the reference ellipsoid, the flattening and the three datum shift parameters (Seeber, 1993). Since generally no absolute coordinate reference is maintained, the datum for the photogrammetric block has to be provided in a way other than by GPS. One possibility is the usage of a few conventional ground control points, usually four xyz control points in the corners of a regular block.

The main problem of on-board GPS, apart from cycle slips, is the high probability of signal interruptions during flight turns, which requires a reassessment of ambiguity problems, in order to maintain a continuous GPS trajectory. The development of more robust estimation procedure in the GPS software improves the ambiguity solution caused by the flight turns. A singularity problem occurs in case GPS measurements are applied stripwise with a standard overlap and four control points. It can be compensated by either a chain of vertical control points at either end of a block or preferably by flying two cross strips (Ackermann, 1996c). Jacobsen and Schmitz (1996) extended the model for the combined bundle block adjustment considering also the geometric relationship between the airstrips. This approach makes crossing flight strips negligible and requires only four ground control points.

The ultimate goal of using GPS for aerial photogrammetry is to become independent from any ground control (Ackermann, 1996c). This requires continuous GPS trajectories of high quality with regard to a GPS datum as well as the transformation to a national reference system.

### 4.1.3 Radar techniques

Besides radar interferometry, there are a few other techniques developed for the generation of digital elevation models from radar imagery. Existing techniques for the derivation of DEMs based on optical imagery have been adapted to the radar approach. These techniques include *radargrammetry* as well as *radarclinometry*.

Leberl *et al.* (1986) developed a mathematical model for radar stereomapping to determine the optimum incidence angle combination of radargrammetric stereoscopy for visual interpretation of a geologic site and for topographic mapping. The radargrammetric technique can be implemented in different ways. The conventional stereoplotter can be modified to incorporate the radar geometry, whereas an analytical plotter realises the stereo geometry using a software algorithm. The setup of the stereomodel consists of several steps. With the inner orientation the relation between plotter coordinates and image coordinates is determined. The image coordinates of ground control points are iteratively calculated using approximations for sensor position and velocity vector of the antenna. A final least squares adjustment using ground control and additional orientation points ensures a parallax-free stereomodel for the data collection. In mountainous areas the

problem of layover, foreshortening and shadows occurs. There are various approaches to overcome or at least reduce these effects. On the one hand, the airborne configuration allows a stereo data acquisition of the area from the same direction in different flying heights. On the other hand, the area can be covered from different directions.

A comprehensive introduction to radargrammetric image processing is given by Leberl (1990). The improvement of the radargrammetric technique by advanced automatic correlation methods and the availability of more suitable data sets led to a revival of radargrammetry. Raggam and Almer (1996) created a DEM calculated from JERS-1 imagery using a parametric model. The good orbital information of the ERS-1 satellite allowed the derivation of a digital elevation model from ERS-1 data even without ground control points (Chen and Dowman, 1996). Stereoscopic data from RADARSAT offer a great potential for radargrammetry, since RADARSAT is able to acquire fine resolution data with variable incidence angles (Dowman *et al.*, 1997). Dowman *et al.* (1997) pointed out that due to the less precise orbit and system parameters (compared to the ERS satellites), the use of ground control points for reconstructing the image geometry is required.

The radargrammetric technique is in operational use for a long time by various Canadian companies (Intera, Intermap etc.) mainly using airborne systems (e.g. Mercer *et al.*, 1994). Recently, the existing system for stereoscopic DEM extraction has been extended for the use of RADARSAT imagery (De Col *et al.*, 1997).

The first practical application of radarclinometry, also referred to as shape-from-shading, was published by Wildley (1984). He also presented the underlying mathematical theory of radarclinometry (Wildley, 1986). The basic principle of radarclinometry is adapted from photoclinometry which is based on the idea that the surface brightness is predictable by the photometric function for a given illumination considering the normal albedo of a terrain point. Using this relation between the geometry and the terrain, the inversion of the radiometric incidence angle correction enables an estimate of the local terrain slope given as the brightness of a pixel. The integration of the pixel values in range direction leads to a height profile of the terrain. By further integration in range and azimuth including filtering, a digital elevation model can be derived from a single SAR image.

#### **4.1.4 Stereoscopy using optical satellite imagery**

Since the first *SPOT* satellite was launched in February 1986, stereo pairs from SPOT PAN imagery with ten metres pixel size have been available on request using the viewing geometry shown in Figure 4-3.



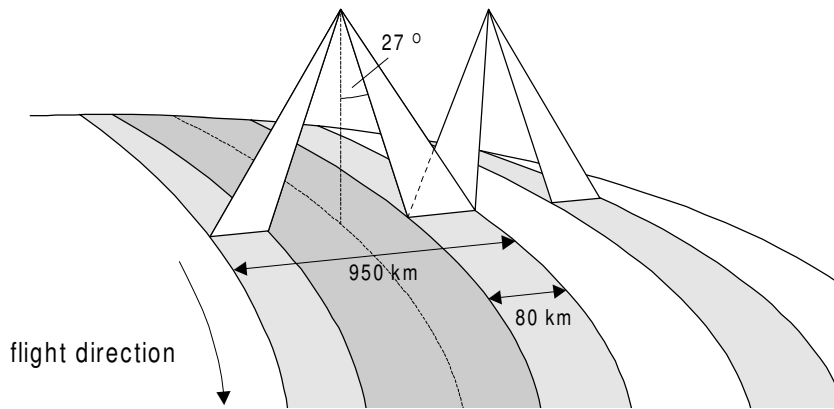


**Figure 4-3:** Stereoscopic viewing geometry of the SPOT satellite

There are two types of product which are suitable for the derivation of elevation models. For the radiometric correction of the Level 1A product only a detector normalisation is performed using a linear model, i.e. the difference in sensitivity between CCD detectors are equalised. Besides the radiometric correction, the Level 1B product is also geometrically corrected. These corrections consider systematic distortions such as panoramic effects, earth rotation and earth curvature effects, and the variation in orbital altitude with respect to the reference ellipsoid.

The geometrical model of a CCD line scanner such as SPOT has been clearly described by Toutin (1985). Konecny *et al.* (1987) evaluated the stereo capabilities of hardcopy SPOT Level 1A imagery by adapting the CCD line geometry to analytical instruments. They modified an existing bundle block adjustment program introducing additional parameters to account for non-uniform movements and the Earth rotation. The unknowns were approximated based on satellite orbital data. This approach is hardware independent and easy to implement as it is similar to the standard bundle block adjustment with central perspective projections. A list of publications about the development and the evaluation of algorithms for estimating elevations from SPOT was given by Sasowsky *et al.* (1992). Meanwhile, with the development of digital photogrammetry various automatic image matching techniques were available. The production and validation of digital elevation models from SPOT Level 1B imagery were evaluated by Al-Rousan *et al.* (1997). Their approach used a normal cross-correlation method for matching with sub-pixel accuracy. The results were particularly encouraging because the SPOT Level 1B stereo imagery is widely used by the geoscientific community (Al-Rousan *et al.*, 1997).

The *Modular Optoelectronic Multispectral Scanner (MOMS)*, a development from the Deutsche Aerospace AG (DASA), is another promising system for the generation of digital elevation models which is still in a pre-operational stage. It offers three different modes for the data acquisition, illustrated in Figure 4-4. In the along-track stereo mode a scene is recorded line by line with the forward, the nadir and the backward looking channels with a time offset of two times 20 seconds, i.e. almost simultaneously. Another mode allows multispectral imaging with four channels. Finally, both modes can be combined.

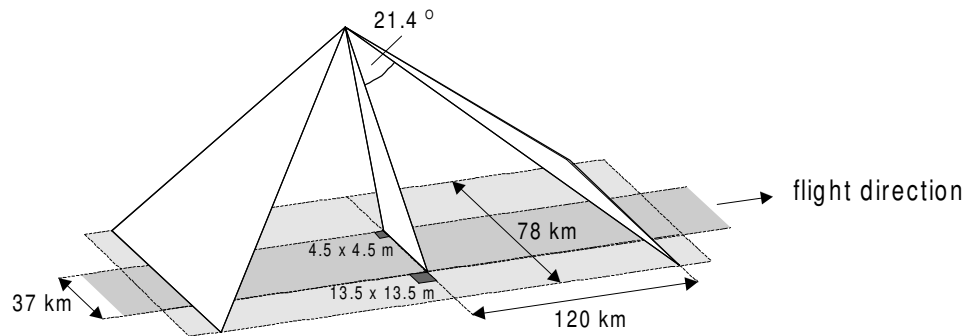


**Figure 4-4:** Along-track stereoscopic viewing geometry of the MOMS sensor

Ackermann *et al.* (1995) pointed out that the stereo acquisition in along-track direction has a significant advantage compared to the generally used two-pass scanning systems such as SPOT, since it allows quasi simultaneous data captures. This approach avoids any changes between the data acquisitions which could reduce the data quality. For the automatic mensuration process as many points as possible are measured to describe the terrain surface in the required detail. The shape of the surface is then reconstructed by finite element modelling. According to Ackermann *et al.* (1995), some aspects of the processing still need to be further investigated. One of the main tasks is the fusion of the high resolution nadir channel (4.5 m spatial resolution) and the two stereo channels (13.5 m spatial resolution). For high geometric precision the calibration of the camera system has to be improved. Finally, the strategies for identifying ground control and check points need to be further developed.

Apart from the SPOT satellite and MOMS sensor, there are other systems potentially suitable for stereoscopic viewing. The Indian Remote Sensing Satellite IRS-1C has a panchromatic sensor with 5.8 m pixel size. By using three separate CCD line sensors the scanner acquires data with a small overlapping area. The off-nadir viewing capability ( $\pm 26$  degrees across-track) can reduce the repeat cycle from 24 days to five days. First results of the stereoscopic use were presented by Jacobsen (1997). With the successful launch of IRS-1D in October 1997 another satellite with the same specifications is available to provide a larger number of suitable data sets.

#### 4.1.5 Laser scanning

The development of airborne laser systems, illustrated in Figure 4-5, started in the 1980s. This was technically possible with the achievements in the development of the fields of global positioning systems (GPS) and inertial navigation systems (INS). For a comprehensive introduction into laser altimetry, the reader is referred to Measures (1984). The laser scanner provides three kinds of measurements: (1) The laser range to the Earth's surface, (2) the spatial location and orientation of the platform and (3) the kinematic trajectory of the aircraft (Vaughan *et al.*, 1996).

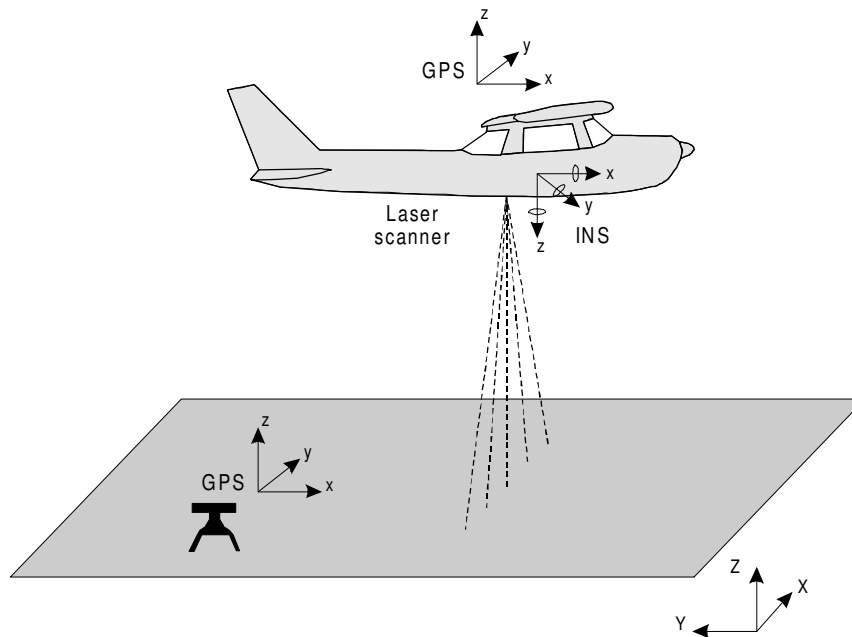


**Figure 4-5:** Data acquisition of a laser scanning system

For kinematic positioning the same GPS techniques are used as already described in section 4.1.2. One GPS receiver is deployed at a known position in the area to be measured. The other receiver is mounted on the aircraft together with a gyroscope for measuring the aircraft motion (Vaughan *et al.*, 1996). Laser scanner systems can also be implemented using a helicopter (Flood and Gutelius, 1997). These systems can achieve vertical accuracies in the order of 10-20 centimetres. The density of the laser measurements is high enough to provide return signals from different vegetation layers. This is used in forested areas to distinguish between the signals and to produce DEMs with reference to the ground surface and to the top canopy (Ackermann, 1996a).

The measurement of the laser range is affected by the travel time of the signal, which depends on the distance between the sensor and the surface, on the atmospheric refraction, and on the range dispersion within the size of the laser spot on the terrain surface. One potential error source of laser altimetry is the synchronisation of the laser, GPS and INS measurements in time.

Digital elevation models measured by laser scanners have the following main applications: measurements of coastal zones, forested areas and powerline locations (Flood and Gutelius, 1997). Furthermore, the high resolution laser measurements are the basis of city models (Ackermann, 1996a) and topographic maps in largely forested areas (Hoss, 1996).

The overall performance of a laser system can be optimised in time and automatism because all the necessary steps from the data acquisition to the final product are performed in a digital way. On the other hand, this measures only geometric information in form of co-ordinates. It does not provide any further object information. Ackermann (1996a) anticipated the integration of laser scanning data with photogrammetric image data to merge high resolution geometric information with optical image information. The number of commercially used laser systems is increasing and it is assumed that laser scanning will

be established on the market especially for difficult areas where the conventional methods have their limitations (Flood and Gutelius, 1997).

## 4.2 TECHNIQUES FOR QUALITY CONTROL

In the field of digital elevation modelling there is a trend from the development of interpolation techniques to the assessment and control of DEM quality (Li, 1994). The assessment found in the literature generally estimates the result but not the process of generation. The problem of quantitatively checking the performance of algorithms is difficult because of the dependence of the estimated surface on the morphology of the sample area which determines the relief of the terrain.

### 4.2.1 Theoretical background

The standards for the collection, processing and quality control of digital elevation data, proposed by the USGS (1997) recently, provide the theoretical background for the quality assessment of digital elevation models.

Any data sets, therefore also DEM data, contain three types of error. *Blunders* are large vertical errors usually exceeding the maximum error (3 sigma) and are caused by careless observations, misreading contours, transposing numeric values or erroneous correlations. *Systematic errors* are introduced by procedures and systems, and follow some fixed rule or pattern. They appear as bias or artefacts in the final DEM. These errors include vertical elevation shifts, fictitious features such as phantom tops, ridges or benches, and interpretation errors due to effects of buildings, shadows and trees. After the removal of blunders and systematic errors, the remaining distortions are caused by *random errors* (USGS, 1997). During processing, blunders must be removed. Systematic errors can be substantially reduced if not completely eliminated.

The vertical accuracy of a DEM is described by the vertical root mean square (rms) error (discussed in detail in subsection 4.2.2) which is computed from a minimum of 28 test points (USGS, 1997). These test points (20 interior points and eight edge points) should be well distributed and representative for the terrain. Ackermann (1996b) proposed the consideration of the slope accuracy or the variation accuracy as a function of slope, breakline effects etc. for a more precise description.

Before the calculated DEMs can be included into the National Digital Cartographic Data Base, the data sets need to be verified (USGS, 1997). The statistical accuracy, described by the rms error, is calculated for the required number of test points. The logical and physical format of the data is checked for consistency. Finally, a visual verification helps to identify blunders in the DEM.

Ackermann (1996b) pointed out that the quality of the software for the interpolation method needs to be considered. It is required that the software is able to consider breaklines and morphological features as well as to identify and delete outliers. Furthermore, the program should provide some figures about the accuracy and reliability of the calculated DEM (Ackermann, 1996b).

### 4.2.2 Quality measures

In order to assess the quality of digital elevation models, a suitable quality measure needs to be defined. A generally used quality measure for DEMs is the rms error  $\mu$  defined as follows (Grossmann, 1969):

$$\mu = \pm \sqrt{\frac{[\varepsilon\varepsilon]}{n}}, \quad (4-2)$$

with the true error  $\varepsilon$  and the number of points  $n$ . Ackermann (1996b) stated that the quality of a DEM covers, apart from the accuracy, also aspects such as completeness, reliability, consistency and uniformity of the accuracy distribution within the DEM.

A comprehensive study about spatial data quality has been initiated by the International Cartographic Association (ICA). The goal of the commission established by the ICA was to define seven elements to describe spatial data quality:

- lineage,
- positional accuracy,
- attribute accuracy,
- data completeness,
- logical consistency,
- semantic accuracy and
- temporal information.

An overview about the results is given by Morrison (1995).

The *lineage*, also referred to as metadata, contains the information about the data history, i.e. how the data sets were acquired, what kind of processing steps (conversions, transformations, analyses etc.) were performed and which assumptions and criteria were applied at various stages.

The major quality measure is still the *positional accuracy*. The root mean square error serves as a measure of overall accuracy and the standard deviation as a measure of precision. Furthermore, the maximum error serves as an additional indicator for the quality of a data set. The definition of the features has a large influence on the positional accuracy. A well defined feature has a higher accuracy than a less well defined feature.

The third element proposed by the commission was the *attribute accuracy*. An attribute defines a fact about some location or feature and helps to distinguish between them.

The *data completeness* describes an error of omission which is a measurable component of the data quality. This needs to be distinguished from the model completeness which is an aspect of the fitness of use.

The *logical consistency* deals with structural integrity of the data and describes the fidelity of relationships within this structure.

The *semantic accuracy* represents the number of features, relationships or attributes which agree with the selected model.

Finally, the temporal aspect of the data quality about the acquisition date, the type of update and the validity period of the data set is stored as *temporal information*.

As mentioned previously, Ackermann (1996b) proposed a more detailed quality measure using the slope accuracy or the variation of vertical accuracy as a function of slope, breakline effects etc. This refers to the derivatives of the height which are more sensitive to changes than the height. The definition of the first two derivatives of the altitude surface (slope and convexity) can be found in Evans (1980). A plane tangent to the terrain surface at a point defines the slope which has two components. The *slope gradient* is the maximum rate of change of altitude whereas the *slope aspect* gives the compass direction of this maximum. These components are measured in the range of 0-90 degrees and 0-360 degrees, respectively. The convexity is defined as the rate of change of slope and is measured in degrees per 100 metres. It can be split up in the two components viz. *profile convexity*, the rate of change of gradient, and *plan convexity*, the rate of change of aspect (Evans, 1980). The slope gradient and aspect can be calculated in several ways. According to a comparative study of these methods by Skidmore (1989), the third-order finite difference method proposed by Horn (1981) appeared to be optimal for the calculation of slope gradient and aspect from a gridded DEM.

There are only a few publications on quality assessment of DEM derivatives. Sasowsky *et al.* (1992) tested the accuracy of slope gradient and aspect derived from a SPOT DEM by comparing it with two reference DEMs. The greatest slope gradient error occurred in areas with steep slopes where the elevation accuracy is the poorest. These results were confirmed by the study carried out by Bolstad and Stowe (1994). They evaluated the accuracy of the elevation, the slope gradient and aspect of a DEM based on stereoscopic SPOT imagery by using field measurements. Bolstad and Stowe (1994) pointed out the importance of the quality assessment of derived DEM products since errors in the input data will propagate through the spatial analysis. Giles and Franklin (1996) assessed also the quality of the second-order derivatives of a SPOT DEM. The effect of errors in elevation on the local neighbourhood increases with each higher order of derivative. The quality, especially of the higher derivatives, is generally difficult to estimate due to a lack of suitable reference data. Therefore, the correlation between the derived value and the actual landscape needs to be considered by the user (Giles and Franklin, 1996). The investigation showed that a better correlation between DEM and field measurements for the slope gradient can be achieved by filtering the elevation model.

### 4.2.3 Ground control points

One way to assess the quality of a digital elevation model is performed by using ground control points (GCPs). This approach is also a part of the standards for DEMs proposed by the United States Geological Survey (USGS, 1997). As mentioned earlier, before a DEM is included in the National Digital Cartographic Data Base (NDCDB), a minimum of 28 points (20 interior and eight edge points) needs to be measured to determine the root mean square (rms) error. The accuracy is computed by comparison of linear interpolated DEM elevations with the corresponding known elevations. In order to be suitable for this single test, the test points have to fulfil the following requirements. They should be well distributed and representative for the terrain. Their accuracy has to be well within the DEM accuracy.

The USGS (1997) gave a list for the order of preference for accepting test points from the following sources: field control, aerotriangulated test points, SPOT elevations, or contour points from maps with appropriate contour interval.

Adkins and Merry (1994) evaluated the accuracy of digital elevation model and topographic maps of different scales by GPS measurements of nineteen road intersections. The relative errors for all tested models and maps were within the acceptable margins, whereas the absolute error of one model exceeded this margin, most likely due to errors in the process of the conversion between different height systems.

#### 4.2.4 Reference DEMs

The use of reference DEMs for the quality assessment of digital elevation models is still a standard approach since it provides the possibility of comparing the complete DEM with a reference. The availability of such a reference DEM, especially considering that it should be, from the statistical point of view, at least one order better than the DEM to be evaluated, significantly reduces the number of suitable reference data sets. DEMs from different sources such as laser altimetry (Joughin *et al.*, 1996a), stereoscopic SPOT imagery (Renouard *et al.*, 1995), digitised contour lines (Schwäbisch *et al.*, 1996) etc. were used for this purpose.

Apart from the assessment of the quality, the comparison with another digital elevation model also gives more insight into other characteristics. The study of Renouard *et al.* (1995), for example, confirmed that interferometric DEMs are very sensitive to terrain slopes perpendicular to the flight direction. Furthermore, the visibility of certain details in ERS DEMs and SPOT DEMs was different due to layover effects in the ERS DEM caused by steep slopes. Schwäbisch *et al.* (1996) showed the loss of coherence of hilly slopes covered by forest.

#### 4.2.5 User requirements

All efforts spent on the development of reliable and accurate procedures to create digital elevation models are not effective if the requirements and needs of the user are not met. Producing a digital elevation model with certain specifications in terms of accuracy, grid size, data volume etc. implies already the decision about the usability for a specific application. Therefore, the question about who is going to use the product and for what kind of application should be taken into account if it comes to the point of defining suitable specifications. These considerations have their impact on the quality estimation of digital elevation models. The quality estimation procedure should provide quality measures which allow the user to decide in a simple way whether the DEM is suitable for his particular application or not.

Burrough (1986) presented a list of products that can be derived from DEMs, given in Table 4-1. It clearly shows the large variety of products which can be used for various purposes. On the other hand, it highlights the problem of having different expectations a user might have in a digital elevation model in terms of accuracy, grid size etc. A cartographer will be less critical about the quality of a DEM for his improved map visualisation than a civil engineer whose volume estimate is required for accurate costing.

With an ever increasing number of digital elevation models becoming available on the market and with an increasing number of applications, the awareness of the data quality problem has grown, but the number of studies carried out especially on the quantitative quality analysis of DEM based products is still limited. As stated by Ackermann (1996b), no standard procedure for this kind of assessment as well as generally accepted specifications about the accuracy of DEMs, e.g. in relation to the type of terrain or to the grid size, do not exist.

Products	Application	Example of potential usage
<b>Block diagram, profiles and horizons</b>	Landscape design	- displaying many kinds of landscape information - showing the variation of the value of a quantitative variable
<b>Volume estimation by numerical integration</b>	Civil engineering	- estimate the volume of material needed to be removed or to be brought in
<b>Contour maps</b>	Cartography	- simple environmental mapping
<b>Line of sight maps</b>	Military Communication	- determine the intervisibility of points in the landscape - network planning
<b>Maps of slope, convexity, concavity and aspect</b>	Geomorphology	- describing and comparing terrain
<b>Shaded relief maps</b>	Cartography	- improving visual qualities of maps - quantitative landform analysis
<b>Drainage network and drainage basing delineation</b>	Hydrology	- detecting ridges and stream lines - determining the boundary of a catchment

**Table 4-1:** Products derived from digital elevation models, their applications and usage (modified from Burrough, 1986)

In the field of hydrology, a few results of studies about the influence of errors in the DEM and the grid size on hydrological modelling were presented. Lagacherie *et al.* (1996) evaluated how errors in the digital elevation model propagate to inputs for hydrological models (the delineation of the subcatchments of each of the nodes of the manmade drainage network, the determination of the slope of the reaches of these drainage networks, and the determination of the mean slope of each subcatchment). The results showed that the quality of a DEM cannot be determined by a single criterion and that the estimation of DEM quality is highly use-specific. Lee and Chu (1996) analysed the impact of potential errors on extracted drainage networks from DEMs by applying simulated random errors of various magnitudes to the digital elevation model. They pointed out that the extracted hydrological features showed a very large sensitivity to potential errors in the DEM and concluded that DEM data should be used with careful consideration regarding their accuracy. Zhang and Montgomery (1994) examined the effect of the DEM grid size on the representation of the land surface and hydrological simulations and reported a lack of systematic studies in this field. Their study confirmed that the grid size of a DEM significantly affects the representation of the land surface as well as the deduced hydrological simulations. Furthermore, they stressed that a reliable representation of the



land surface also depends on the accuracy and the distribution of the original survey for the DEM. Zhang and Montgomery (1994) suggested a grid size of ten metres as sufficient for many applications of geomorphological and hydrological modelling based on digital elevation models.

The above mentioned studies indicate that the users of digital elevation models are becoming much more aware of the data quality problem. It also shows that there is still a lack of specific requirements for DEMs from the user's side about the accuracy level needed for their application, since digital elevation models are often created for general use and not for a specific application. A large number of parameters can be derived from DEMs for various purposes, at different scales and with different accuracy levels. Therefore, it is difficult to find a general quality measure which suits most of the potential applications. As already pointed out by Lagacherie *et al.* (1996), the DEM quality cannot be determined by a single criterion. It cannot include any information about the density and spatial distribution of the observations and how correct and detailed the surface is represented. The quality measure should be user or application oriented. The quality of the height derivatives, the slope with the components gradient and aspect as well as profile and plan convexity, introduced in subsection 4.2.2, which are even directly used by some applications (e.g. geomorphology), could be used for this purpose.

Another aspect that needs to be considered is the level at which the quality measure should be provided. As mentioned before, a single value for a whole DEM is certainly not sufficient. A quality measure at the pixel level would be ideal but causes some practical problems. The "quality DEM" containing the quality measure for each corresponding pixel in the digital elevation model would have at least the same size as the "original DEM". This storage problem could be solved by choosing a larger grid size. The calculation of a quality DEM of this size needs to be based on a functional error model. An implementation using a numerical error propagation approach, as proposed in this study, is not possible due to time constraints for the necessary processing. A compromise between the most accurate information possible and a suitable practical implementation is required.

The user might be interested in certain features in the DEM (e.g. a catchment with a clearly defined boundary). The definition of such features for the quality assessment during the production of the digital elevation model is only possible if the application for which the DEM is used as basis is known. Furthermore, the features of interest will also vary in scale depending on the type of study carried out with the data set. Therefore, the areas for which a quality measure is calculated have to be representative for the whole digital elevation model. Mapping units e.g. land use classes could be used to identify representative areas. The definition of these mapping units will differ from application to application, so that there is no general and objective way to define these areas independent from their application and the scale of study. An area can be described in many different ways depending on the perspective and need. Geological parameters can be used for identifying the site on the basis types of rock exposures, geological structures etc. In geomorphological terms, areas can be separated in features such as rivers, mountains, slopes, terrain etc. They can also be distinguished in several land use categories. All the classifications are generally visually assessed. The statistical measures are hardly representative of areas with such mixed signatures or categories.

### **4.3 PROPOSED METHOD**

The method proposed for quality assessment in this study takes into consideration all the user requirements and other aspects discussed earlier.

The quality of an interferometric product is a result of a number of processing steps. Since the quality of the result depends on the performance of the various processing steps which can be influenced by choosing different approaches and algorithms. Care has been taken to evaluate each single processing step during the quality assessment. In order to avoid the problems related to the accuracy and availability of suitable reference data sets, the method has been designed to be independent of any reference. The aim has been to provide a quality measure at a suitable level, ideally at the pixel level.

In this study an error propagation approach has been proposed which provides a quality measure for each single processing step. Furthermore, it allows an estimation of the loss of quality caused by introducing any assumptions or simplifications into the processing algorithm. Since the knowledge about the exact implementation of the different processing steps in the various software packages is very limited, an empirical approach for the error propagation has been chosen. This does not require any knowledge about the derivatives of the mathematical function of the calculation algorithms involved. The resulting quality measure is theoretically given at the pixel level. Using this approach, the method can be easily adapted for the quality assessment using another software package. To reduce the required processing time, however, this quality assessment has been done only for a small, selected area (about 512 x 512 pixels).

The factors influencing the interferometric processing such as the choice of data sets, the sensitivity of input parameters and the processing algorithms are studied in the next chapter. The theoretical background of the error propagation approach and the practical implementation of this method is described in more detail in chapter 6.

## 5 FACTORS INFLUENCING THE INTERFEROMETRIC PROCESSING

---

There are basically three sources affecting the quality of SAR interferometric products on which the user has a certain influence. His data selection already determines the suitability for different applications. By choosing a software package the input parameters which are used during the processing are determined. The sensitivity of these input parameters is an important aspect. Finally, the choice of the available algorithms, usually a compromise between the most accurate and the fastest, has a major impact on the quality of the final interferometric product. These three aspects are analysed and discussed in detail in this chapter.

### 5.1 CHOICE OF DATA SETS

The choice of suitable data sets for interferometric processing has a significant influence on the final result. For hazard monitoring, for example, the data sets have to be acquired at a certain time, preferably as close as possible to the event and with the minimum time difference to avoid any other disturbances in the data set. The sensor transmits signals of a certain wavelength and polarisation in a given viewing geometry (satellite height, look angle, baseline etc.). Therefore, the characteristics of the radar sensor and the data sets determine the suitability of the imagery for a certain application.

The use of precise orbit parameters causes a shift in phase (shown in Figure 5-1) in the interferogram but does not improve the geometry to an extent that significantly more details are visible. Furthermore, no improvement has been achieved by introducing more than five precise orbit state vectors. The difference of the interferograms (depicted in Figure 5-2) confirms this observation.

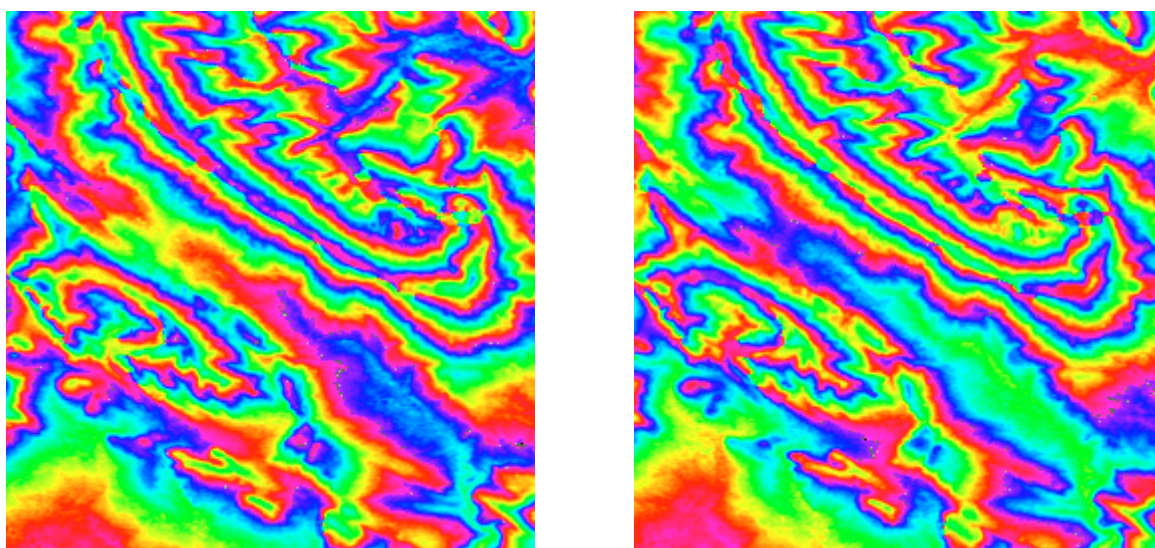


**Figure 5-1:** *Interferograms calculated with non-precise (left) and precise orbit state vectors (right). It shows a general shift in phase. There are no significantly more topographic details visible.*

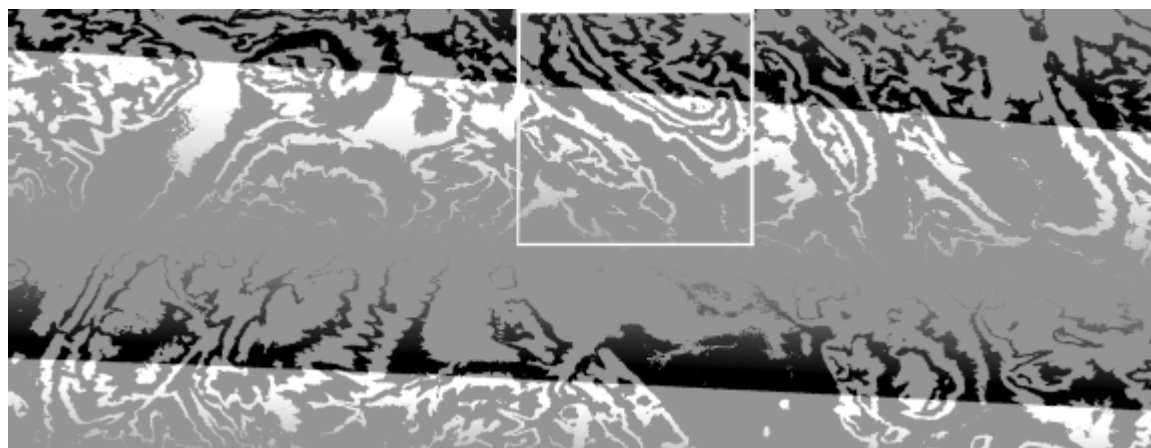


**Figure 5-2:** *Difference interferogram. This figure is derived from the difference between an interferogram calculated with five precise orbit state vectors and an interferogram calculated with five non-precise orbit state vectors. The box indicates the area shown in Figure 5-1.*

The data sets are affected by two types of decorrelation: the baseline decorrelation and the temporal decorrelation. The length of the baseline indicates the sensitivity to height changes (cf. Table 2-1) and the amount of baseline decorrelation. The difference in time between the two data acquisitions is the second source of decorrelation in the data sets. Both sources of decorrelation occur in the imagery. The differences while comparing data sets with a similar baseline length acquired one and 35 days apart tend to indicate only the temporal component of the decorrelation. The loss of coherence in data sets with the same repeat cycle in data acquisition are most likely due to baseline decorrelation. However, despite these indications it is not possible to distinguish between these two effects.

## 5.2 SENSITIVITY OF INPUT PARAMETERS

The error propagation model, described in more detail in chapter 6, is used to investigate two aspects of the interferometric processing, namely, the sensitivity of the processing to changes and the quality estimation of the processed result. A change in any input parameter causes a change in the processing result. The sensitivity study provides the means to estimate the magnitude of a change in the result caused by a slight alteration in an input parameter. It also indicates trends caused by the change in the input parameters which might need to be accounted for in a further development of the algorithms. The error propagation model gives the opportunity to evaluate different algorithms used for carrying out the same processing step. It can give an idea about the computational efficiency of different implementations of the same algorithms and allows the comparison of different algorithms for the same purpose.

The sensitivity study was carried out using ERS data sets from an area in Groningen, the Netherlands (for details see Table 5-2). This area was chosen because it meets all the necessary requirements to serve as an ideal calibration site. The selected area is basically flat so that the influence of any topography in form of slopes etc. is negligible. Furthermore, the density of the vegetation is low since the area is mainly used for agricultural purposes. This ensures that the received signals are backscattered from the same vegetation level and volume scattering does not have to be considered.

	Data sets	
<b>Test site</b>	Groningen, the Netherlands	
<b>Images</b>	Sensors	Data acquisition
Master image	ERS-1	19-Aug-95
Slave image	ERS-2	20-Aug-95
<b>Subset</b>	Row	Column
Upper left corner	3000	700
Bottom right corner	6000	1300

**Table 5-2:** Data sets used for the sensitivity study

The sensitivity study has been carried out following the processing scheme as illustrated in Figure 5-3. The interferometric processing is performed once with unchanged parameters to obtain an interferogram as the original processing result. In the next step, the interferogram is calculated with changed input parameters. For each input parameter a suitable range of change was chosen which led to a number of processing results. The difference image between the changed and original processing was then further evaluated.

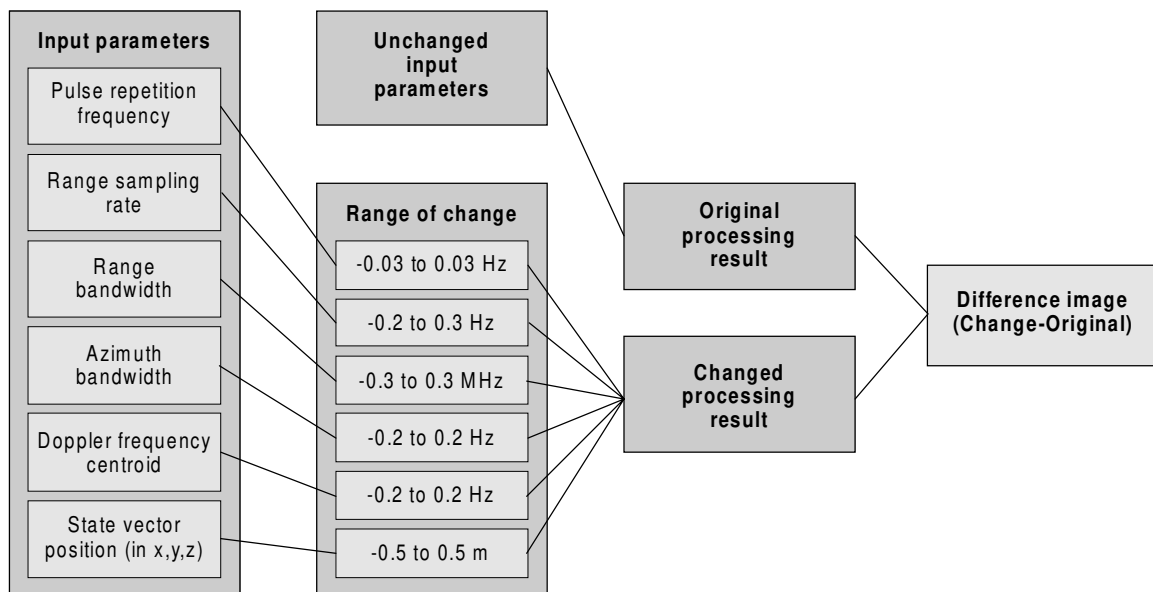


**Figure 5-3:** Processing scheme of the sensitivity study

16 randomly distributed points were selected for the sensitivity study (Figure 5-4). The points had a phase value of about zero in the original interferogram in order to ensure that the results with changed input parameters are in the same phase cycle assuming that the change is not larger than  $\pm \pi$ . For these points, the values in the various difference images were measured. These measurements served as the basis for the sensitivity curves presented later in this chapter.

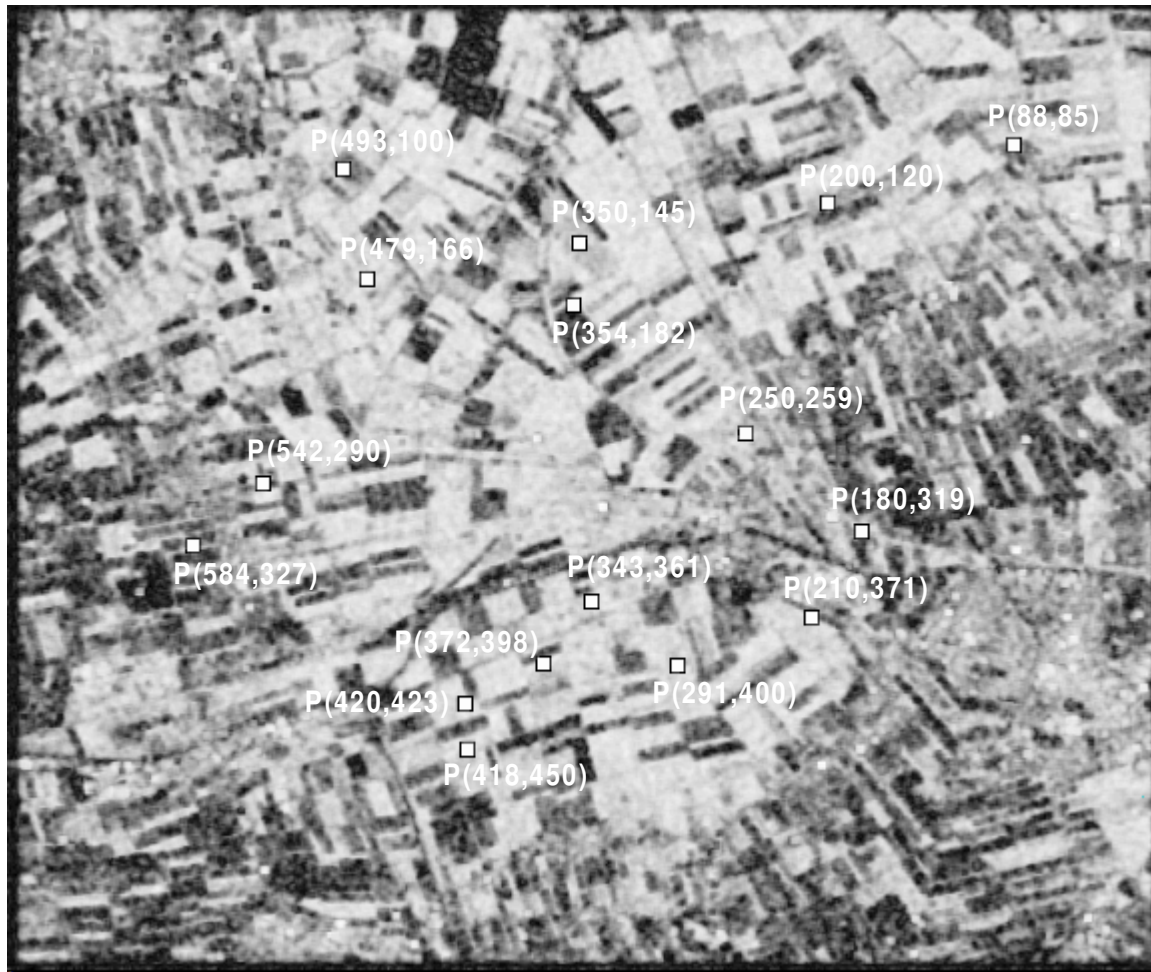


**Figure 5-4:** Location of the 16 points used for the sensitivity study on the coherence image. These points were randomly selected taking care that the values in the original interferogram were about zero in order to avoid phase cycle shift caused by the changed output.

### 5.2.1 Input parameters

The radar sensor transmits signals with a fixed rate per time interval referred to as *pulse repetition frequency* (PRF). Together with the *range sampling rate* the PRF determines the sample spacing in azimuth and range direction.

The *range* and *azimuth bandwidths* are fundamental parameters in the stage of forming a radar image since they determine the resolution of the radar image. For the interferometric processing they are of minor importance. In the Atlantis software the range and azimuth bandwidth are used for the calculation of the range and azimuth filtering as well as for the assessment of the quality of the co-registration since they give information about the resolution in range and azimuth direction (Armour, Atlantis Scientific Inc., personal communication, 1997).

Points in a radar image have no positional meaning as they do in optical imagery since they depend on the measured distance between the sensor and the imaged surface point which is in fact a function of time. Therefore, the pixels in a radar image are given in reference to

a time, in case of the ERS satellite data, in a zero-Doppler projection. The central parameter for this system is the *Doppler centroid frequency* which represents the Doppler frequency at the beam centre time.

The orbit of the satellite is described in the leader file by the position and velocity of a number of *state vectors* (in case of the ERS satellite data, five state vectors are given). However, for a reliable co-registration precise orbit vectors are a prerequisite. This information is maintained by a number of institutions such as the European Space Research Institute (ESRIN) via the DLR in Germany, the Delft Institute for Earth-Oriented Space Research (DEOS) in the Netherlands or the Center of Space Research (CSR) of the University of Texas at Austin, Texas.

### 5.2.2 Sensitivity study

For the comparison of results obtained from processing with changed input parameters, a reference interferogram with unchanged parameters was required. This original interferogram, illustrated in Figure 5-5, shows a typical fringe pattern for very flat areas. The height difference is too low to produce several countable fringes. The original coherence image (Figure 5-6) shows generally a good correlation in agricultural fields. The coherence level of the settlements is slightly lower.

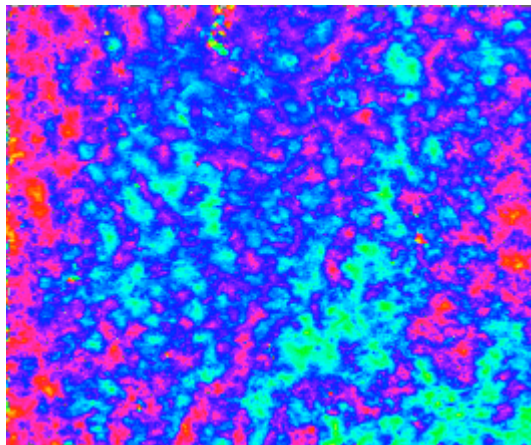


**Figure 5-5:** *Original interferogram*

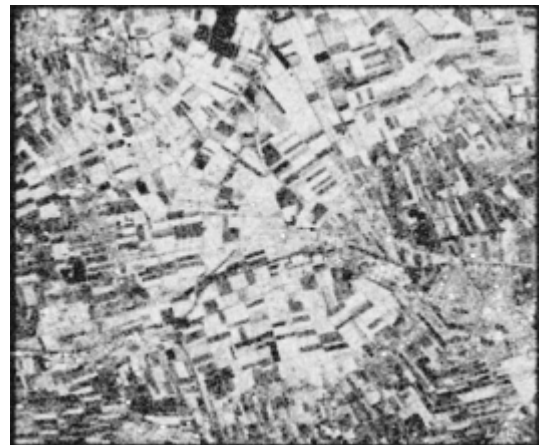


**Figure 5-6:** *Original coherence image*

The actual phase values in the interferograms had to be calculated using the arc tangent function since the file was stored in complex form. The range of the phase values should theoretically cover the full range of  $-\pi$  to  $\pi$ . Due to the fact that the arc tangent function is not well defined at the range margins, the calculation introduced some uncertainties which are visible in the difference images.

The graphs in the following figures show the relation between a change in an input parameter and a change in the resulting interferogram. The continuous graphs exclude the zero value for the change in the input parameter since there is obviously no change in the resulting interferogram if there is no change in an input parameter.

### Pulse repetition frequency

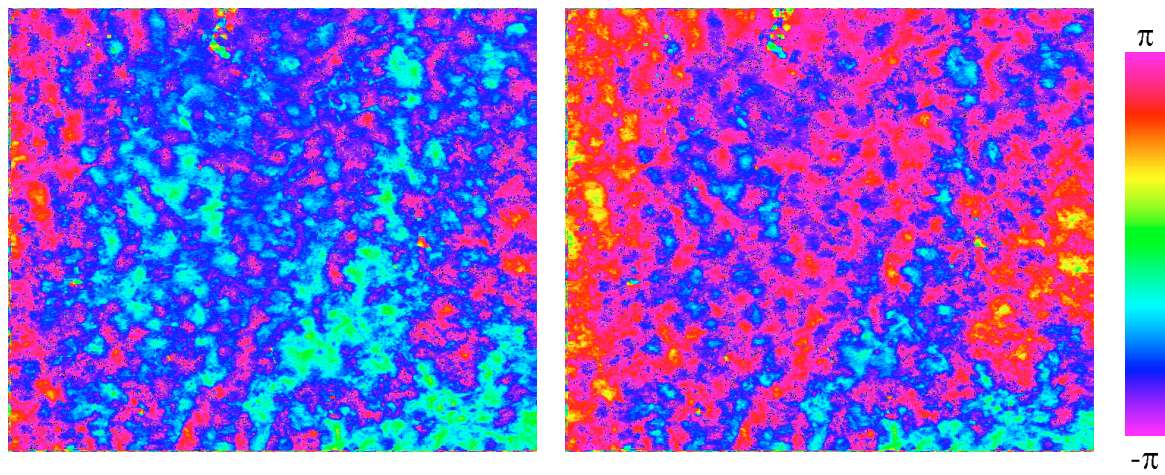


**Figure 5-7:** Original interferogram (left) and interferogram with a change of  $-0.01$  Hz in the pulse repetition frequency (right)

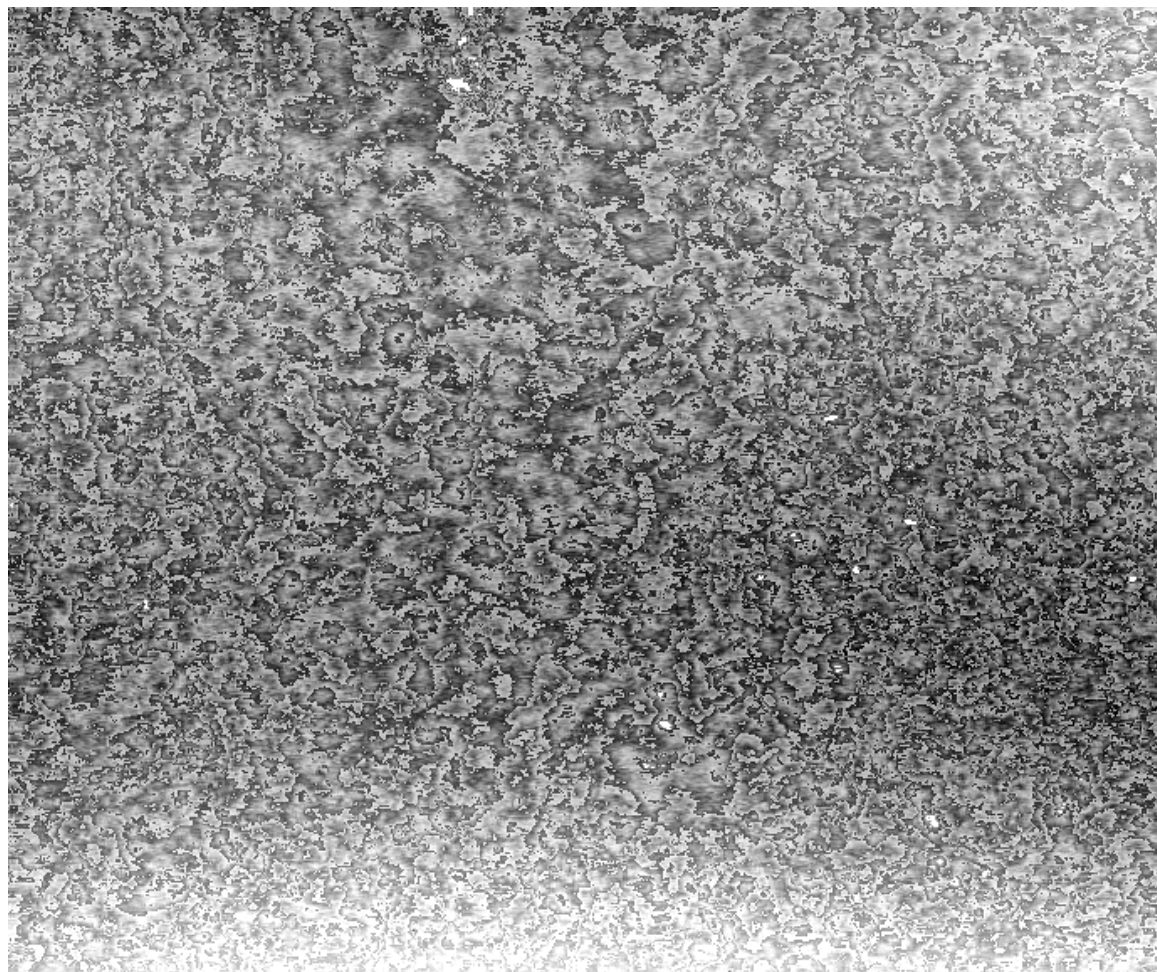


**Figure 5-8:** Difference image (PRF changed by  $-0.01$  Hz minus original)



The change in the fringe pattern between the original and the changed interferogram (Figure 5-7) is clearly visible. The shape of the fringes basically remains similar. A part of the fringes has shifted to another phase cycle.

The difference image (Figure 5-8) shows a pattern which is related to the distribution of the fringes. A second trend in the vertical direction is creating different brightness levels from a medium brightness at the top of the image to a lower level in the middle and finally to a bright level at the bottom of the image.

The impact of a change in the pulse repetition frequency (PRF), illustrated in Figure 5-9, clearly shows that the interferometric processing cannot account for changes in the PRF of any magnitude. The change in the interferogram given in radians indicates the shift in phase for the positions of the sixteen randomly selected points caused by a change in the PRF. All selected points have basically the same values with respect to the change in input but the graph does not have a clear trend which could be removed by a specific processing step. Considering the fact that the pulse repetition frequency is often given as a nominal value in ERS leader files, this input parameter has to be considered as critical. The PRF value, which can be calculated using the zero-Doppler azimuth times and number of lines of the specific data set, generally differs significantly from the given value.

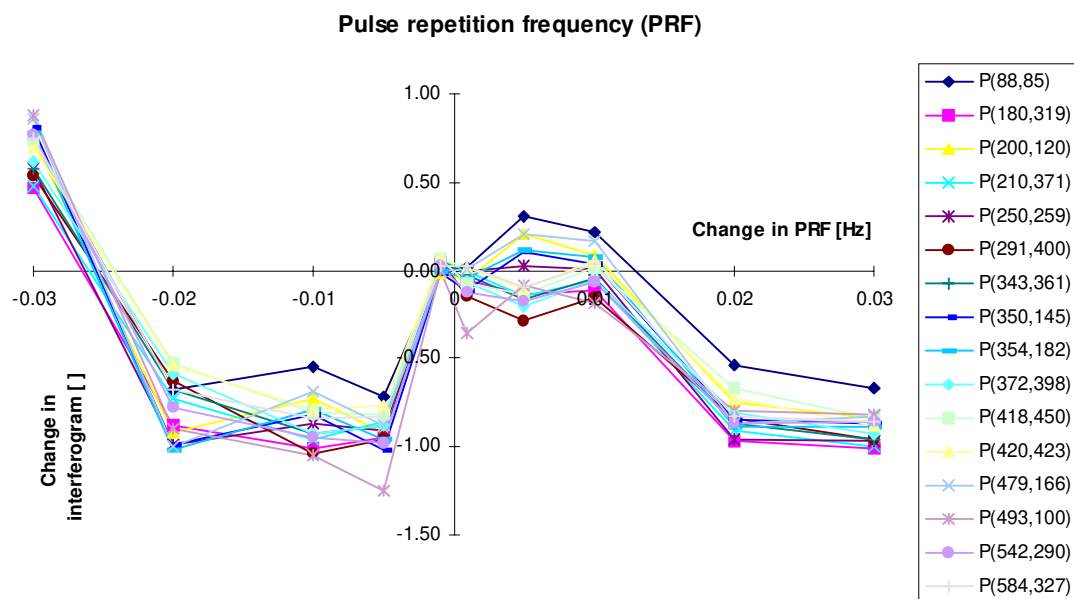


**Figure 5-9:** Graph showing the relation between a change in the pulse repetition frequency and the change in the resulting interferogram. The change in the interferogram is given in radians and indicates the shift in the phase values at the position of the sixteen randomly selected points in case of any change.

### Range sampling rate

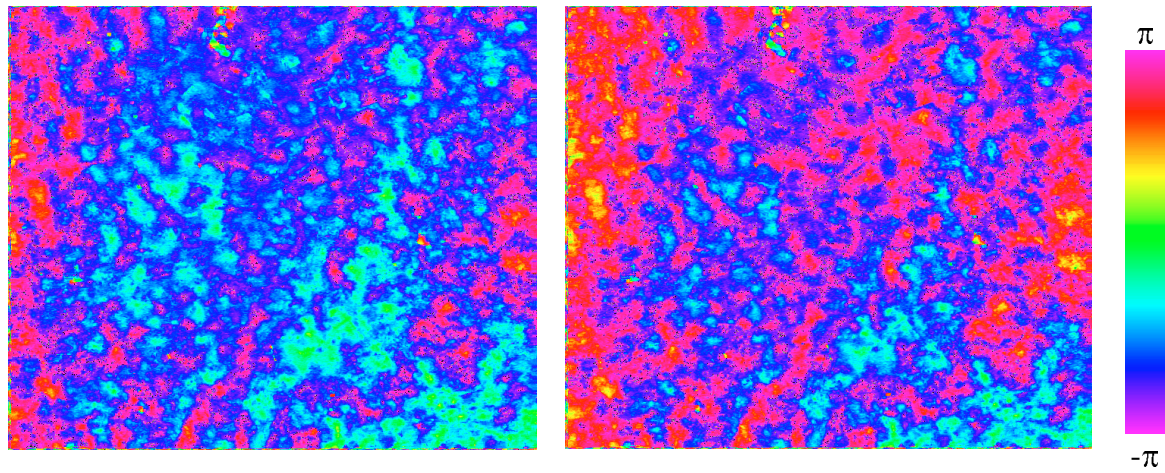


**Figure 5-10:** Original interferogram (left) and interferogram with a change of 0.1 Hz in the range sampling rate (right)

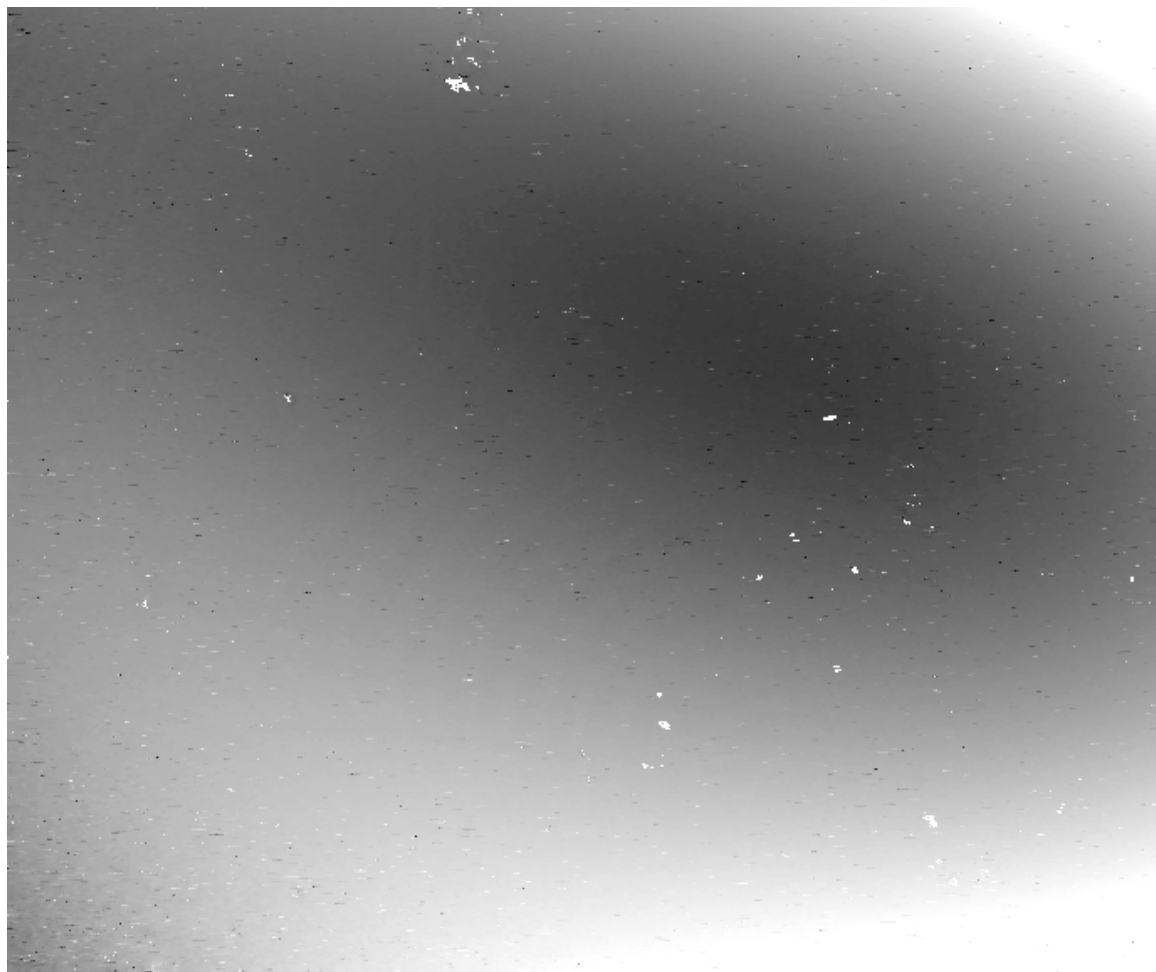


**Figure 5-11:** Difference image (Range sampling rate changed by 0.1 Hz minus original)

The shape of the resulting fringes in the changed interferogram (Figure 5-10) looks very similar to the interferogram with a change in the pulse repetition frequency.

The difference image (Figure 5-11) shows homogeneous changes in an elliptical shape. The centre of these elliptical patterns is slightly shifted from the middle to the upper right direction.

The influence of a change in the range sampling rate on the resulting interferogram, shown in Figure 5-12, is comparable to the influence of a change in the pulse repetition frequency, although the impact is smaller. It passes the interferometric processing without being corrected in any way. The small amount of resulting change and the fact that the range sampling rate can be considered as relatively stable lets this factor appear as being less critical for the propagation of large errors. However, the range resampling rate appeared to be very sensitive to larger changes. The algorithm has problems to perform the surface fit during the automatic matching for the co-registration. An increased number of patches is supposed to solve this problem but it does not lead to any acceptable processing result.

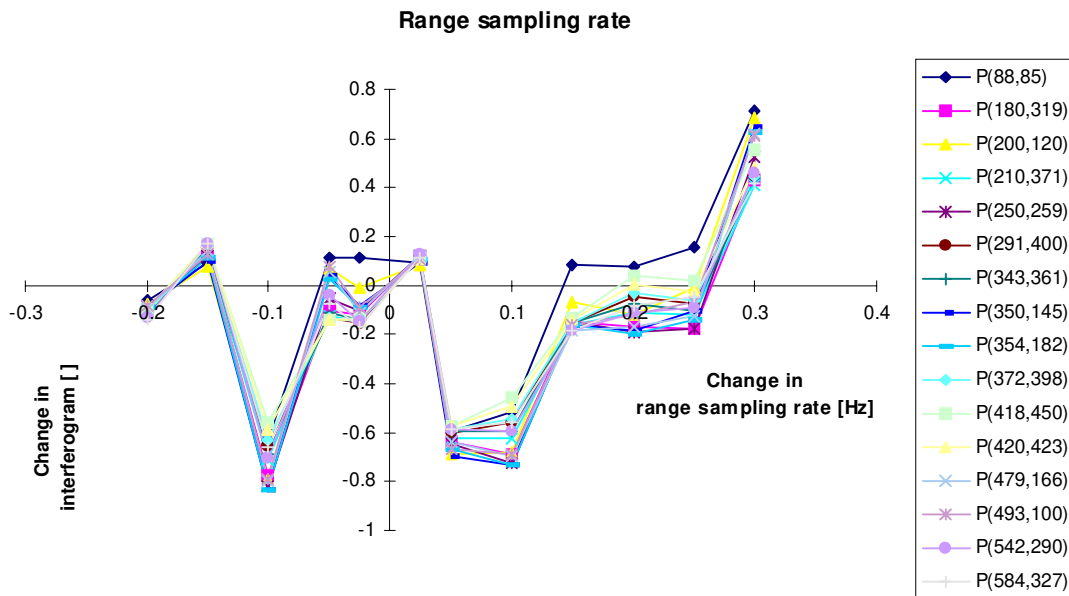


**Figure 5-12:** Graph showing the relation between a change in the range sampling rate and the change in the resulting interferogram

## Range bandwidth

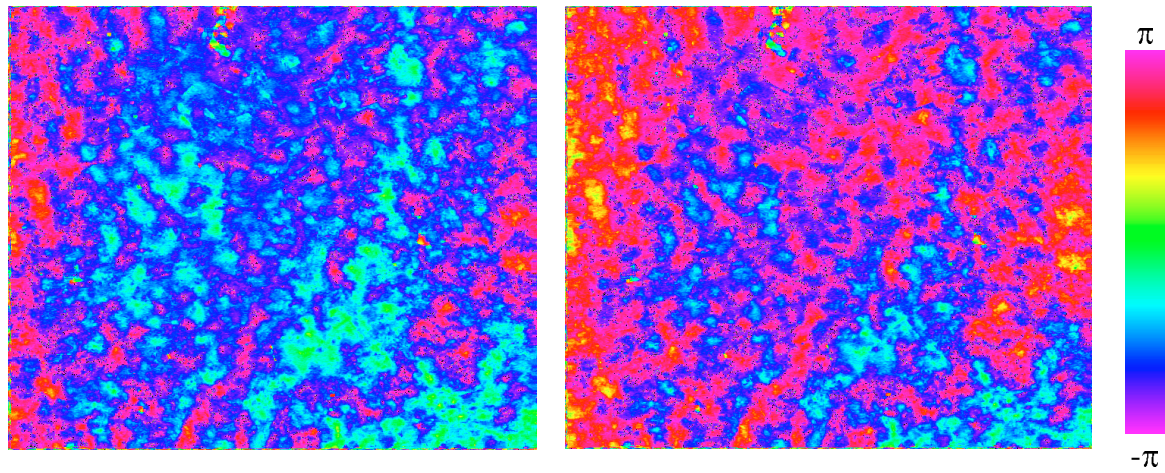


**Figure 5-13:** Original interferogram (left) and interferogram with a change of 0.005 MHz in the range bandwidth (right)

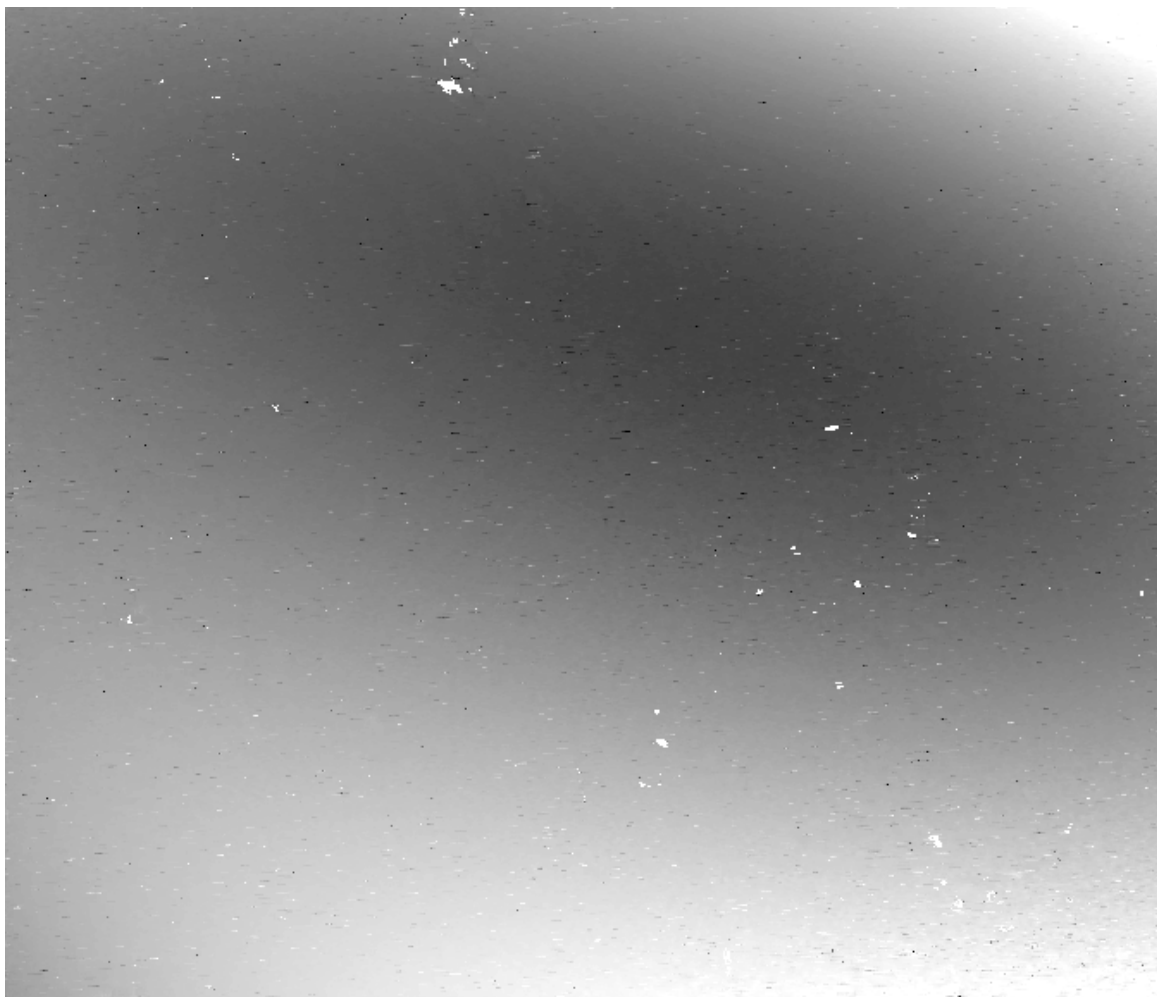


**Figure 5-14:** Difference image (Range bandwidth changed by 0.005 MHz minus original)

As mentioned before, the range bandwidth is used in the Atlantis software to calculate the characteristics for the filtering applied before the interferogram generation. The small change of 0.005 MHz in the range bandwidth results in an interferogram (Figure 5-13) similar to the ones shown before.

The difference image (Figure 5-14) also appears similar to the one from the range sampling rate with a comparable distribution and homogeneity in the change.

Small changes in the input value result in a change in the interferogram which is almost constant (Figure 5-15). The amount of change varies from point to point. It can be assumed that this effect depends on the varying backscatter due to different surface characteristics. The different graphs are symmetric, i.e. the sign of the change is not relevant for the impact. If the change in the input value exceeds a certain threshold the software accounts for it and changes the characteristics for the filtering. Therefore, the range bandwidth does not appear to be a critical input parameter for interferometric processing.

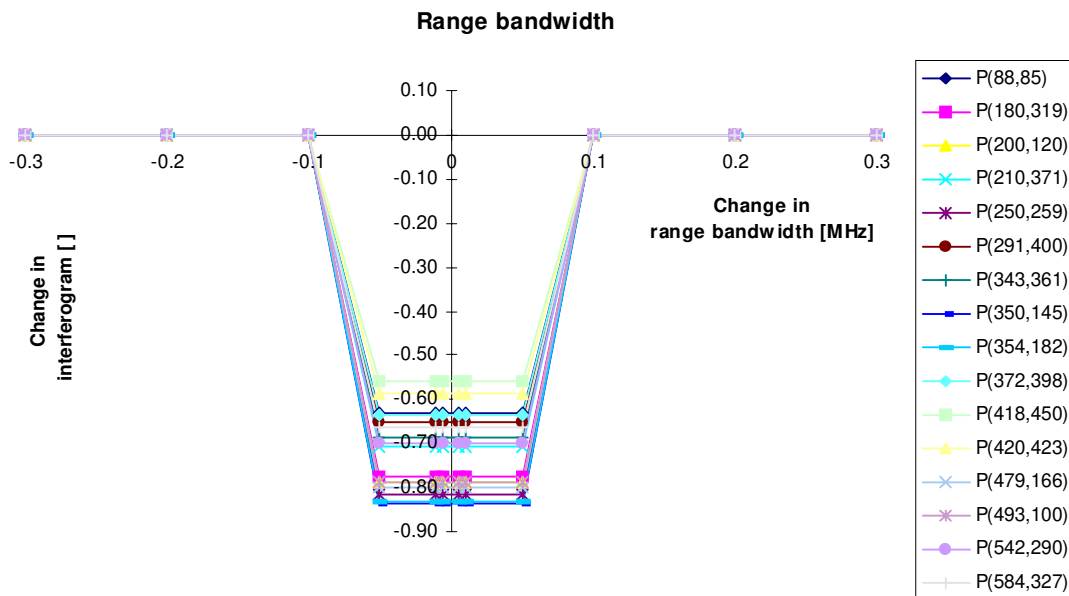


**Figure 5-15:** Graph showing the relation between a change in the range bandwidth and the change in the resulting interferogram

### Azimuth bandwidth

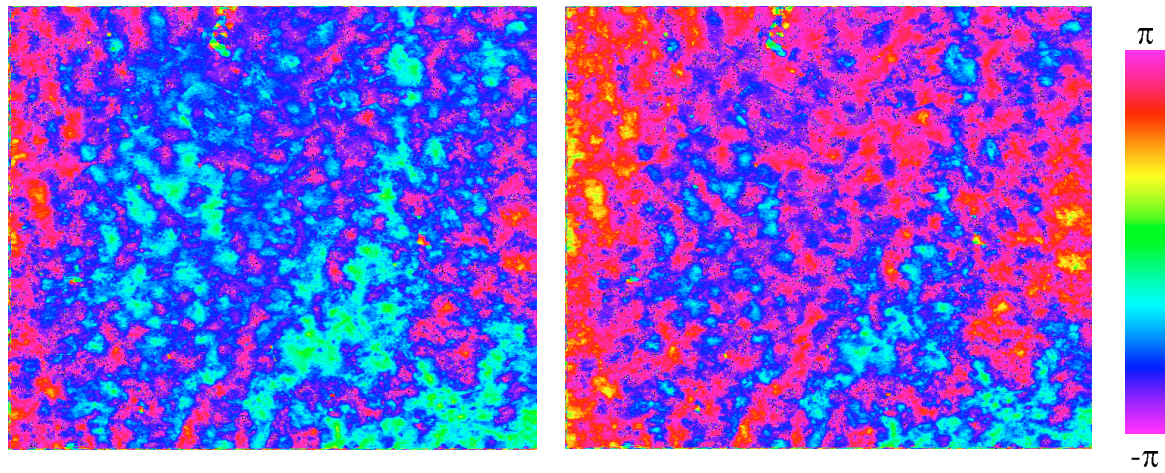


**Figure 5-16:** Original interferogram (left) and interferogram with a change of 0.01 Hz in the azimuth bandwidth (right)

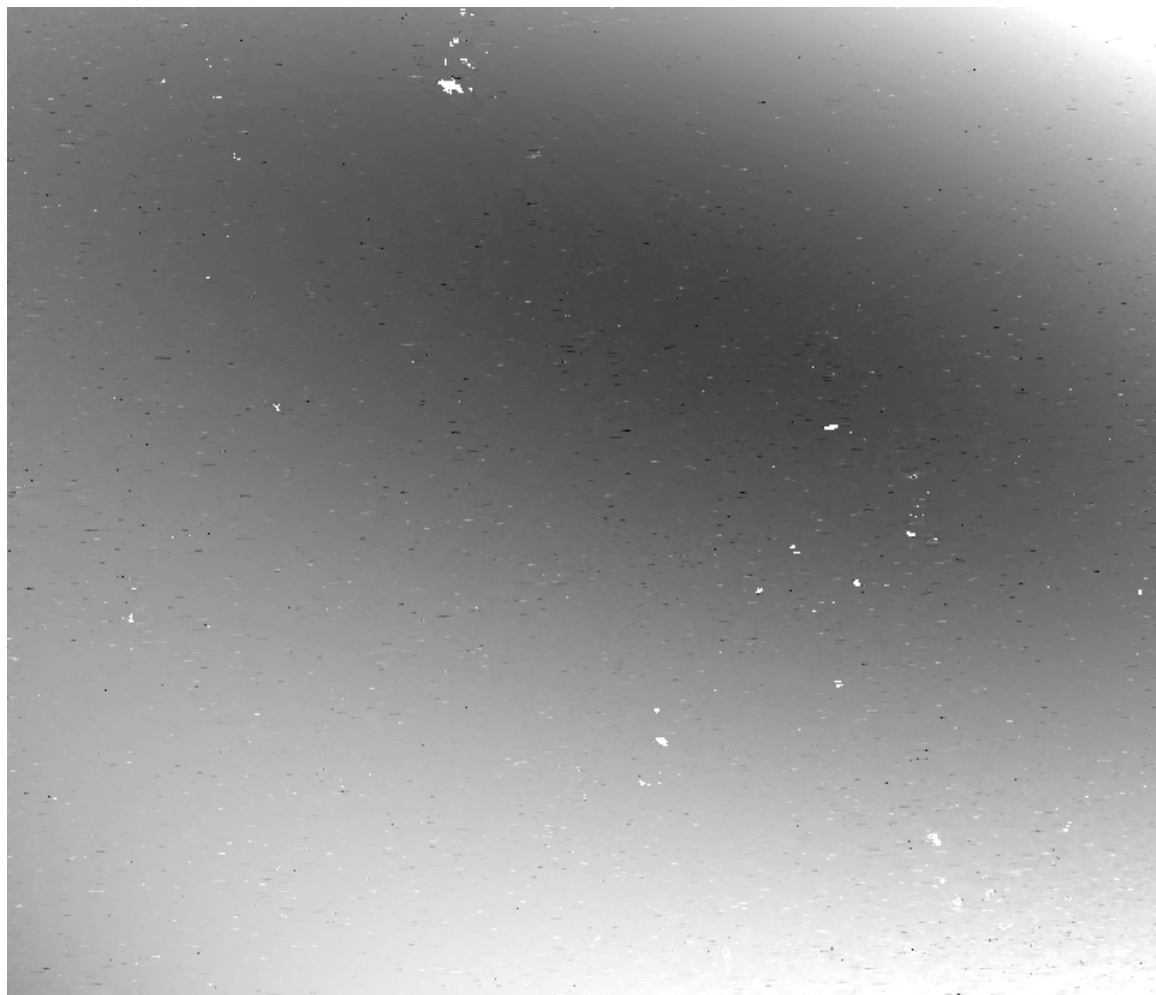


**Figure 5-17:** Difference image (Azimuth bandwidth changed by 0.01 Hz minus original)

Besides the range bandwidth, the azimuth bandwidth is the other fundamental parameter for the generation of a SAR image.

A comparison with the results obtained for the range bandwidth shows that the impact of the azimuth bandwidth is almost identical. The fringe shape caused by a change of 0.01 Hz in azimuth bandwidth (Figure 5-16) as well as the difference image (Figure 5-17) have very similar characteristics.

Therefore, the comparable performance of the software due to the amount of change in the input value shown in Figure 5-18 is not surprising and the azimuth bandwidth can also be considered as a non-critical parameter.

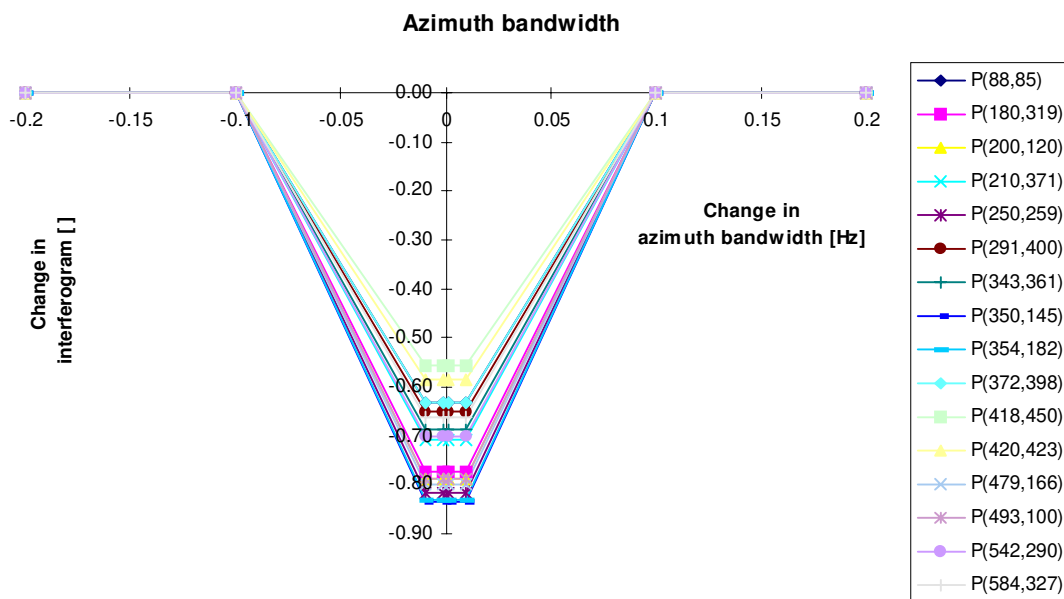


**Figure 5-18:** Graph showing the relation between a change in the azimuth bandwidth and the change in the resulting interferogram

### Doppler centroid frequency

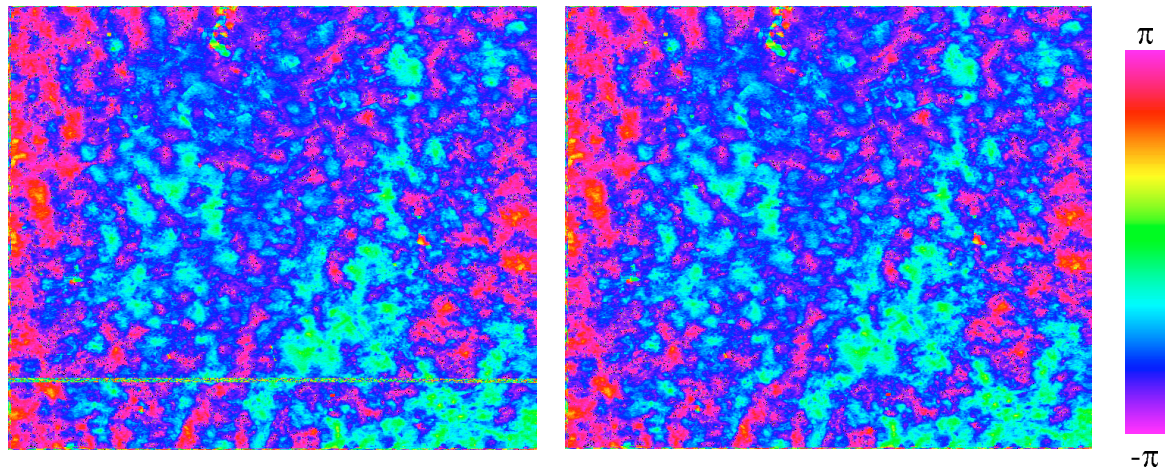


**Figure 5-19:** Original interferogram (left) and interferogram with a change of -0.1 Hz in the Doppler centroid frequency (right)

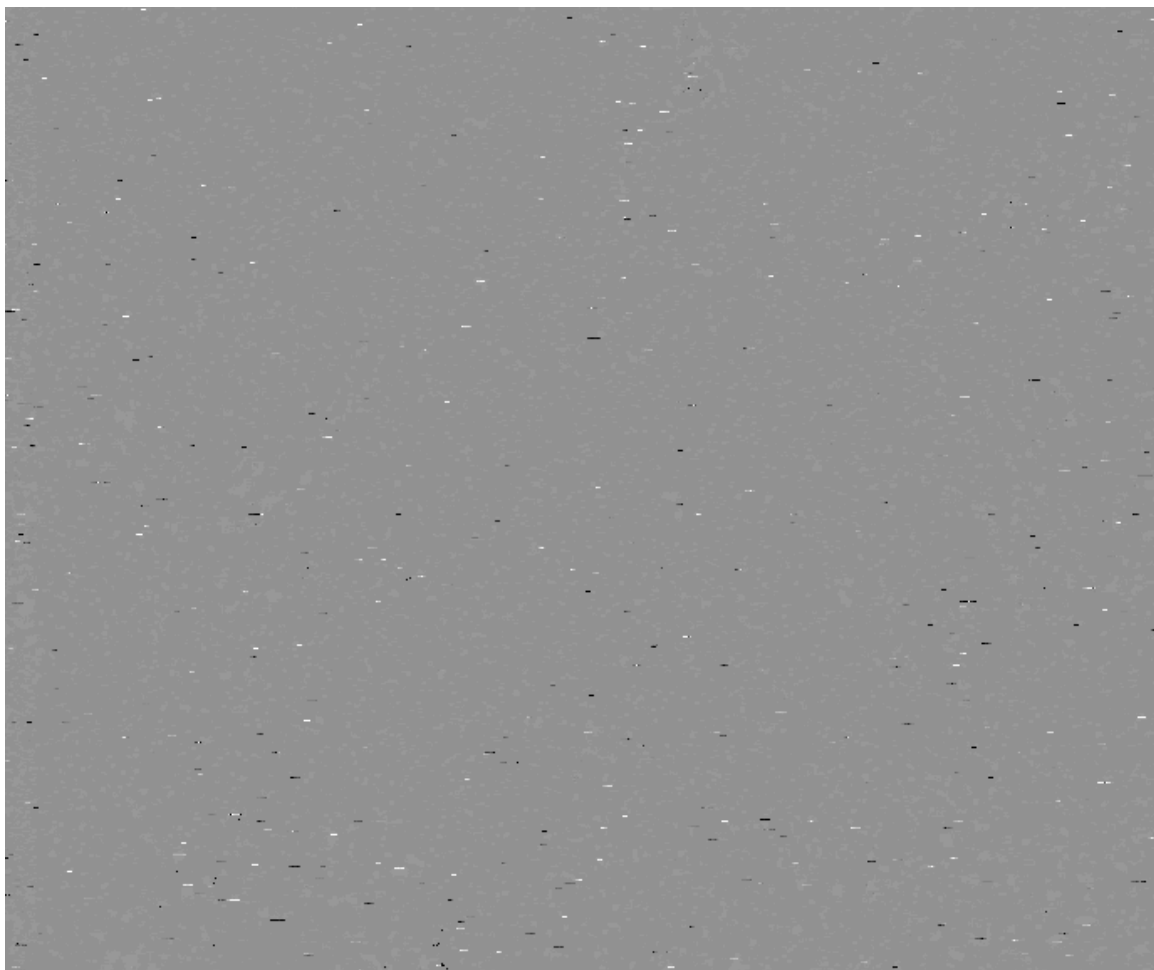


**Figure 5-20:** Difference image (Doppler centroid frequency changed by -0.1 Hz minus original)



As mentioned above, the Doppler centroid frequency determines the location of a pixel in an image. Therefore, it can be assumed that a change in the Doppler centroid frequency only affects the position of a pixel and its physical properties.

The change of -0.1 Hz in the Doppler centroid frequency causes such a small variation in the resulting interferogram that visually no difference can be identified between it and the original interferogram (Figure 5-19).

The difference image (Figure 5-20) confirms this impression. Apart from very small locally distributed linear features in horizontal direction the whole image appears very homogeneous.

For the 16 measured points the impact is almost constant (Figure 5-21). The impact of the Doppler centroid frequency on the resulting interferogram is measurable but considerably small. Hence, the influence of this input parameter on the interferometric processing can be considered negligible.

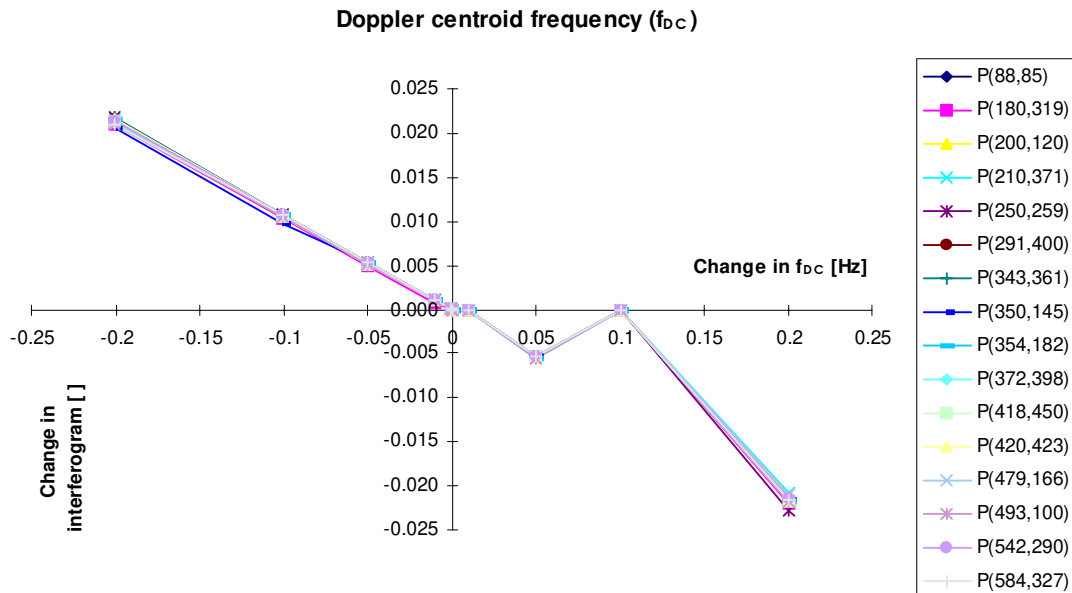


**Figure 5-21:** Graph showing the relation between a change in the Doppler centroid frequency and the change in the resulting interferogram

### State vector position

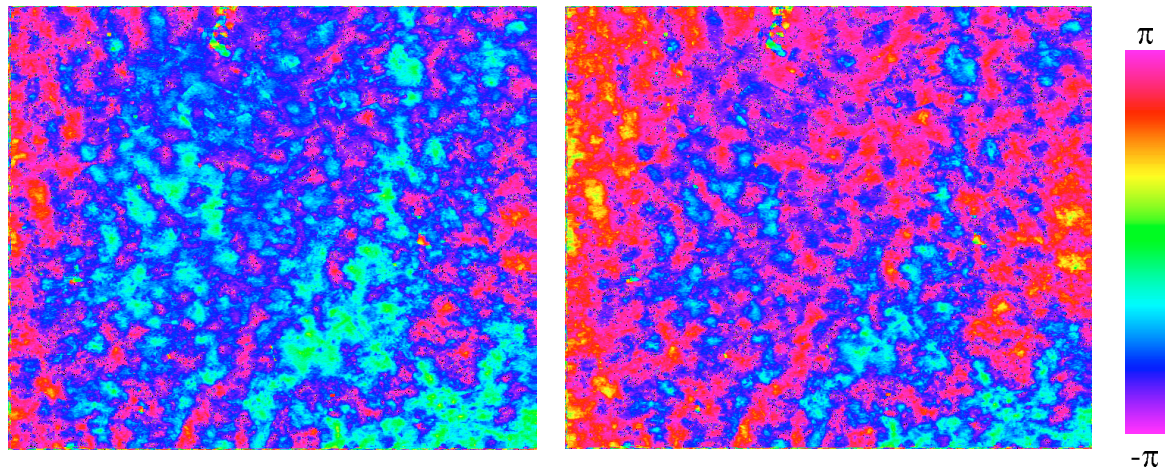


**Figure 5-22:** Original interferogram (left) and interferogram with a change of 0.01 m in the state vector position in  $x$  (right)

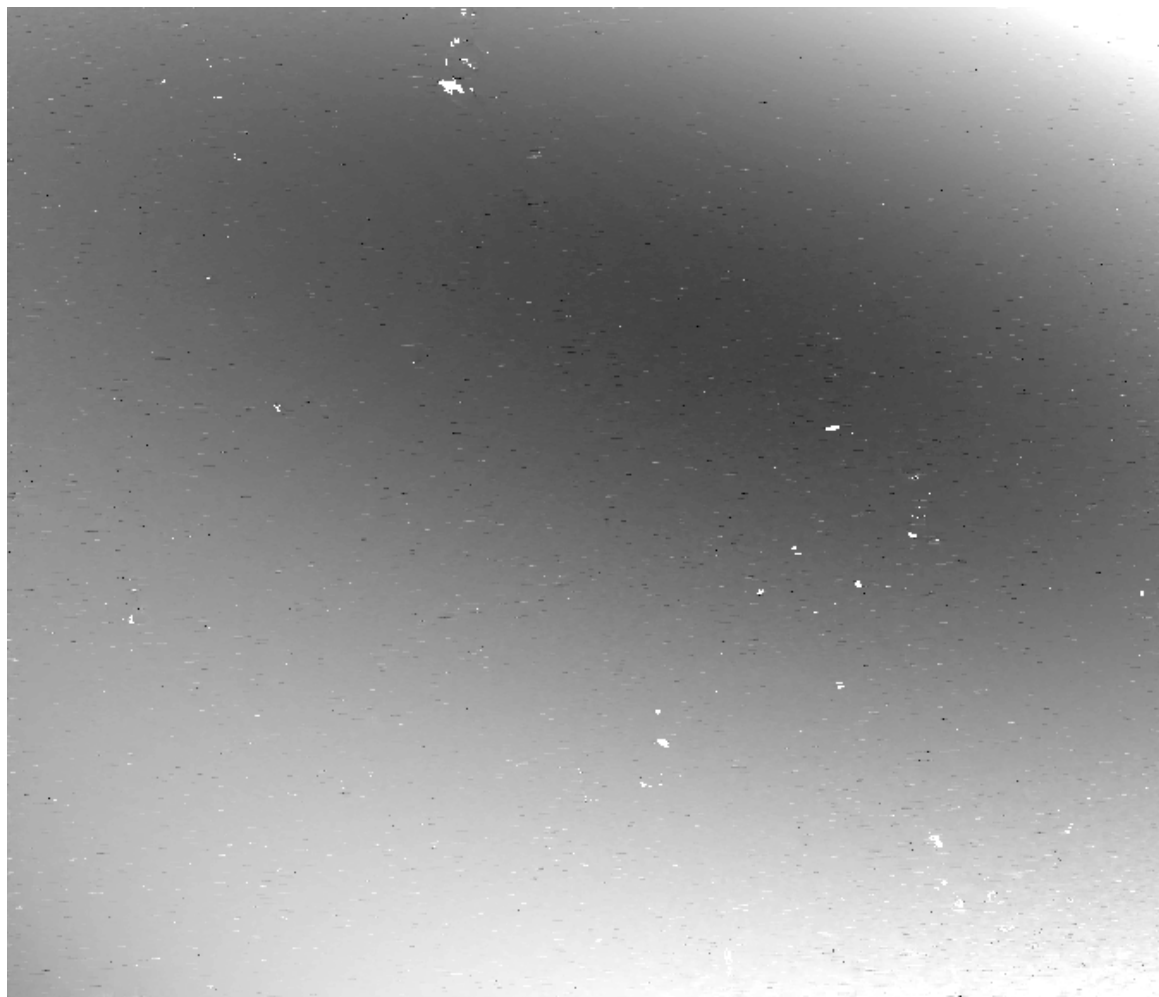


**Figure 5-23:** Difference image (State vector position in  $x$  changed by 0.01 m minus original)

The position of the state vector is given in a three-dimensional way for the directions in x, y and z. The sensitivity study showed that all three components perform in a similar way. Therefore, only the results for a change in the state vector position in x are presented here.

The performance of the state vector position in terms of sensitivity is basically the same as the one of azimuth and range bandwidth. A change of 0.01 metres (Figure 5-22) leads to a difference image with a homogeneous distribution of an elliptical change (Figure 5-23).

The graphs showing the relation between a change in the input value and the result are symmetric and have the same trend as presented for the bandwidths. The software accounts for larger errors introduced in the processing whereas small errors remain uncorrected.

The quality of orbit information is well known as a factor with significant influence on the interferometric data quality. Hence, the user of interferometric data sets should be aware of this error source and pay attention to the quality of this input parameter. The usage of precise orbit information appears to be a prerequisite in order to be able to obtain reliable results.

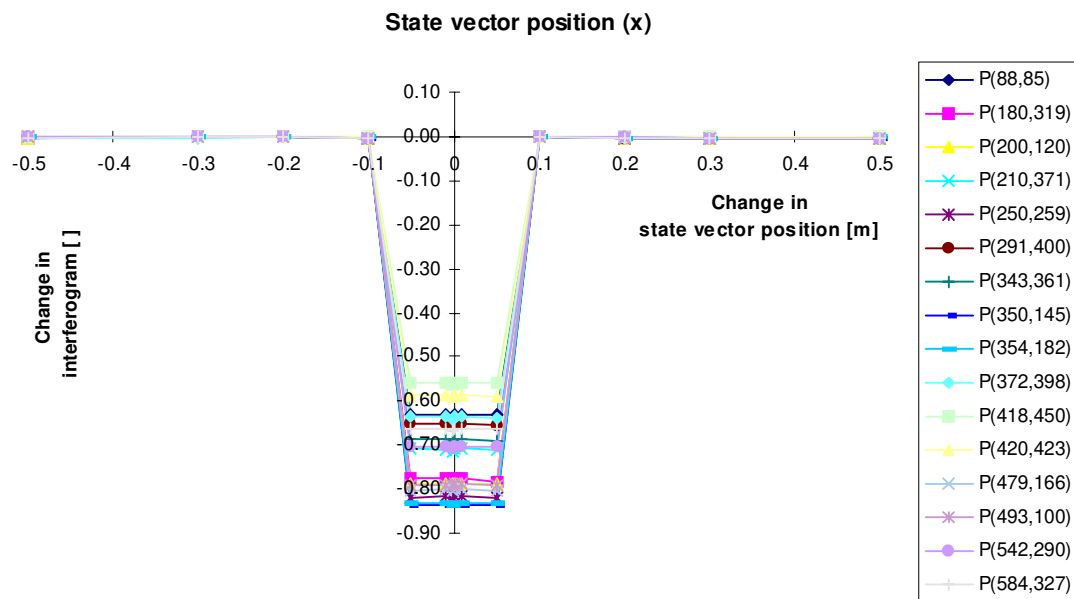


**Figure 5-24:** Graph showing the relation between a change in the state vector position in the x direction and the change in the resulting interferogram

### 5.2.3 Combination of input parameters

So far, the influence of a change in the input parameters has been studied for each input parameter separately. For the error propagation model it has been assumed that the input parameters are statistically independent from each other. The influence of a combination of various parameters on the interferometric result can give an indication about the potential cross-correlation between two input parameters.

For this part of the investigation three different combinations were chosen: (1) the three components of the state vector position, (2) the azimuth and range bandwidths, and (3) the pulse repetition frequency combined with the range sampling rate.

The input parameters of the first two combinations showed a similar performance in the sensitivity study. If the error introduced for an input parameter was large enough the software was able to correct for that. For the combination study the change values for each parameter were chosen in the range which passed the interferometric processing uncorrected. All calculated combinations showed that influence of the summation of the individual contribution was large enough to be corrected during the processing. However, it is assumed that the actual uncertainty of the input parameters is small enough that it still passes the processing and influences the interferometric result. The values chosen for this approach are not necessarily representative for all possible combinations of these parameters.

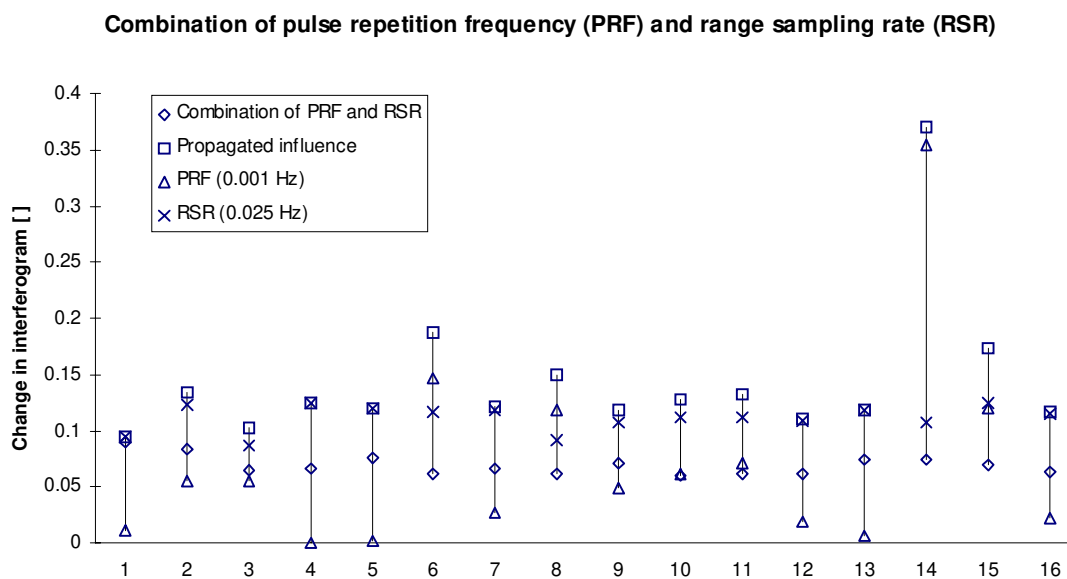


**Figure 5-25:** Change in interferogram caused by a combination of changed input parameters. The absolute change in the interferogram as result of a combination of a change in pulse repetition frequency and range sampling rate is compared with the influence of the individual changes propagated using the variances of the measurements in the sensitivity study.

The pulse repetition frequency (PRF) and the range sampling rate (RSR) were the two parameters whose changes significantly influenced the interferometric product. The result of the sensitivity study indicated that their changes are not accounted for during the processing regardless of the magnitude of change. A combination of both parameters with a change of 0.02 Hz in PRF and 0.1 Hz in RSR showed a similar result as the other above mentioned combinations. The difference between the “changed” and “original” interferogram was very small which means that the software also adapts to changes in these parameters. The result of a combination with smaller values is shown in Figure 5-25.

The absolute change in the interferogram caused by a change in the pulse frequency of 0.001 Hz is compared with the propagated influence of the individual changes using the variances of the parameters. The measurements for this comparison were taken at the same positions as in the sensitivity study. The result clearly shows that the propagated influence in all measured points is larger than the value from the combination approach. Assuming that the two input parameters are statistically independent both results should be approximately the same. The difference between them indicates that the cross-correlation between the two parameters exists. It needs some further research to investigate whether this correlation between parameters is homogeneous over the whole area, related to the coherence level or any surface characteristics.

### **5.3 PROCESSING ALGORITHMS**

Besides the analysis of the input parameters, the sensitivity study also provides the opportunity to investigate the algorithms used for interferometric processing. Due to the complexity of the processing, there are various possibilities to implement the different processing steps. Many different techniques have been proposed but no processing scheme has been generally accepted to achieve the best possible results.

#### **5.3.1 Co-registration**

For some of the processing steps, studies comparing different techniques have been carried out but no systematic approach for the whole interferometric processing chain has yet been presented. Nevertheless, it is also possible to draw conclusions about certain processing steps by theoretical studies. For the co-registration, for example, the following methods can be used: the co-registration based on (1) intensity values, (2) complex values and (3) on the signal-to-noise ratio. Comparing these three methods, it is obvious that a method only using the intensity values is easy to implement and computationally efficient but the least accurate. The complex value contains in addition to the intensity also the phase information. Finally, a method based on the signal-to-noise ratio is able to optimise the co-registration by minimising the introduced noise level. This generally leads to the best results. The interpolation method for the resampling of the slave image also has its influence on the co-registration result. As shown in section 3.3, a higher order polynomial is needed to correct the effect of non-linear parameters. The loss of accuracy by choosing a simplified approach for the implementation is well known but computational efficiency and the processing time is sometimes considered to be more important.

Since there is no interferometric software package available in which several co-registration methods are implemented, no direct comparison of different techniques could be performed. However, the limitations of the co-registration using an auto-matching procedure based on intensity values can be practically shown. The problem of co-registration based on intensities arises if the area covered by a data set is heterogeneous and the backscatter behaviour is significantly different during the two data acquisitions. The intensity images of two ERS-1 scenes acquired 35 days apart (Figure 5-26) show large intensity differences over large parts of the image due to temporal decorrelation caused by harvest activities.

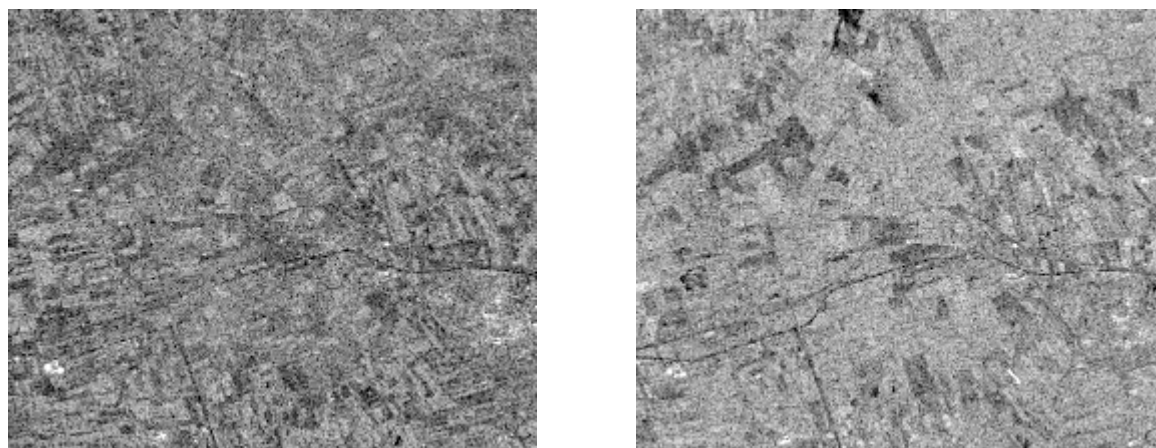


**Figure 5-26:** *Intensity images of the Groningen area. The left image was acquired on 19-Aug-95. The right image (acquired 23-Sep-95) is more homogeneous and the man-made features such as roads and settlement are even more pronounced than in the earlier image.*

The automatic matching algorithm, even using precise orbit information, leads to an unsatisfactory result depicted in Figure 5-27. Compared to the coherence image derived from tandem data (cf. Figure 5-5) this result does not show any structure of agricultural fields or the settlements.

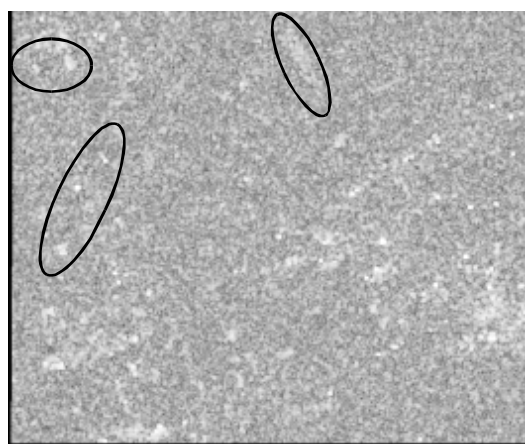


**Figure 5-27:** *Result of the auto-matching algorithm. Different features are enhanced compared to Figure 5-28.*

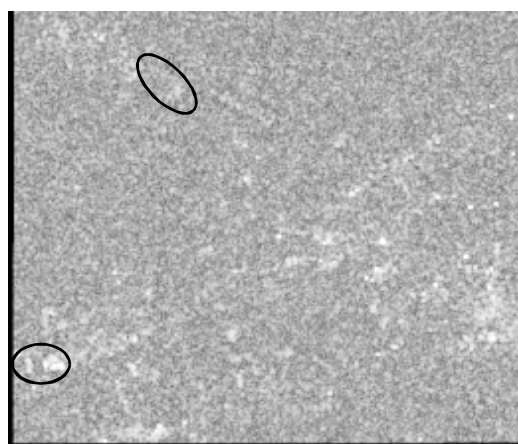


**Figure 5-28:** *Result of the manual tie pointing. Different features are enhanced compared to Figure 5-27.*

Tie points which were clearly identifiable in the intensity images were manually selected and automatically refined by the matching algorithm. This procedure reduced the rms error of the transformation to 0.034 pixels in range direction and 0.065 pixels in azimuth direction. The result (Figure 5-28) of this manual approach which is not assumed to give the best achievable results, visually does not show more details compared to the auto-matching approach but leads to a different shift used for the co-registration. The two results indicate different coherence levels for several features highlighted in Figure 5-27 and Figure 5-28. It can be assumed that there are more potentially well correlated features in the imagery but the correlation calculation based only on intensity values has its limitations with areas with a partly low coherence level due to mainly temporal decorrelation.

### 5.3.2 Filtering

Filtering of the data sets can be applied at different stages of the interferometric processing. Each filtering step can reduce disturbing effects such as speckle or noise which are in the data sets, at the expense of losing a part of the original information. Before the interferogram generation, azimuth spectral overlap filtering of the slave image is performed using the Doppler centroid frequencies. In range direction, a baseline decorrelation filtering is applied to the master and slave image. These filtering techniques can also be applied before the co-registration of the two complex images. After the generation of the interferogram a second filtering step is introduced to reduce the noise level either by a multi-look approach or by adaptive filtering.

### 5.3.3 Phase unwrapping

A quantitative comparison of different techniques is very difficult because the different algorithms need to be implemented in the same software system in order to avoid the influence of any processing step other than the one that is supposed to be tested. Since the interferometric processing (e.g. phase unwrapping) is a very complex task, generally only a limited number of algorithms for the same processing step is implemented. The use of selected algorithms from different software packages for comparison is difficult because no data standard is established which allows an easy exchange of data sets among different software packages. Most software packages use their own internal data format and are therefore not compatible with each other (for details see Appendix A). Since there is only a limited number of software packages commercially available, this part of the study could not be performed with desired detail.

In order to perform a comprehensive study for the comparison of the different algorithms implemented for a processing step, it is necessary to create an environment which allows a quantitative assessment under controlled conditions. This could be achieved by generating an artificial data set which considers all relevant error sources indicated in this study. The other aspect which would make a comprehensive comparison of different algorithms easier is the introduction of a standard format for interferometric data sets which allows an easier exchange of data sets among software packages.

## 6 ERROR PROPAGATION MODEL

---

The implementation of a method for the quality assessment of SAR interferometric data is the main part of this study. After introducing the theoretical background of the proposed error propagation model, the issues concerning the practical implementation of the empirical approach are discussed. Results of the quality assessment of digital elevation models are presented. Finally, the limitations and advantages of the proposed method are highlighted.

### 6.1 BACKGROUND OF ERROR PROPAGATION

From the statistical point of view, interferometric processing is a very complex mathematical function  $f(x)$  depending on a number of input parameters which are introduced at various stages into the processing. The input parameters as well as the function that the interferometric processing is actually representing have their uncertainties. Therefore, they introduce an error into the calculation which propagates with every subsequent processing step. The aim of error propagation is to estimate the influence of the error introduced at a certain stage on the result of a given function  $f(x)$ .

If the function  $f(x)$  is simple or even linear and normally distributed, the error propagation problem can be solved by analytical means. These solutions are not applicable for complex processing schemes such as the one for SAR interferometry. Heuvelink (1993) presented four alternative methods for the propagation of errors in local GIS operations: the first and second order Taylor methods, Rosenblueth's method and the method of Monte Carlo simulation. The first three methods are not discussed here as they require knowledge about the mathematical formulation of the function  $f(x)$  which is actually not given for the interferometric processing.

Error propagation by the Monte Carlo method, described in detail by Hammersley and Handscomb (1979), follows a completely different approach. A Monte Carlo simulation is based on the repeated  $n$  computations of the function  $f(x)$  with input values that are randomly sampled in a certain range. If the number of computations  $n$  is sufficiently large, the entire distribution is represented and a reliable accuracy measure can be derived. An error propagation using the Monte Carlo simulation is generally applicable but computationally very intensive.

Nevertheless, the whole approach can be significantly simplified by introducing quality estimates for each input parameter. In this way only one computation per input parameter, with an input value changed in the order of the standard deviation, is required which needs to be compared to the original processing result. This simplification is only valid assuming that all input parameters are normally distributed and statistically independent.

This error propagation method was chosen for the quality assessment of SAR interferometric data as it allows the assessment of a result calculated by a commercially available software package with a limited knowledge about the practical implementation of the algorithms. Furthermore, a sensitivity study can be carried out indicating which of the



input parameters have a larger impact on the interferometric product and which algorithm implemented for a certain processing step gives the best result.

## 6.2 EMPIRICAL APPROACH

The implementation of the error propagation model is done in an empirical way in order to keep the approach as flexible as possible. There is no additional information needed on how the data processing or a single processing step is actually performed. The schematic representation of the error propagation model as proposed by Gens and van Genderen (1996a) is shown in Figure 6-1.

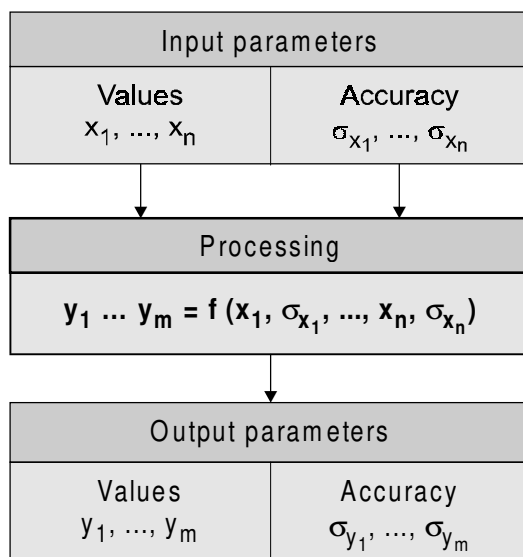


**Figure 6-1:** Schematic representation of the error propagation model (Gens and van Genderen, 1996a)

For each single processing step the values  $x_i$  and the accuracies of all  $n$  input parameters  $\sigma_{x_i}$  as well as a list of  $m$  output parameters  $y_i$  have to be known. The data set is then processed once with the original values and afterwards  $n$  times with one slightly changed input parameter. The accuracy of the output parameters  $\sigma_{y_i}$  is then derived from the changes of the adapted and the original calculation by numerical differentiation. The empirical approach can be performed for a single processing step, for larger parts or even the complete processing chain. Therefore, it can be adapted for the quality assessment of all mentioned interferometric products as long as all relevant input parameters and their accuracies are considered.

There are a number of parameters given in the leader file (for details of file structures see Gråbak, 1995) used for the interferometric processing. For the quality estimation only those parameters are used which are independent of each other. Therefore, parameters such as azimuth and range sample spacing which can be derived from the sampling rates are not included in the quality estimation. The parameters used for the calculation and their standard deviations are listed in Table 6-1.

The standard deviations for some of the input parameters are published in the literature. The quality of the determination of the orbit state vectors mainly depends on the amount of measurements introduced in the calculation. The ERS-2 orbits are mainly based on satellite laser ranging and PRARE observations which leads to a higher accuracy compared to ERS-1 orbits. However, for the ERS tandem mission the orbits of the ERS-1 satellite could be improved by simultaneous orbit determination of both ERS satellites (Scharroo and Visser, 1997). In addition to that, the development of the underlying gravity models led to a further improvements of the orbit determination. The other standard deviations are based on logical assumptions and the experience gained from the sensitivity study. It is difficult to estimate the impact of other influencing factors such as the atmosphere,

processing algorithms etc. The atmosphere causes local inhomogeneities which can lead to phase shift up to a phase cycle. Since it is a local phenomenon there is no way to estimate an average value for the influence on the whole data set. Without further knowledge about the actual implementation of a particular processing no estimation can be made as to what extent assumptions or simplifications in the processing have their effect on the processed result.

Parameter	Standard deviation	Information source
Pulse repetition frequency	0.1 Hz	assumption
Range sampling rate	0.3 Hz	assumption
Azimuth bandwidth	0.1 Hz	assumption
Range bandwidth	1 Hz	Francis et al. (1995)
Doppler centroid	0.1 Hz	assumption
State vector position		Reigber et al. (1996)
along-track	0.31 m	
across-track	0.33 m	
radial	0.07 m	

**Table 6-1:** Input parameters used for interferometric processing of ERS satellite data

### 6.3 ESTIMATION OF THE DEM ACCURACY

For the estimation of the quality of a digital elevation model data sets from two different test sites have been selected.

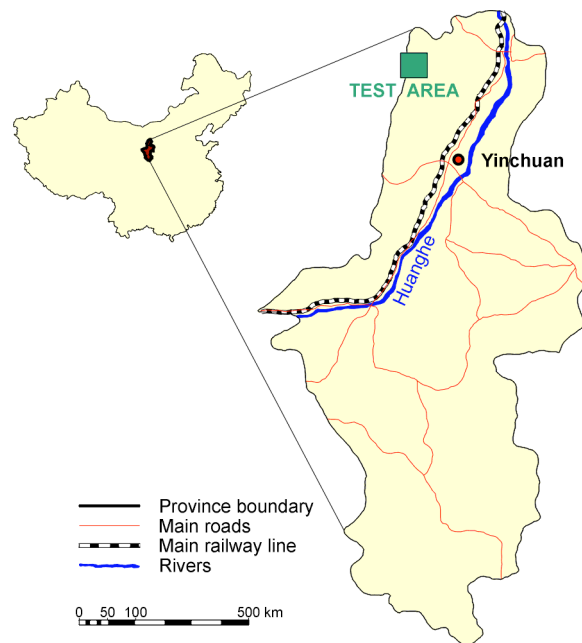


**Figure 6-2:** Map of the test site in Ningxia, China

A mountainous area in Ningxia, an autonomous region in North-west China, has been chosen as a test site because it provides a large variation in terrain types and land forms. Furthermore, the influence of the vegetation on the acquired imagery can be neglected since in most parts the area is devoid of all vegetation and is covered by bare soils and rock outcrops. Since there were no suitable topographic maps nor a reference DEM available for this area, no comparison with an absolute reference has been carried out. This case represents the worst situation in the evaluation of an interferometric DEM where no reference is available to estimate the quality of the calculated result.

An ERS tandem data set (for details see Table 6-2) has been chosen for the estimation of the DEM accuracy in this difficult test site.

	Data sets	
<b>Test site</b>	Ningxia, China	
<b>Images</b>	Sensors	Data acquisition
Master image	ERS-1	16-Jan-96
Slave image	ERS-2	17-Jan-96
<b>Subset</b>	Row	Column
Upper left corner	1410	11
Bottom right corner	4008	526

**Table 6-2:** Data sets used for the study of the Ningxia test site

The other test site located in Lower Saxony, Germany, represents a hilly terrain with large forest areas and some agricultural fields. A digital elevation model derived from photogrammetric measurements serving as a reference model was available for this test site.

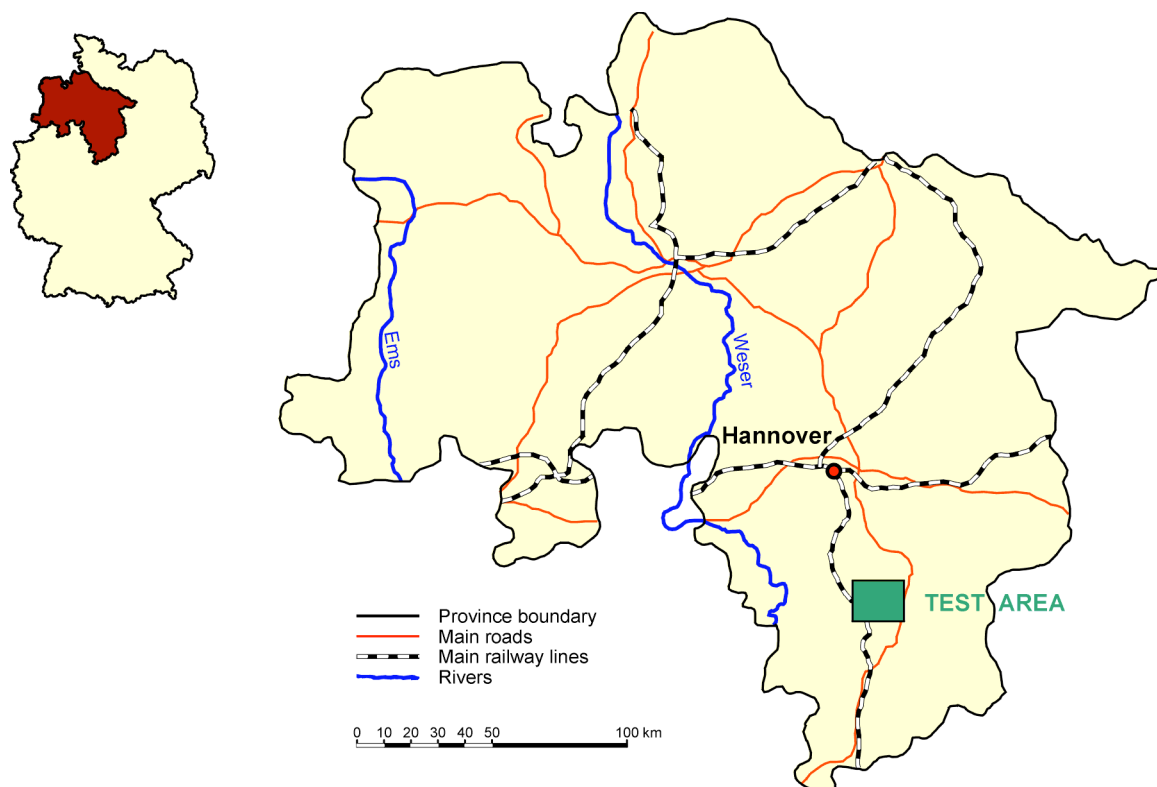


**Figure 6-3:** Map of the test site in Lower Saxony, Germany

	Data sets	
<b>Test site</b>	Lower Saxony, Germany	
<b>Images</b>	Sensors	Data acquisition
Master image	ERS-1	21-Apr-96
Slave image	ERS-2	22-Apr-96
<b>Subset</b>	Row	Column
Upper left corner	8875	0
Bottom right corner	14900	2475

**Table 6-3:** Data sets used for the study of the Lower Saxony test site

The tandem data set used for the Lower Saxony test site was acquired in spring (for details see Table 6-3). Therefore, no disturbances due to agricultural activities etc. are expected. As the tandem pair has a relatively small overlap in azimuth direction the chosen subset represents the largest extractable area of this interferometric image pair.

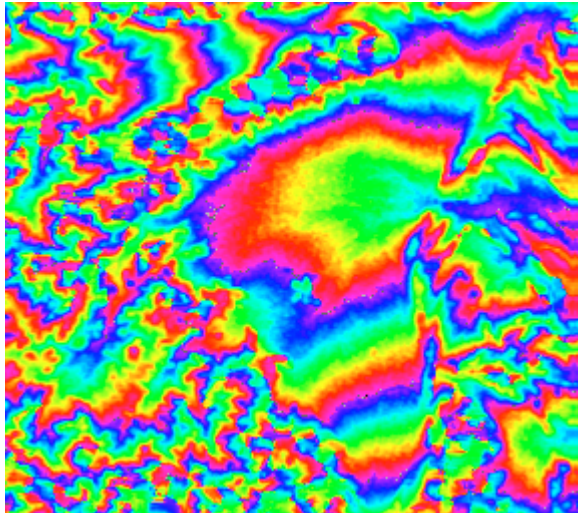
### 6.3.1 Results from the Ningxia area, China

As mentioned before the Ningxia test site was chosen to show that the proposed method is able to provide a reasonable quality estimation of an interferometrically derived DEM in an area where no suitable reference information whatsoever is available. Since there is no way of comparing the calculated result with a reference, the only possibility to evaluate the InSAR DEM is to assess whether the estimated accuracy is within the expected range given in the literature.



As can be seen from the coherence image (Figure 6-4), the correlation level is only reasonably high in some parts of the scene which are flat whereas the slopes (in the top part) and rugged topography (see bottom centre) cause a significant decorrelation. The resolution of the sensor is not able to represent the detailed structure of the terrain. The loss of coherence in the curvilinear features on the right side of the image is due to the moving water surface of the small tributaries of a river.

**Figure 6-4:** Coherence image of the Ningxia area



The corresponding interferogram (Figure 6-5) confirms the observation made on the coherence image. In the hilly parts of the terrain some discontinuities in the phase occur which cause serious problems in solving all ambiguities during the phase unwrapping process. Clear fringes are only detectable in reasonably flat areas. The shape of the rest of the fringes indicates how rugged the terrain is.

**Figure 6-5:** Interferogram of the Ningxia area

Following the calculation scheme given in Table 6-4 the contribution of each input parameter to the standard deviation of the DEM has been calculated. The variance for each parameter ( $vv$ ) is derived from the difference in the result of the adapted and original processing ( $\Delta y_i$ ), the change in the input values introduced for the adapted calculation ( $\Delta x_i$ ) and the standard deviation of the input parameters ( $\sigma_i$ ). The summation of all contributions results in the estimation of the variance for one point ( $\Sigma vv$ ). The square root of the variance ( $\sqrt{[vv]}$ ), finally, determines the standard deviation for one point.

Parameter	Change in input $\Delta x_i$	Difference in result $\Delta y_i$	Standard deviation $\sigma_i$	$\left(\frac{\Delta y_i}{\Delta x_i} \cdot \sigma_i\right)^2$ $vv$
Pulse repetition frequency	0.03 Hz	1.4800 m	0.1 Hz	24.33889 m <sup>2</sup>
Range sampling rate	0.3 Hz	-3.7633 m	0.3 MHz	14.16258 m <sup>2</sup>
Azimuth bandwidth	0.05 Hz	0.0001 m	0.1 Hz	1.87 E-08 m <sup>2</sup>
Range bandwidth	0.05 MHz	0.0001 m	1.0 MHz	1.92 E-06 m <sup>2</sup>
Doppler centroid	0.1 Hz	-0.0001 m	0.1 Hz	1.68 E-08 m <sup>2</sup>
State vector position in x	0.05 m	-0.0040 m	0.31 m	0.00062 m <sup>2</sup>
State vector position in y	0.05 m	0.0269 m	0.33 m	0.03145 m <sup>2</sup>
State vector position in z	0.05 m	0.0149 m	0.07 m	0.00044 m <sup>2</sup>
Variance [vv] of the interferometric height P(275,275)= $\Sigma$				38.53399 m <sup>2</sup>
Standard deviation of the interferometric height P(275,275)= $\sqrt{[vv]}$				6.208 m

**Table 6-4:** Calculation scheme for the empirical error propagation model

From Table 6-4 and other computations it is clear that the size of the variance in the pulse repetition frequency and the range sampling rates confirms the results from the sensitivity study. These parameters have the largest impact on the interferometric result. The influence of the state vector position is less but still significant. The contribution of the other parameters is much smaller and can be neglected.

The final product of the interferometric process, the digital elevation model (Figure 6-6), shows quite some detail although the processed area is rather small (8.8 km x 9.9 km). The middle part of the area is homogeneously flat whereas the lower left part indicates a rugged surface with significant slopes.

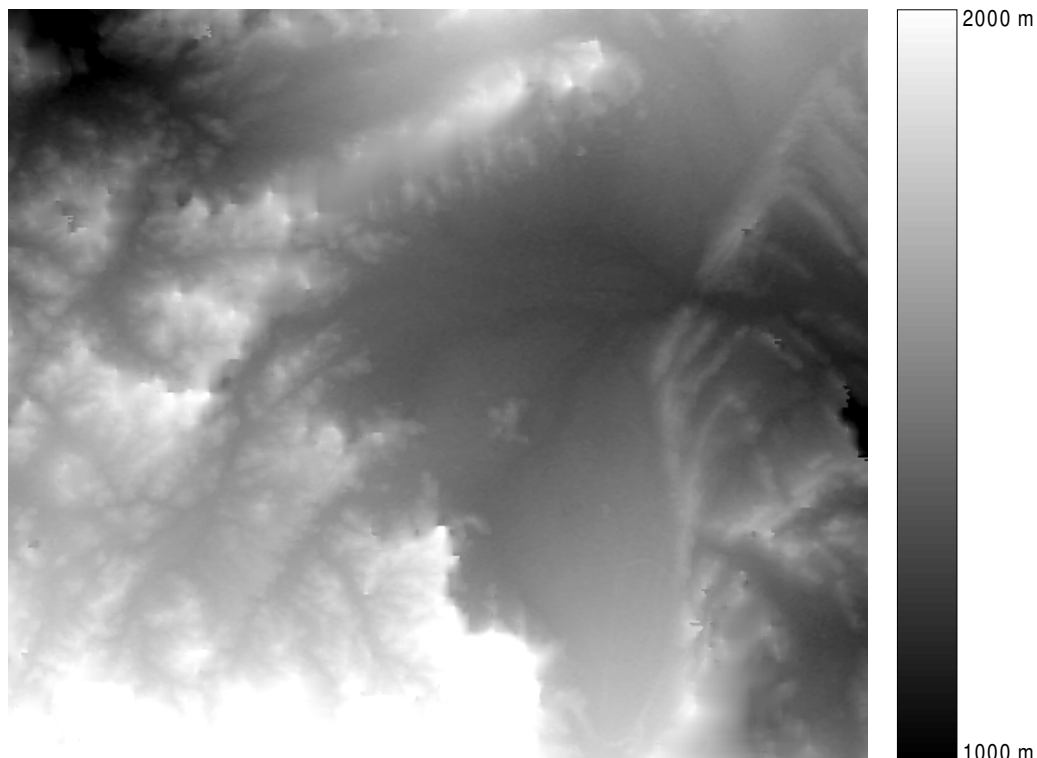


**Figure 6-6:** Digital elevation model (Ningxia, China)

Using the empirical approach proposed here it is possible to estimate the quality of the interferometric DEM on pixel level. Based on the calculation scheme shown in Table 6-4, an error map for the whole DEM has been computed (Figure 6-7). The visual inspection of the histogram helped to determine the threshold for masking out the artefacts in the digital elevation model caused by phase discontinuities. The maximum error in height for this small subset is 10 metres. The mean height difference is 1.6 metres which leads to a standard deviation of 0.8 metres in the height values. The values in the error map do not show any relation to the actual topography and are too optimistic. The small size of the subset is probably the main reason for this far from expected result. The number of artefacts also indicates the difficulties that occurred during the phase unwrapping process. From this it can be concluded that for some test sites such as the one presented here, error propagation model does not appear to be suitable to reliably estimate the quality of interferometric DEM.

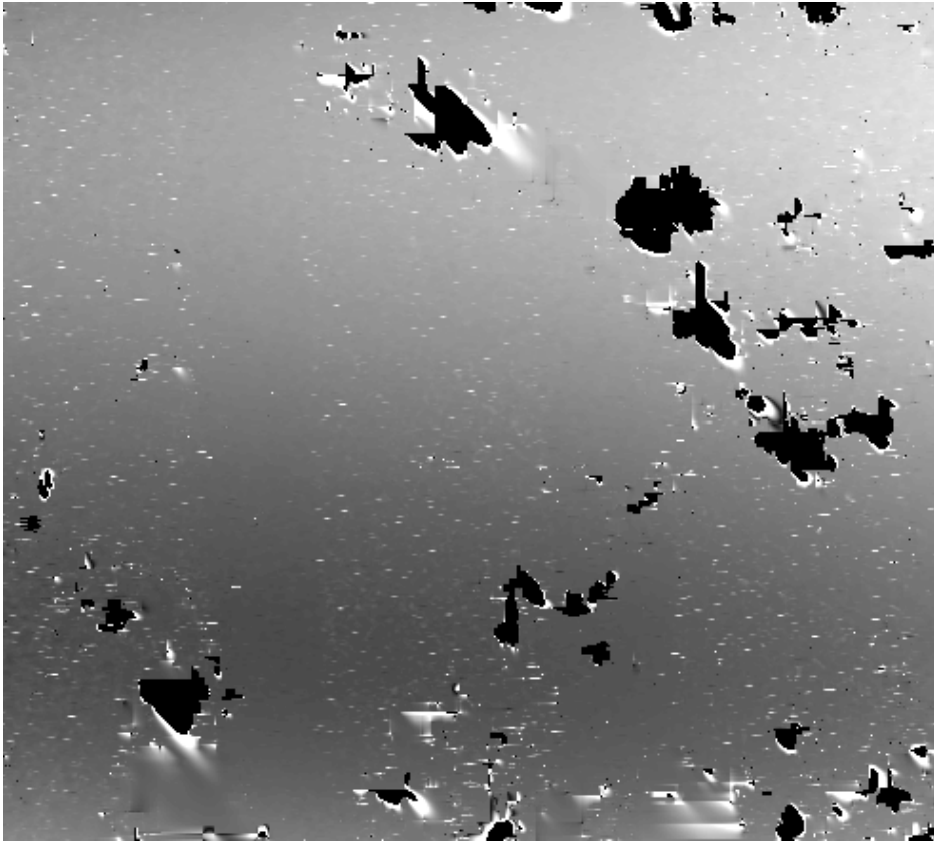


**Figure 6-7:** *Error map of the Ningxia DEM (artefacts caused by phase discontinuities masked out in black)*

### 6.3.2 Results from the Lower Saxony area, Germany

The interferogram calculated for the Lower Saxony area (Figure 6-8) gives a good indication about the variety in the landscape. Flat areas represented by just one fringe can easily be distinguished from the hilly parts where several fringes indicate steeper slopes. Visually, no phase discontinuities can be detected.

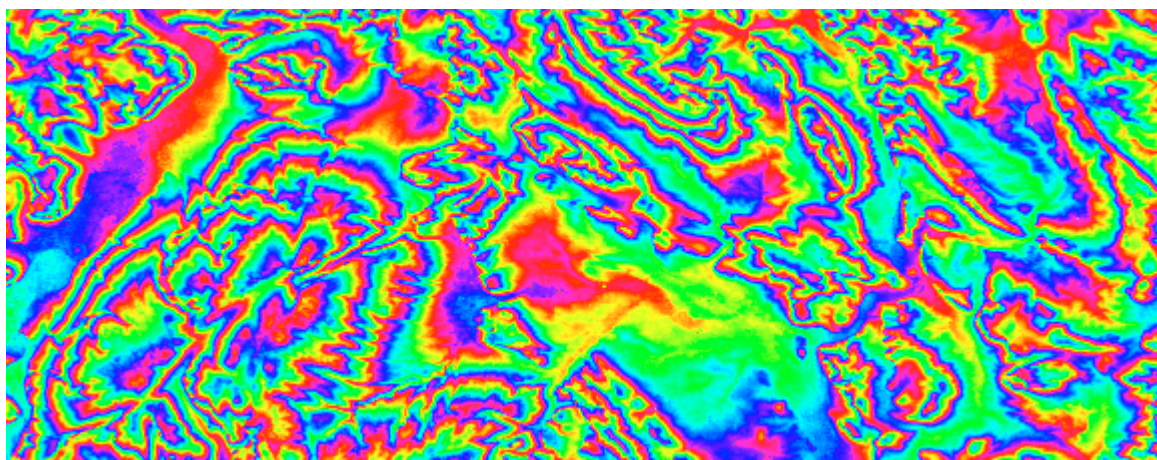


**Figure 6-8:** *Interferogram of the Lower Saxony area. The fringes in the interferogram show that a large variety of land forms is present and give a good indication about the actual landscape.*

The coherence image for this area (Figure 6-9) shows a generally high level of coherence. Most of the highly correlated parts are mainly agricultural fields. The homogeneity of these fields indicates that the conditions during the two data acquisitions have been very similar. The small dark spots in the light homogeneous areas are settlements. Furthermore, some rivers can be identified. Areas of lower coherence are mainly forest covers. It is even possible to distinguish different densities of the forest cover from the different shades in the dark parts on the coherence image.

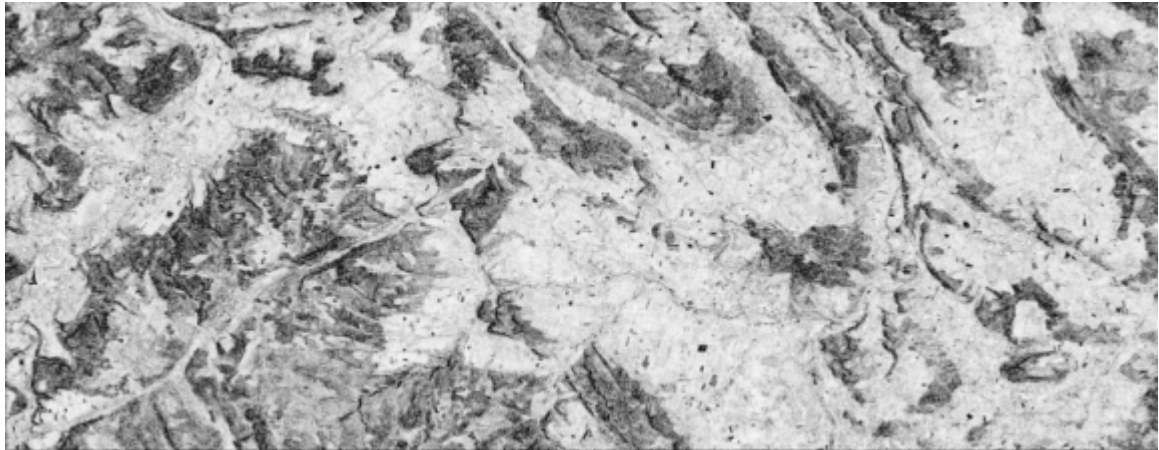


**Figure 6-9:** *Coherence image of the Lower Saxony area. The coherence image of this area serves as a good indicator for forested areas. Highly correlated parts indicate agricultural areas whereas low coherence areas are covered mainly by forest.*

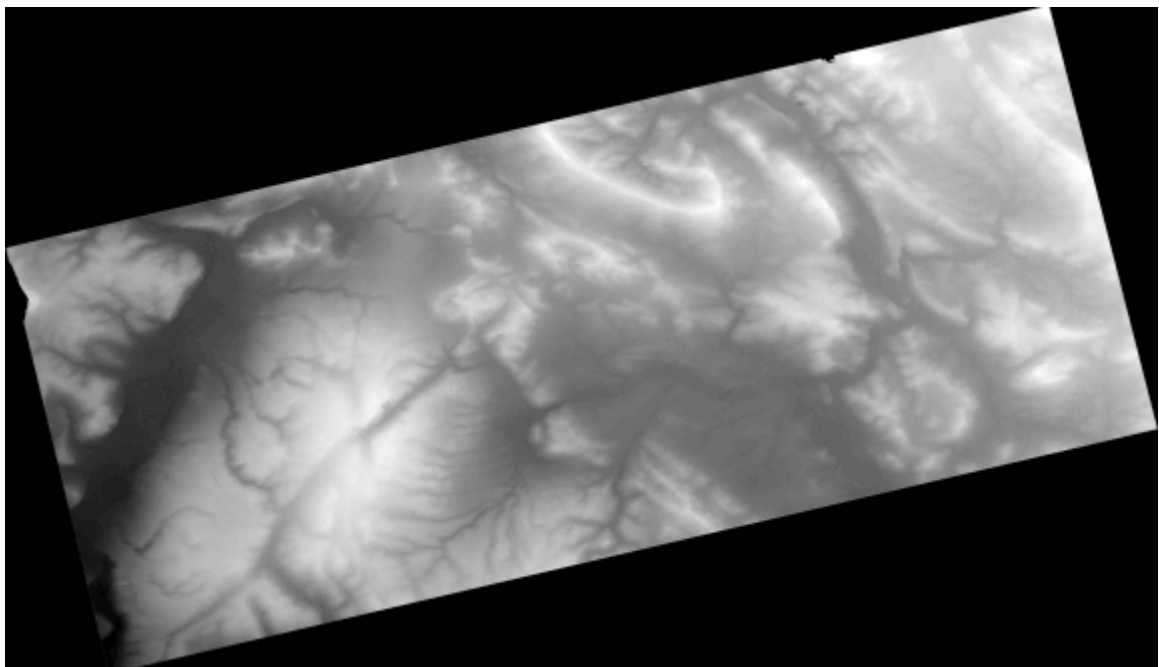


**Figure 6-10:** *Digital elevation model of the Lower Saxony area*



The resulting digital elevation model shown in Figure 6-10 has a pixel size of 20 metres and covers an area of 16 km x 24 km. The height ranges from 20 to 580 metres. It has been geocoded using one height reference point from the topographic map (scale 1:50 000) of the study area and projected into the Gauss-Krüger coordinate system in order to be able to compare it with the reference DEM.

A three-dimensional perspective view of the interferometrically derived digital elevation model (Figure 6-11) can be used to give a better visual impression of the terrain surface. The grid size of the mesh of 30 metres was chosen to represent the general terrain structure. Furthermore, the perspective view overlaid on the corresponding interferogram shows the relation between the calculated phase differences and the height values. It also gives an idea about the complex issue of phase unwrapping where for each point the exact number of phase cycles needs to be determined to reconstruct the correct height.

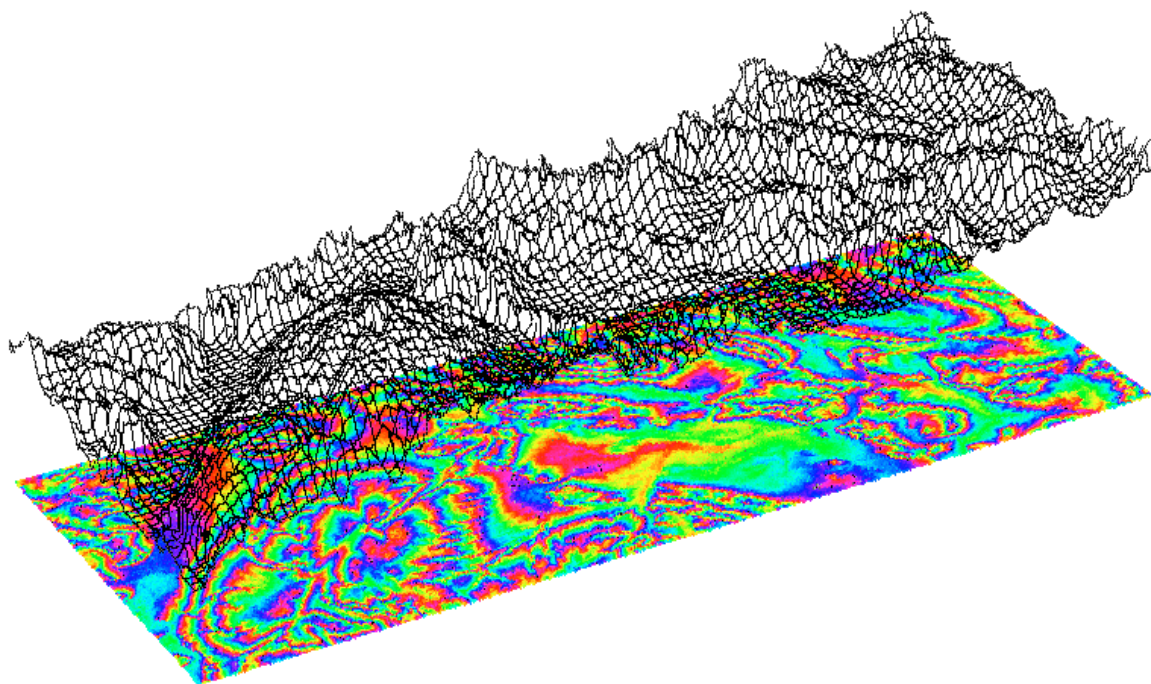


**Figure 6-11:** *Perspective view of the interferometrically derived digital elevation model of the Lower Saxony area overlaid on the corresponding interferogram. This perspective highlights the relation between the measured phase value and the final calculated height value.*

For generating the error map of the Lower Saxony area (shown in Figure 6-12) the calculation scheme presented in Table 6-4 has been used. It was observed that the orbit state vectors were very sensitive to changes. For some parts of the area the phase unwrapping algorithm had problems to calculate a reliable result using the proposed standard values. Therefore, the error map for this area is based on a smaller subset. The contribution of the different input parameters to the overall height error confirmed the observation of the sensitivity study. The parameters with the largest influence on the final result were the pulse repetition frequency (depicted in Figure 6-13) and the range sampling rate. The error map of the Lower Saxony area shows less artefacts compared to the one from the Ningxia area. The visual inspection of the histogram here led to setting a threshold of 80 metres as maximum error for masking out the artefacts caused by phase

inconsistencies. The mean height error is 36 metres resulting in a standard deviation of 15.4 metres for the height. This result is within the expected range.

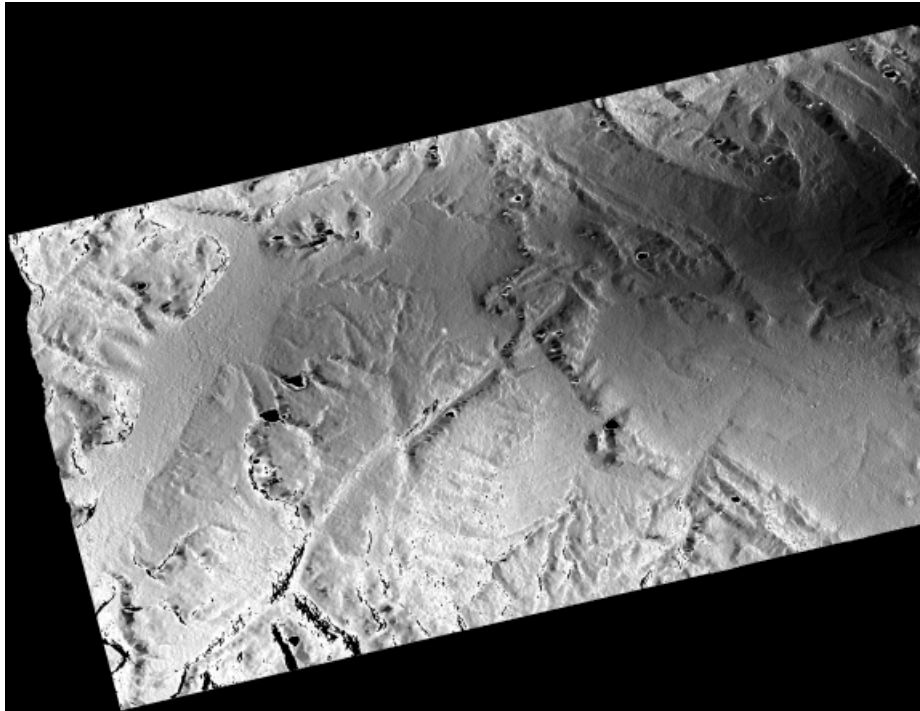


**Figure 6-12:** *Error map of the Lower Saxony DEM*

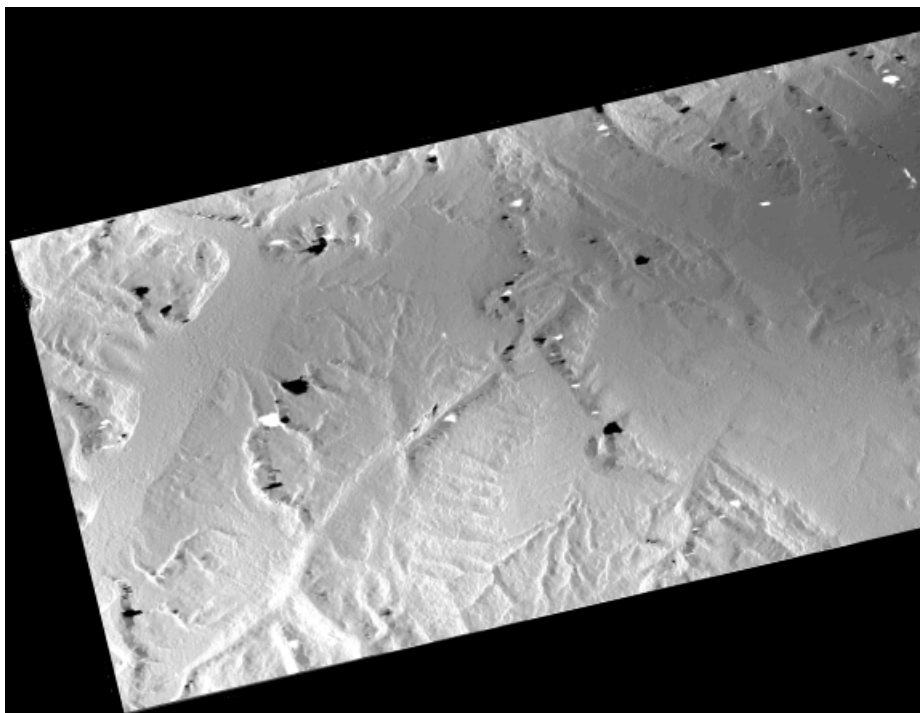


**Figure 6-13:** *Difference image (Pulse repetition frequency changed by 0.03 Hz minus original digital elevation model)*

The reference DEM shown in Figure 6-14 is derived mainly from photogrammetric and some terrestrial measurements. The accuracy is in the range of 0.5 to 2.0 metres. The size of the original raster is 12.5 metres which has been resampled to 25 metres.

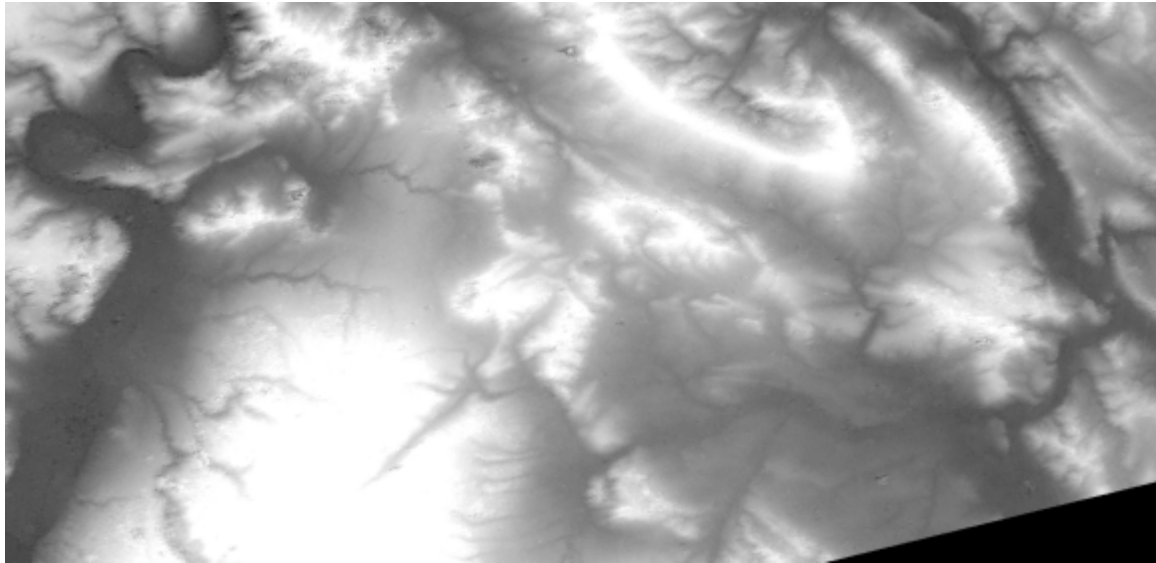


**Figure 6-14:** Reference DEM of the Lower Saxony area

In order to be able to compare the interferometric DEM with the reference DEM both elevation models need to be in the same coordinate system, i.e. in the same map projection. Therefore, the interferometric DEM has to be properly geocoded. As mentioned before, the interferometric software allows the geocoding of the digital elevation model for several different projections based on one reference height point and the orbit geometry. Assuming that this geocoded interferometric product is reliable ideally two translations should be enough to fit the two elevation models to each other. However, this geocoding method was not sufficient as an additional rotation of 2.1 degrees and a substantial correction of the height trend had to be performed in order to achieve a precise fit of the two elevation models. With the refinement tool of the interferometric software only the height trend was removed using twelve reference height points identified in the topographic map. Finally, a third-order polynomial transformation was performed for the rotation and the subsampling of the interferometric DEM from originally 20 m pixel size down to 25 m pixel size of the reference DEM using 18 ground control points. By following this procedure errors introduced by resampling the interferometric DEM twice have been avoided.

The difference between the interferometrically derived and the reference DEM (depicted in Figure 6-15) indicates a good fit in the centre part of the area but also some problems in the hilly parts. After removing some obvious artefacts the difference between the two elevation models ranges from -75 to 15 metres. The mean difference is at -20 metres resulting in a standard deviation of 23.7 metres. There are a few potential error sources. First, it has to be assumed that the reference DEM is free of any errors which may not be valid for the whole area. Some parts of the area are covered by forest so that there are difference due to the fact that the interferometric height is referring to the top tree layer

and the reference DEM is most likely based on terrestrial measurement which refer to the actual ground. The problems having occurred during the geocoding of the interferometric DEM based on the orbit geometry and a reference height point lead to the assumption that the transformation of the terrain corrected DEM into the map projection was not correctly performed. A second source of error is the removal of the height trend with the refinement tool. The number of height control points might not have been sufficient or well distributed to correct the height trend in a satisfactory way. Finally, the slight misregistration of the interferometric DEM to the reference DEM is possible although the rms error did not exceed 1.6 pixels.

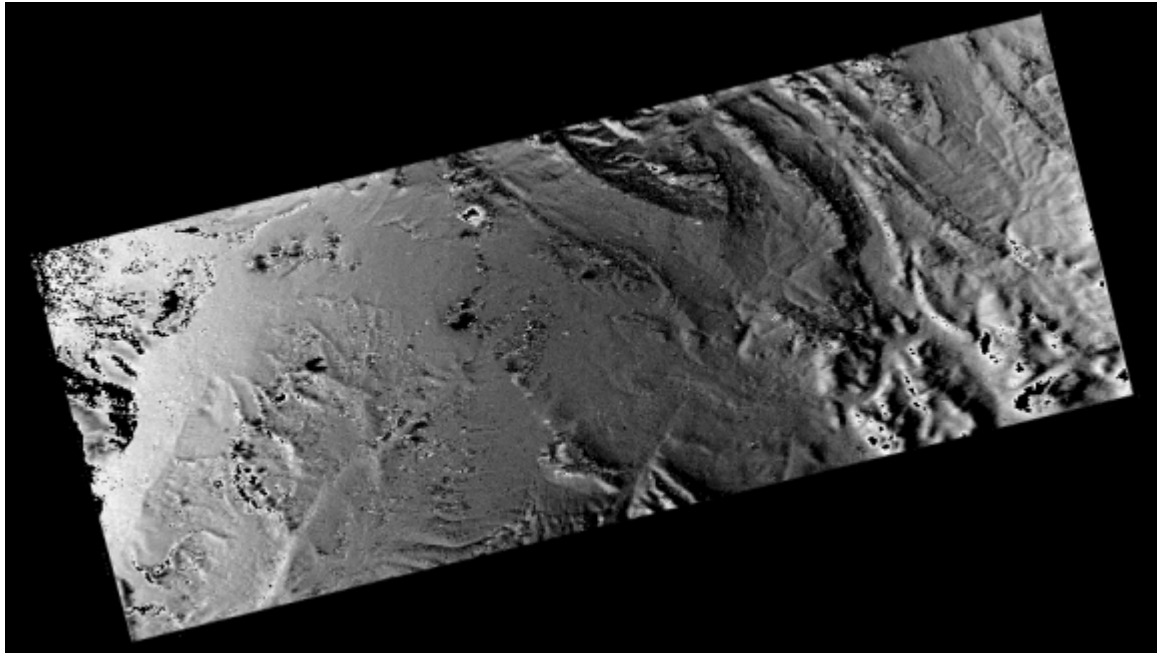


**Figure 6-15:** *Difference between the interferometrically derived and the reference DEM of the Lower Saxony area*

## 6.4 LIMITATIONS

The use of an error propagation model for the quality assessment of SAR interferometric data has its limitations although most of these do not originate from the model itself but the parameters that influence the acquired signal. If these effects are not corrected in one of the processing steps, the influence remains in all the subsequent results and is also not taken into account in the error propagation model. For example, the influence of atmospheric effects, the different backscatter behaviour due to various surface covers etc. are not modelled for. Also, systematic errors introduced by assumptions in the implemented algorithms are not included. The assumption that the input parameters are statistically independent has to be further investigated. In case of a significant correlation between the input parameters the proposed error propagation model needs to be adapted. The problem of an empirical approach such as the proposed one is the limited flexibility for interactive processing methods such as choosing tie points or correcting phase unwrapping results.

## 6.5 ADVANTAGES

Despite some limitations of the proposed method as discussed above, the biggest advantage of using an empirical approach for the quality assessment is its flexibility in the adaptation to different algorithms and software packages, since it needs only limited knowledge about the actual implementation of the algorithms. Besides the input parameters and their accuracies, no further knowledge about implemented algorithms is required.

Furthermore, the error propagation model provides a quality measure directly related to the data processing method. It allows the quantitative comparison of different algorithms for co-registration, filtering etc.

In addition to this, the error propagation model can give detailed information about specific objects in the data set as it enables a quality assessment at the pixel level, although this approach becomes time consuming in terms of processing speed for larger areas.

The chosen approach fits into the frame of spatial data quality with respect to lineage information (Guptill and Morrison, 1995). All the algorithms used during the data processing can be specified and can be attached as metadata to the interferometric product.

Finally, not being dependent on a reference data set can be advantageous, especially in areas where no suitable reference data sets of any kind are available.

## 7 CONCLUSIONS AND RECOMMENDATIONS

---

The results presented in this thesis represent the first systematic approach for the development of an alternative quality assessment procedure for SAR interferometric data based on error propagation. The approach generally used earlier was based on the comparison of the interferometric DEM with a reference data set. Because the quality and availability of suitable reference data cannot be guaranteed this approach can not always be followed.

The interferometric techniques, applications and processing have been reviewed and the orbits, the atmospheric effects, temporal and baseline decorrelation as well as the performance of the interferometric processing have been identified as potential error sources. Furthermore, the need for quality assessment of SAR interferometric data sets have been identified.

The input parameters for the interferometric processing such as the pulse repetition frequency, the range sampling rate, the azimuth and range bandwidths, the Doppler centroid frequency and the state vectors have been systematically investigated. Their impact on the interferometric products has been evaluated. For this purpose a sensitivity study has been carried out. This study has shown that the pulse repetition frequency and the range sampling rate are the most critical input parameters which are not corrected by the interferometric processing. The other input parameters given in the ERS leader file can be accounted for if the amount of change in the input parameters is large enough. A study on the influence of a combination of input parameters has indicated that a cross-correlation between some input parameters exists. The input parameters are, therefore, not statistically independent. Further research is needed to investigate the magnitude of the correlation and its dependence on coherence, surface characteristics etc.

The user requirements for potential applications using digital elevation models as input for further analysis have been investigated which showed a lack of quantitative study on the aspects of quality. It has also shown that an awareness of the quality aspect for DEMs as input for the various applications hardly exists.

A quality assessment has been carried out with all user requirements in mind and following a systematic, scientific approach. A detailed method for quality assessment has been worked out with due consideration to the theoretical background.

The theoretical background of error propagation has been provided and an empirical implementation of the error propagation model based on an adapted Monte Carlo simulation has been worked out.

The output of the error propagation model underlines the result of the sensitivity study. The main contribution in the error budget has come from the pulse repetition frequency and the range sampling rate. The influence of the orbit errors are less prominent but still significant. The error propagation model has been applied to results of two test sites. The results achieved emphasise different aspects. The size of the test site in Ningxia, China, is not sufficient to perform the quality assessment adequately. There is no relation to topographic feature visible in the error map. Comparing the estimated height accuracy with

the results of earlier studies (e.g. Zebker *et al.*, 1994b) show that the achieved result is too optimistic. For the second area in Lower Saxony, Germany, the result of the quality estimation with a standard deviation of 23.7 metres seems to be more realistic. The comparison to the reference DEM has indicated some of the general problems with the quality estimation of digital elevation models. In areas with forest cover, for example, the heights obtained from SAR interferometry and from terrestrial measurements are not comparable.

Basic information about technical specifications of available commercial and non-commercial software packages has been collected (Appendix A).

The SAR interferometric product should be accompanied by a metadata set containing detailed information about the data set itself and each single processing step. That should include information about the following aspects:

- data set identification (sensor, orbit, frame, date of acquisition, product etc.)
- length of baseline
- co-registration method (based on intensity, complex values or SNR)
- interpolation method used for resampling during the co-registration
- filtering methods applied
- phase unwrapping method used
- for DEM: map projection, grid size etc.

The developed approach should be seen as a first step for a further research in the field of quality assessment of SAR interferometric data in a systematic way. A number of issues have been considered in this study. Some of these need to be investigated in greater detail.

One interesting task is the definition of representative areas for which the quality assessment should be carried out. An area can be described in many different ways depending on the perspective and need.

After these representative areas are defined properly, user related quality measures such as a standard deviation for slope gradient etc. for a certain area of interest can be calculated based on the proposed error propagation approach. This aspect certainly needs more detailed knowledge about the user requirements which is still lacking in some of the applications. This means that there is also a need for further investigation of these aspects from the application side.

Another field of interest is the further investigation of the quality of processing algorithms in terms of accuracy and processing speed. At the moment, there is no generally accepted scheme used for the processing of SAR interferometric data in order to achieve optimal results. An artificial data set for the simulation of different scenarios within a controlled environment is a prerequisite for a systematic investigation of each single processing step. This synthetic data set can be used for several aspects.

For the continuation of the sensitivity study, the influence of each input parameter due to factors such as slope, land cover, noise etc. could be investigated.

Furthermore, a simulated data set allows a comparison of results with an absolute reference as the correct result is known beforehand. It allows for the introduction of

different error sources separately or in a combination. This enables conclusions to be derived about the interrelation among different error sources.

The approach of controlled scenarios based on simulated data can be used for checking models developed for corrections of some factors such as atmospheric effects etc.

This raises the question as to what kind of characteristics should a simulated data set have. Since most of the users of DEMs take the elevation model as basis for their application and often make use of the derivatives of the height, one aspect for the simulation is a representation of the different derivatives at various scales. Different terrain types can be simulated by using backscatter models developed by various institutes (e.g. Ulaby *et al.*, 1990). Noise as well as speckle can be introduced from various sources. Finally, the parameters which influence the viewing geometry also need to be included.

The results presented in this thesis have clearly shown that a systematic investigation in the field of quality assessment of SAR interferometric data is not only necessary and feasible but that many aspects related to this topic still require more research. The results have also indicated that further research in this line would be most rewarding in terms of the user requirements to produce digital elevation models by means of SAR interferometry at an operational level.



## REFERENCES

---

The references indicated with \* are available online on the World Wide Web.

ESA Fringe'96 Workshop in Zurich, Switzerland:

<http://www.geo.unizh.ch/rsl/fringe96/> .

Third ERS Symposium in Florence, Italy:

<http://florence97.ers-symposium.org/> .

---

ACKERMANN, F., 1961, Ein Verfahren zur programmgesteuerten Ausgleichung von Triangulationsstreifen. *Bildmessung und Luftbildwesen*, **36**, 108-123.

ACKERMANN, F., 1992, Operational rules and accuracy models for GPS-aerotriangulation. *International Archives of Photogrammetry and Remote Sensing*, **29** (B3), Washington, D.C., 691-700.

ACKERMANN, F., 1996a, Airborne laser scanning for elevation models. *International Journal for Geomatics*, **10** (10), 24-25.

ACKERMANN, F., 1996b, Techniques and strategies for DEM generation. in *Digital Photogrammetry: An Addendum to the Manual of Photogrammetry*, pp. 135-141.

ACKERMANN, F., 1996c, The status and accuracy performance of GPS photogrammetry. *Digital Photogrammetry: Addendum of the Manual of Photogrammetry*, pp. 108-114.

ACKERMANN, F., FRITSCH, D., HAHN, M., SCHNEIDER, F. and TSINGAS, V., 1995, Automatic generation of digital terrain models with MOMS-02/D2 data. *Proceedings of the MOMS-02 Symposium*, Cologne, Germany, pp. 79-86.

ADKINS, K.F. and MERRY, C.J., 1994, Accuracy assessment of elevation data sets using the global positioning system. *Photogrammetric Engineering and Remote Sensing*, **60**, 195-202.

AHUJA, R.K., MAGNANTI, T.L. and ORLIN, J.B., 1993, *Network flows: Theory, algorithms and applications*. (Englewood Cliffs:Prentice-Hall), 846 p.

AINSWORTH, T.L., CHUBB, S.R., FUSINA, R.A., GOLDSTEIN, R.M., JANSEN, R.W., LEE, J.-S. and VALENZUELA, G.R., 1995, INSAR Imagery of Surface Currents, Wave Fields, and Fronts. *IEEE Transactions on Geoscience and Remote Sensing*, **33**, 1117-1123.

AL-ROUSAN, N., CHENG, P., PETRIE, G., TOUTIN, TH. and VALADAN ZOEJ, M.J., 1997, Automated DEM extraction and orthoimage generation from SPOT Level 1B imagery. *Photogrammetric Engineering and Remote Sensing*, **63**, 965-974.

ARMOUR, B., 1997, Personal communication.

- ASKNE, J.I.H., DAMMERT, P.B.G., ULANDER, L.M.H. and SMITH, G., 1997, C-band repeat-pass interferometric SAR observations of the forest. *IEEE Transactions on Geoscience and Remote Sensing*, **35**, 25-35.
- BAO, M., BRÜNING, C. and ALPERS, W., 1997, Simulation of ocean waves imaging by an along-track interferometric synthetic aperture radar. *IEEE Transactions on Geoscience and Remote Sensing*, **35**, 618-631.
- BARMETTLER, A., PASQUALI, P., SMALL, D. and NÜESCH, D., 1996, Cross-compatibility of ERS-SLC products. *ESA Fringe'96 Workshop*, Zurich, Switzerland.\*
- BAUER, H. and MÜLLER, J., 1972, Height accuracy of blocks and bundle adjustment with additional parameters. *International Archives for Photogrammetry*, Commission III, Ottawa, Canada.
- BOLSTAD, P.V. and STOWE, T., 1994, An evaluation of DEM accuracy: Elevation, slope, and aspect. *Photogrammetric Engineering and Remote Sensing*, **60**, 1327-1332.
- BRIOLE, P., MASSONNET, D. and DELACOURT, C., 1997, Post-eruptive deformation associated with the 1986-87 and 1989 lava flows of Etna, detected by radar interferometry. *Geophysical Research Letters*, **24**, 37-40.
- BRUZZI, S., LOUET, J. and PFEIFFER, B., 1995, ENVISAT-1 system and mission. *Space Technology*, **15**, 145-155.
- BURROUGH, P.A., 1986, *Principles of geographical information systems for land resources assessment*. (Oxford:Clarendon Press), 194 p.
- CARANDE, R.E., 1994, Estimating ocean coherence time using dual-baseline interferometer synthetic aperture radar. *IEEE Transactions on Geoscience and Remote Sensing*, **32**, 846-854.
- CARRARA, A., BITELLI, G. and CARLA, R., 1997, Comparison of techniques for generating digital terrain models from contour lines. *International Journal of Geographical Information Science*, **11**, 451-473.
- CARRASCO, D., ALONSO, J. and BROQUETAS, A., 1995, Accuracy assessment of SAR interferometry using the ERS-1. *Proceedings of IGARSS '95*, Florence, Italy, pp. 781-783.
- CARRASCO, D., DÍAZ, J., BROQUETAS, A., ARBIOL, R., CASTILLO, M. and PALÀ, V., 1997, Ascending-descending orbit combination SAR interferometry assessment. *Proceedings of the Third ERS Symposium*, Florence, Italy.\*
- CHEN, P.-H. and DOWMAN, I., 1996, Space intersection from ERS-1 synthetic aperture radar images. *Photogrammetric Record*, **88**, 561-573.
- CLARKE, A.L., GRUEN, A. and LOON, J.C., 1982, The application of contour data for generating high fidelity grid digital elevation models. *Proceedings of AutoCarto V*, Falls Church, Virginia, pp. 381-400.

- COSTANTINI, M., 1996, A phase unwrapping method based on network programming. *ESA Fringe'96 Workshop*, Zurich, Switzerland.\*
- COULSON, S.N., 1993, SAR interferometry with ERS-1. *Earth Observation Quarterly*, **40**, 20-23.
- CUMMING, I. and HAWKINS, D., 1990, All-weather mapping with interferometric radar. *Proceedings of the 23rd International Symposium on Remote Sensing of Environment*, Bangkok, Thailand, pp. 1249-1262.
- DE COL, E., GRIFFITHS, S., THORNTON, S., COMIN, L., SPOERING, T. and IRVING, R.E.L., 1997, Digital elevation model (DEM) extraction from stereo RADARSAT. *Proceedings of the Twelfth International Conference and Workshops on Applied Geologic Remote Sensing*, Denver, Colorado, Vol. II, p. 485-493.
- DE FAZIO, M. and VINELLI, F., 1993, DEM reconstruction in SAR interferometry: Practical experiences with ERS-1 SAR data. *Proceedings of IGARSS '93*, Tokyo, Japan, pp. 1207-1209.
- DOWMAN, I., TWU, Z.-G. and PU-HUAI, C., 1997, DEM generation from stereoscopic SAR data. *International Symposium Geomatics in the Era of RADARSAT*, Ottawa, Canada. (<http://www.ccrs.nrcan.gc.ca/ger97/ger97fme.html>)
- EVANS, D.L., FARR, T.G., ZEBKER, H.A. and MOUGINIS-MARK, P.J., 1992, Radar interferometry studies of the earth's topography. *EOS, Transactions, American Geophysical Union*, **73**, 553, 557-558.
- EVANS, I.S., 1980, An integrated system of terrain analysis and slope mapping. in Hagedorn, H. and Thomas, M. (eds.) *Zeitschrift für Geomorphologie*, Supplementband 36, Perspectives in geomorphology, pp. 274-295.
- FALLER, N.P. and MEIER, E.H., 1995, First results with the airborne single-pass DO-SAR interferometer. *IEEE Transactions on Geoscience and Remote Sensing*, **33**, 1230-1237.
- FEIGL, K.L., SERGENT, A. and JACQ, D., 1995, Estimation of an earthquake focal mechanism from a satellite radar interferogram: Application to the December 4, 1992 Landers after shock. *Geophysical Research Letters*, **22**, 1037-1040.
- FERNANDES, M.J., 1993, *Precise satellite orbit determination with particular application to ERS-1*. Doctoral thesis, University College of London, 301 p.
- FERRETTI, A., MONTI GUARNIERI, A., PRATI, C. and ROCCA, F., 1996, Multi-baseline interferometric techniques and applications. *ESA Fringe'96 Workshop*, Zurich, Switzerland.\*
- FERRETTI, A., MONTI GUARNIERI, A., PRATI, C. and ROCCA, F., 1997, Multi-baseline SAR interferometry for automatic DEM reconstruction. *Proceedings of the Third ERS Symposium*, Florence, Italy.\*

- FIELDING, E.J., BLOM, R.G. and GOLDSTEIN, R.M., 1997, Detection and monitoring of rapid subsidence over Lost Hills and Belridge oil fields by SAR interferometry. *Proceedings of the Twelfth International Conference and Workshops on Applied Geologic Remote Sensing*, Denver, Colorado, Vol. I, p. 84.
- FINSTERWALDER, R., 1952, *Photogrammetrie*. (Berlin:De Gruyter), 377 p.
- FLOOD, M. and GUTELIUS, B., 1997, Commercial implications of topographic terrain mapping using scanning airborne laser radar. *Photogrammetric Engineering and Remote Sensing*, **63**, 327-329, 363-366.
- FRANCESCHETTI, G., IODICE, A., MIGLIACCIO, M. and RICCIO, D., 1996, On the baseline decorrelation. *Proceedings of IGARSS '96*, Lincoln, Nebraska, pp. 680-682.
- FRANCIS, C.R., GRAF, G., EDWARDS, P.G., MCCAIG, M., MCCARTHY, C., LEFEBVRE, A., PIEPER, B., POUVREAU, P.-Y., WALL, R., WESCHLER, F., LOUET, J., SCHUMANN, W. and ZOBL, R., 1995, The ERS-2 Spacecraft and its Potential. *ESA bulletin*, **83**, 13-31.
- FREI, U., GRAF, K.C. and MEIER, E., 1993, Cartographic reference systems. In Schreier, G. (ed.) *SAR Geocoding: Data and Systems*. (Karlsruhe:Wichmann), pp. 213-234.
- FRIED, D.L., 1977, Least-squares fitting a wave-front distortion estimate to an array of phase-difference measurements. *Journal of the Optical Society of America*, **67**, 370-375.
- GABRIEL, A.K. and GOLDSTEIN, R.M., 1988, Crossed orbit interferometry: Theory and experimental results from SIR-B. *International Journal of Remote Sensing*, **9**, 857-872.
- GABRIEL, A.K., GOLDSTEIN, R.M. and ZEBKER, H.A., 1989, Mapping small elevation changes over large areas: Differential radar interferometry. *Journal of Geophysical Research*, **94** (B7), 9183-9191.
- GATELLI, F., MONTI GUARNIERI, A., PARIZZI, F., PASQUALI, P., PRATI, C. and ROCCA, F., 1994, The wavenumber shift in SAR interferometry. *IEEE Transactions on Geoscience and Remote Sensing*, **32**, 855-864.
- GENS, R. and GENDEREN, J.L. VAN, 1996a, An approach to Error Propagation Modeling of SAR interferometric data. *ESA Fringe'96 Workshop*, Zurich, Switzerland.\*
- GENS, R. and GENDEREN, J.L. VAN, 1996b, SAR interferometry - issues, techniques, applications. *International Journal of Remote Sensing*, **17**, 1803-1835.
- GEUDTNER, D., 1995, *Die interferometrische Verarbeitung von SAR-Daten des ERS-1*. Doctoral thesis, University of Stuttgart, DLR-Forschungsbericht 95-28, 141 p.
- GHIGLIA, D.C. and ROMERO, L.A., 1994, Robust two-dimensional weighted and unweighted phase unwrapping that uses fast transform and iterative methods. *Journal of the Optical Society of America A*, **11**, 107-117.

- GILES, P.T. and FRANKLIN, S.E., 1996, Comparison of derivative topographic surfaces of a DEM generated from stereoscopic SPOT images with field measurements. *Photogrammetric Engineering and Remote Sensing*, **62**, 1165-1171.
- GOBLIRSCH, W., WERNER, C., NÜESCH, D. and FALLER, N., 1995, Accuracy of interferometric elevation models generated from DOSAR airborne data. *Proceedings of IGARSS '95*, Florence, Italy, pp. 770-774.
- GOLDSTEIN, R.M., 1995, Atmospheric limitations to repeat-track radar interferometry. *Geophysical Research Letters*, **22**, 2517-2520.
- GOLDSTEIN, R.M. and ZEBKER, H.A., 1987, Interferometric radar measurement of ocean surface currents. *Nature*, **328**, 707-709.
- GOLDSTEIN, R.M., BARNETT, T.P. and ZEBKER, H.A., 1989, Remote sensing of ocean currents. *Science*, **246**, 1282-1285.
- GOLDSTEIN, R.M., ENGELHARDT, H., KAMB, B. and FROLICH, R.M., 1993, Satellite radar interferometry for monitoring ice sheet motion: Application to an Antarctic ice stream. *Science*, **262**, 1525-1530.
- GOLDSTEIN, R.M., ZEBKER, H.A. and WERNER, C.L., 1988, Satellite radar interferometry: Two-dimensional phase unwrapping. *Radio Science*, **23**, 713-720.
- GRÅBAK, O., 1995, *SAR products CCT format specifications, Annex C, SAR SLC CCT and exabyte format specifications*. ESA report ES-IS-EPO-GS-5902.3.
- GRAHAM, L.C., 1974, Synthetic interferometer radar for topographic mapping. *Proceedings of the IEEE*, **62**, 763-768.
- GRAY, A.L. and FARRIS-MANNING, P.L., 1993, Repeat-pass interferometry with airborne synthetic aperture radar. *IEEE Transactions on Geoscience and Remote Sensing*, **31**, 180-191.
- GRAY, A.L., MATTAR, K.E. and FARRIS-MANNING, P.J., 1992, Airborne SAR interferometry for terrain elevation. *Proceedings of IGARSS '92*, Houston, Texas, pp.1589-1591.
- GROSSMANN, W., 1969, *Grundzüge der Ausgleichsrechnung nach der Methode der kleinsten Quadrate nebst Anwendung in der Geodäsie*. (Berlin: Springer-Verlag), 425 p.
- GUERRE, L.-F., HIRSCHFELD, A., DEMARGE, L. and FOUCHER, C., 1996, The digital elevation model market: Current situation and perspectives. *ESA Fringe'96 Workshop*, Zurich, Switzerland.\*
- GUPTILL, S.C. AND MORRISON, J.L., 1995, *Elements of spatial data quality*. (Oxford:Elsevier Science), 202 p.

- HAGBERG, J.O. and ULANDER, L.M.H., 1993, On the optimization of interferometric SAR for topographic mapping. *IEEE Transactions on Geoscience and Remote Sensing*, **31**, 303-306.
- HAGBERG, J.O., ULANDER, L.M.H. and ASKNE, J., 1995, Repeat-pass SAR interferometry over forested terrain. *IEEE Transactions on Geoscience and Remote Sensing*, **33**, 331-340.
- HALSEMA, D. VAN, KOOIJ, M.W.A. VAN DER, GROENEWOUD, W., HUISING, J., AMBROSIUS, B.A.C. and KLEES, R., 1995, SAR interferometrie in Nederlands. *Remote Sensing Nieuwsbrief*, Juni 1995, pp. 31-34.
- HAMMERLEY, J.M. and HANDSCOMB, D.C., 1979, *Monte Carlo methods*. (London:Chapman and Hall), 178 p.
- HARTL, PH. and THIEL, K.-H., 1993, Bestimmung von topographischen Feinstrukturen mit interferometrischem ERS-1-SAR. *Zeitschrift für Photogrammetrie und Fernerkundung*, **3**, 108-113.
- HARTL, PH. and WU, X., 1993, SAR interferometry: Experiences with various phase unwrapping methods. *Proceedings of the Second ERS-1 Symposium*, Hamburg, Germany, pp. 727-732.
- HARTL, PH. and XIA, Y., 1993, Besonderheiten der Datenverarbeitung bei der SAR-Interferometrie. *Zeitschrift für Photogrammetrie und Fernerkundung*, **3**, 214-222.
- HARTL, PH., REICH, M., THIEL, K.-H. and XIA, Y., 1992, SAR-interferometry applying ERS-1 - some preliminary test results -. *Proceedings of the First ERS-1 Symposium*, Cannes, France, pp. 219-222.
- HARTL, PH., THIEL, K.-H., WU, X., DOAKE, CH. and SIEVERS, J., 1994, Application of SAR interferometry with ERS-1 in the Antarctic. *Earth Observation Quarterly*, **43**, 1-4.
- HEISKANEN, W.A. and MORITZ, H., 1990, *Physical Geodesy*. Reprint, Institute of Physical Geodesy, Technical University Graz, Austria.
- HEUVELINK, G.B.M., 1993, *Error propagation in quantitative spatial modelling - Applications in geographical information systems*. Doctoral thesis, University of Utrecht, 151 p.
- HOLECZ, F., MEIER, E., PIESBERGEN, J., NÜESCH, D. AND MOREIRA, J., 1994, Rigorous derivation of backscattering coefficient. *Proceedings of CEOS SAR Calibration Workshop*, Ann Arbor, Michigan, pp. 143-155.
- HORN, B.K.P., 1981, Hill shading and the reflectance map. *Proceedings of the IEEE*, **69**, 14.
- HOSS, H., 1996, DTM derivation with laser scanner data. *International Journal for Geomatics*, **10** (10), 28-31.

- HUDGIN, R.H., 1977, Wave-front reconstruction for compensated imaging. *Journal of the Optical Society of America*, **67**, 375-378.
- JACOBSEN, K., 1982, Attempt at obtaining the best possible accuracy in bundle block adjustment. *Photogrammetria*, **37**, 219-235.
- JACOBSEN, K., 1997, Calibration of IRS-1C PAN camera. *Proceedings of the ISPRS workshop 'Sensors and Mapping from Space'*, Hannover, Germany, (in press).
- JACOBSEN, K. and SCHMITZ, M., 1996, A new approach of combined block adjustment using GPS-satellite constellation. *International Archives of Photogrammetry and Remote Sensing*, **31** (B3), 355-359.
- JOUGHIN, I.R., KWOK, R. and FAHNESTOCK, M.A., 1996a, Estimation of ice-sheet motion using satellite radar interferometry - method and error analysis with application to Humboldt glacier, Greenland. *Journal of Glaciology*, **42**, 564-575.
- JOUGHIN, I.R., WINEBRENNER, D.P. and FAHNESTOCK, M.A., 1995, Observation of ice-sheet motion in Greenland using satellite radar interferometry. *Geophysical Research Letters*, **22**, 571-574.
- JOUGHIN, I.R., WINEBRENNER, D.P., FAHNESTOCK, M.A., KWOK, R. and KRABILL, W., 1996b, Measurement of ice-sheet topography using satellite-radar interferometry. *Journal of Glaciology*, **42**, 10-22.
- JUST, D. and BAMLER, R., 1994, Phase statistics of interferograms with applications to synthetic aperture radar. *Applied Optics*, **33**, 4361-4368.
- KAPLAN, E.D. (ED.), 1996, *Understanding GPS: Principles and applications*. (London:Artech House), 554 p.
- KOLOUCH, D., 1983, *Geometrische Auswertung von Sonarbildern und Interferometeraufnahmen mit Hilfe digitaler Bildverarbeitung*. Doctoral thesis, University of Hannover, Germany.
- KONECNY, G. and LEHMANN, G., 1984, *Photogrammetrie*. (Berlin:de Gruyter), 4. edition, 392 p.
- KONECNY, G., LOHMANN, P., ENGEL, H. and KRUCK, E., 1987, Evaluation of SPOT imagery on analytical photogrammetric instruments. *Photogrammetric Engineering and Remote Sensing*, **53**, 1223-1230.
- KOOIJ, M.W.A. VAN DER, HALSEMA, D. VAN, GROENEWOUD, W., METS, G.J., OVERGAAUW, B. and VISSER, P., 1995, *SAR land subsidence monitoring*. Dutch Remote Sensing Board, NRSP-2 95-13.
- KOPPE, C., 1902, Die neue topographische Landeskarte des Herzogtums Braunschweig. *Zeitschrift für Vermessungswesen*, **31**, 397-424.
- KRAMER, H.J., 1994, *Observation of the Earth and its environment*, second edition. (Berlin:Springer), 580 p.

- KWOH, L.K., CHANG, E.C., HENG, W.C.A. and LIM, H., 1994, DTM generation from 35-day repeat pass ERS-1 interferometry. *Proceedings of IGARSS '94*, Pasadena, California, pp. 2288-2290.
- KWOK, R. and FAHNESTOCK, M.A., 1996, Ice sheet motion and topography from radar interferometry. *IEEE Transactions on Geoscience and Remote Sensing*, **34**, 189-200.
- LAGACHERIE, PH., MOUSSA, R., CORMARY, D. and MOLENAT, J., 1996, Effects of DEM data source and sampling pattern on topographical parameters and on a topography-based hydrological model. *Proceedings of HydroGIS '96 'Application on Geographic Information Systems in Hydrology and Water Resources Management'*, Vienna, Austria, pp. 191-199.
- LANARI, R., FORNARO, G., RICCIO, D., MIGLIACCIO, M., PAPATHANASSIOU, K.P., MOREIRA, J.R., SCHWÄBISCH, M., DUTRA, L., PUGLISI, G., FRANCESCHETTI, G. and COLTELLI, M., 1996, Generation of digital elevation models by using SIR-C/X-SAR multifrequency two-pass interferometry: The Etna case study. *IEEE Transactions on Geoscience and Remote Sensing*, **34**, 1097-1115.
- LEBERL, F.W., 1990, *Radargrammetric Image Processing*. (Boston:Artech House), 590 p.
- LEBERL, F.W., DOMIK, G., RAGGAM, J. and KOBRICK, M., 1986, Radar stereomapping techniques and application to SIR-B images of Mt. Shasta. *IEEE Transactions on Geoscience and Remote Sensing*, **24**, 473-481.
- LEE, J. and CHU, CH.-J., 1996, Spatial structures of digital terrain models and hydrological feature extraction. *Proceedings of HydroGIS '96 'Application on Geographic Information Systems in Hydrology and Water Resources Management'*, Vienna, Austria, pp. 201-206.
- LEMMENS, M.J.P.M., 1992, *Image matching strategies for the co-registration of CAESAR sea images: An hierarchical area-based approach*. Dutch Remote Sensing Board, NRSP-1 90-40b.
- LI, F.K. and GOLDSTEIN, R.M., 1990, Studies of multibaseline spaceborne interferometric synthetic aperture radars. *IEEE Transactions on Geoscience and Remote Sensing*, **28**, 88-96.
- LI, Z., 1994, A comparative study of the accuracy of digital terrain models (DTMs) based on various models. *ISPRS Journal of Photogrammetry and Remote Sensing*, **49**, 2-11.
- LIN, Q., VESECKY, J.F. and ZEBKER, H.A., 1992, New approaches in interferometric SAR data processing. *IEEE Transactions on Geoscience and Remote Sensing*, **30**, 560-567.
- LIN, Q., VESECKY, J.F. and ZEBKER, H.A., 1994, Comparison of elevation derived from InSAR data with DEM over large relief terrain. *International Journal of Remote Sensing*, **15**, 1775-1790.



- MADSEN, S.N., MARTIN, J.M. and ZEBKER, H.A., 1995, Analysis and evaluation of the NASA/JPL TOPSAR across-track interferometric SAR system. *IEEE Transactions on Geoscience and Remote Sensing*, **33**, 383-391.
- MADSEN, S.N., ZEBKER, H.A. and MARTIN, J., 1993, Topographic mapping using radar interferometry: Processing techniques. *IEEE Transactions on Geoscience and Remote Sensing*, **31**, 246-256.
- MASSONNET, D. and FEIGL, K.L., 1995, Discrimination of geophysical phenomena in satellite radar interferograms. *Geophysical Research Letters*, **22**, 1537-1540.
- MASSONNET, D., BRIOLE, P. and ARNAUD, A., 1995, Deflation of Mount Etna monitored by spaceborne radar interferometry. *Nature*, **375**, 567-570.
- MASSONNET, D., FEIGL, K., ROSSI, M. and ADRAGNA, F., 1994, Radar interferometric mapping of deformation in the year after the Landers earthquake. *Nature*, **369**, 227-230.
- MASSONNET, D., FEIGL, K.L. and ROSSI, M., 1996, Coseismic deformation field of the M=6.7 Northridge, California earthquake of January 17, 1994 recorded by two radar satellites using interferometry. *Geophysical Research Letters*, **23**, 969-972.
- MASSONNET, D., ROSSI, M., CARMONA, C., ADRAGNA, F., PELTZER, G., FEIGL, K. and RABAUTE, T., 1993, The displacement field of the Landers earthquake mapped by radar interferometry. *Nature*, **364**, 138-142.
- MEASURES, R., 1984, *Laser remote sensing*. (Malabar:Kreiger Publishing), 510 p.
- MEIER, E., FREI, U. and NÜESCH, D., 1993, Precise terrain corrected geocoded images. In Schreier, G. (ed.) *SAR Geocoding: Data and Systems*. (Karlsruhe:Wichmann), pp. 173-185.
- MERCER, J.B., GRIFFITHS, S. and THORNTON, S., 1994, Large area topographic mapping using stereo SAR. *Proceedings of the First International Airborne Remote Sensing Conference*, Strasbourg, France, Vol. I, pp. 269-280.
- MOCCIA, A. and VETRELLA, S., 1992, A tethered interferometric synthetic aperture radar (SAR) for a topographic mission. *IEEE Transactions on Geoscience and Remote Sensing*, **30**, 103-109.
- MOCCIA, A., VETRELLA, S. and D'ERRICO, M., 1995, Twin satellite orbital and doppler parameters for global topographic mapping. *EARSeL Advances in Remote Sensing - Topography from Space*, **4** (2), 55-66.
- MOREIRA, J., SCHWÄBISCH, M., FORNARO, G., LANARI, R., BAMLER, R., JUST, D., STEINBRECHER, U., BREIT, H., EINEDER, M., FRANCESCHETTI, G., GEUDTNER, D. and RINKEL, H., 1995, X-SAR interferometry: First results. *IEEE Transactions on Geoscience and Remote Sensing*, **33**, 950-956.
- MORRISON, J.L., 1995, Spatial data quality. in Guptill, S.C. and Morrison, J.L. (eds.) *Elements of spatial data quality*, (Oxford:Elsevier Science), pp. 1-12.

- MOUGINIS-MARK, P.J. and GARBEIL, H., 1993, Digital topography of volcanoes from radar interferometry: An example from Mt Vesuvius, Italy. *Bulletin Volcanologique*, **55**, 566-570.
- MURAKAMI, M., TOBITA, M., FUJIWARA, S., SAITO, T. and MASAHARU, H., 1996, Coseismic crustal deformations of 1994 Northridge, California, earthquake detected by interferometric JERS-1 synthetic aperture radar. *Journal of Geophysical Research*, **101** (B4), 8605-8614.
- ORWIG, L.P. and HELD, D.N., 1992, Interferometric ocean surface mapping and moving object relocation with a Norden systems Ku-band SAR. *Proceedings of IGARSS '92*, Houston, Texas, pp. 1598-1600.
- PASQUALI, P., 1995, *Generazione di Mappe Altimetriche con Interferometria SAR*. Doctoral thesis, Politecnico di Milano.
- PELTZER, G. and ROSEN, P., 1995, Surface displacement of the 17th May 1993, Eureka Valley, California, earthquake observed by SAR Interferometry. *Science*, **268**, 1333-1336.
- PELTZER, G., HUDNUT, K.W. and FEIGL, K.L., 1994, Analysis of coseismic surface displacement gradients using radar interferometry: New insights into the Landers earthquake. *Journal of Geophysical Research*, **99** (B11), 21971-21981.
- POLIDORI, L., GUILLANDE, R., KASSER, M. and RUDANT, J.-P., 1994, Airborne SAR for small terrain changes detection: A simulation-based evaluation. *Proceedings of the First International Airborne Remote Sensing Conference*, Strasbourg, France, Vol. I, pp. 643-650.
- PRATI, C. and ROCCA, F., 1990, Limits to the resolution of elevation maps from stereo SAR images. *International Journal of Remote Sensing*, **11**, 2215-2235.
- PRATI, C., ROCCA, F. and MONTI GUARNIERI, A., 1992, SAR interferometry experiments with ERS-1. *Proceedings of the First ERS-1 Symposium*, Cannes, France, pp. 211-218.
- PRITT, M.D., 1996, Phase Unwrapping by Means of Multigrid Techniques for Interferometric SAR. *IEEE Transactions on Geoscience and Remote Sensing*, **34**, 728-738.
- RAGGAM, H. and ALMER, A., 1996, Assessment of the potential of JERS-1 for relief mapping using optical and SAR data. *International Archives of Photogrammetry and Remote Sensing*, **23** (B4), 671-676.
- REIGBER, C., XIA, Y., KAUFMANN, H., MASSMANN, F.-H., TIMMEN, L., BODECHTEL, J. and FREI, M., 1996, Impact of Precise Orbits on SAR Interferometry. *ESA Fringe'96 Workshop*, Zurich, Switzerland.\*

- RENOUARD, L., PERLANT, F. and NONIN, 1995, Comparison of DEM generation from SPOT stereo and ERS interferometric SAR data. *EARSeL Advances in Remote Sensing - Topography from Space*, **4** (2), 103-109.
- RIGNOT, E., 1996, Tidal motion, ice velocity, and melt rate of Petermann Gletscher, Greenland, measured from radar interferometry. *Journal of Glaciology*, **42**, 476-485.
- ROGERS, A.E.E. and INGALLS, R.P., 1969, Venus: Mapping the surface reflectivity by radar interferometry. *Science*, **165**, 797-799.
- ROSSI, M., ROGRON, B. and MASSONNET, D., 1996, JERS-1 SAR image quality and interferometric potential. *IEEE Transactions on Geoscience and Remote Sensing*, **34**, 824-827.
- SAMSON, J., 1996, *Coregistration in SAR interferometry*. MSc thesis, Technical University Delft, the Netherlands.
- SASOWSKY, K.C., PETERSEN, G.W. and EVANS, B.M., 1992, Accuracy of SPOT digital elevation model and derivatives: Utility for Alaska's north slope. *Photogrammetric Engineering and Remote Sensing*, **58**, 815-824.
- SCHERMERHORN, W., 1960, History and development of aerial triangulation. *Bolletino di geodesia e scienze affini*, **19** (4), 713-736.
- SCHARROO, R. AND VISSER, P.N.A.M, 1997, ERS Tandem Mission orbits: is 5 cm still a challenge?. *Proceedings of the Third ERS Symposium*, Florence, Italy.\*
- SCHWÄBISCH, M., 1995, *Die SAR-Interferometrie zur Erzeugung digitaler Geländemodelle*. Doctoral thesis, University of Stuttgart, DLR-Forschungsbericht 95-25, 125 p.
- SCHWÄBISCH, M. and WINTER, R., 1995, Erzeugung digitaler Geländemodelle mit Methoden der SAR-Interferometrie. *DLR-Nachrichten*, Heft 79 (August 1995), pp. 20-24.
- SCHWÄBISCH, M., KNÖPFLE, W., MATSCHKE, M. and ROTH, A., 1996, Quality Assessment of InSAR-Derived DEMs Generated with ERS Tandem Data. *Proceedings of the Progress in Electromagnetic Research Symposium (PIERS '96)*, Innsbruck, Austria, pp. 802-804.
- SCHWÄBISCH, M., LEHNER, S. and WINKEL, N., 1997, Coastline extraction using ERS SAR interferometry. *Proceedings of the Third ERS Symposium*, Florence, Italy.\*
- SEEBER, G., 1993, *Satellite geodesy: Foundations, methods, and applications*. (Berlin: de Gruyter), 531 p.
- SHEMER, L., MAROM, M. and MARKMAN, D., 1993, Estimates of currents in the nearshore ocean region using interferometric synthetic aperture radar. *Journal of Geophysical Research*, **98** (C4), 7001-7010.

- SKIDMORE, A.K., 1989, A comparison of techniques for calculating gradient and aspect from a gridded digital elevation model. *International Journal of Geographic Information Systems*, **3**, 323-334.
- SMALL, D., MEIER, E., WEGMÜLLER, U. and NÜESCH, D., 1994, Applications of geocoded ERS-1 InSAR-derived digital terrain information. *Proceedings of CEOS SAR Calibration Workshop*, Ann Arbor, Michigan, pp. 184-190.
- SMALL, D., PASQUALI, P. and FÜGLISTALER, S., 1996, A comparison of phase to height conversion methods for SAR interferometry. *Proceedings of IGARSS '96*, Lincoln, Nebraska, pp. 342-344.
- SMALL, D., WERNER, C.L. and NÜESCH, D., 1993, Baseline modelling for ERS-1 SAR interferometry. *Proceedings of IGARSS '93*, Tokyo, Japan, pp. 1204-1206.
- SMALL, D., WERNER, C.L. and NÜESCH, D., 1995, Geocoding and validation of ERS-1 InSAR derived digital elevation models. *EARSeL Advances in Remote Sensing - Topography from Space*, **4** (2), 26-39.
- SOLAAS, G.A., 1994, *ERS-1 interferometric baseline algorithm verification*. ESA technical report ES-TN-DPE-OM-GS02.
- SOLAAS, G.A., GATELLI, F. and CAMPBELL, G., 1996, *Initial testing of ERS tandem data quality for InSAR applications*. ESA technical report.
- STEVENS, D.R., CUMMING, I.G. and GRAY, A.L., 1995, Options for airborne interferometric SAR motion compensation. *IEEE Transactions on Geoscience and Remote Sensing*, **33**, 409-419.
- STEVENS, N.F., MORLEY, J.G., MULLER, J.-P., MURRY, J.B., UPTON, M. and WAGDE, G., 1997, The volume and morphology of lava flows from orbital radar interferometry. *Proceedings of the 23rd Annual Conference and Exhibition of the Remote Sensing Society*, Reading, United Kingdom, pp. 66-71.
- TAKAJO, H. and TAKAHASHI, T., 1988, Noniterative method for obtaining the exact solution for the normal equation in least-squares phase estimation from the phase difference. *Journal of the Optical Society of America A*, **5**, 1818-1827.
- TARAYRE, H. and MASSONNET, D., 1994, Effects of a refractive atmosphere on interferometric processing. *Proceedings of IGARSS '94*, Pasadena, California, pp. 717-719.
- TARAYRE, H. and MASSONNET, D., 1996, Atmospheric propagation heterogeneities revealed by ERS-1 interferometry. *Geophysical Research Letters*, **23**, 989-992.
- THOMPSON, D.R. and JENSEN, J.R., 1993, Synthetic aperture radar interferometry applied to ship-generated internal waves in the 1989 Loch Linhe experiment. *Journal of Geophysical Research*, **98** (C6), 10259-10269.
- TORGE, W., 1991, *Geodesy*. (Berlin:de Gruyter), 264 p.

- TOUTIN, TH., 1985, *Analyse mathématique des possibilités cartographiques du système SPOT*. Doctoral thesis, Ecole Nationale des Sciences Géographiques, Paris.
- TREUHAFT, R.N., MADSEN, S.N., MOGHADDAM, M. and ZYL, J.J. VAN, 1997, Vegetation characteristics and underlying topography from interferometric radar. *Radio Science*, **31**, 1449-1485.
- TREVETT, J.W., 1986, *Imaging radar for resources surveys*. (London:Chapman&Hall), 313 p.
- ULABY, F.T., SARABANDI, K., McDONALD, K., WHITT, M. and DOBSEN, M.C., 1990, Michigan microwave canopy scattering model. *International Journal of Remote Sensing*, **11**, 1223-1253.
- USGS, 1997, *Standards for digital elevation models*. Technical instructions.  
([http://mapping.usgs.gov/www/ti/DEM/standards\\_dem.html](http://mapping.usgs.gov/www/ti/DEM/standards_dem.html)).
- VACHON, P.W., GEUDTNER, D., GRAY, A.L. and TOUZI, R., 1995, ERS-1 synthetic aperture radar repeat-pass interferometry studies: Implications for RADARSAT. *Canadian Journal of Remote Sensing*, **21**, 441-454.
- VAUGHAN, C.R., BUFTON, J.L., KRABILL, W.B. and RABINE, D., 1996, Georeferencing of airborne laser altimeter measurements. *International Journal of Remote Sensing*, **17**, 2185-2200.
- WADGE, G., ACHACHE, J., FERRETTI, A., FRANCIS, P.W., MORLEY, J., MULLER, J.-P., MURRAY, J.B., PRATI, C., ROCCA, F., STEVENS, N.F., UPTON, M. and WILLIAMS, C.A., 1997, Volcano monitoring using interferometric SAR. *Proceedings of the Third ERS Symposium*, Florence, Italy.\*
- WEGMÜLLER, U., 1996, The potential of ERS SAR interferometry for hydrology. In Parlow, E. (ed.) *Progress in environmental remote sensing research and applications* (Rotterdam:A.A.Balkema), pp. 319-324.
- WEGMÜLLER, U. and WERNER, C.L., 1995, SAR interferometric signatures of forest. *IEEE Transactions on Geoscience and Remote Sensing*, **33**, 1153-1161.
- WEGMÜLLER, U. and WERNER, C.L., 1997, Retrieval of vegetation parameters with SAR interferometry. *IEEE Transactions on Geoscience and Remote Sensing*, **35**, 18-24.
- WERNER, C.L., HENSLEY, S., GOLDSTEIN, R.M., ROSEN, P.A. and ZEBKER, H.A., 1992, Techniques and applications of SAR interferometry for ERS-1: Topographic mapping, change detection and slope measurement. *Proceedings of the First ERS-1 Symposium*, Cannes, France, pp. 205-210.
- WERNER, M., 1997, X-SAR/SRTM - a spaceborne single-pass interferometric SAR. *Proceedings of the ISPRS workshop 'Sensors and Mapping from Space'*, Hannover, Germany, (in press).
- WILDLEY, R.L., 1984, Topography from single radar images. *Science*, **224**, 153-156.

- WILDLEY, R.L., 1986, Radarclinometry for the Venus radar mapper. *Photogrammetric Engineering and Remote Sensing*, **52**, 41-50.
- WOOD, J.D. and FISHER, P.F., 1993, Assessing interpolation accuracy in elevation models. *IEEE Computer Graphics and Applications*, **13** (2), 48-56.
- ZEBKER, H.A. and GOLDSTEIN, R.M., 1986, Topographic mapping from interferometry synthetic aperture radar observations. *Journal of Geophysical Research*, **91** (B5), 4993-4999.
- ZEBKER, H.A. and VILLASENOR, J., 1992, Decorrelation in interferometric radar echoes. *IEEE Transactions on Geoscience and Remote Sensing*, **30**, 950-959.
- ZEBKER, H.A., MADSEN, S.N., MARTIN, J., WHEELER, K.B., MILLER, T., LOU, Y., ALBERTI, G., VETRELLA, S. and CUCCI, A., 1992, The TOPSAR interferometric radar topographic mapping instrument. *IEEE Transactions on Geoscience and Remote Sensing*, **30**, 933-939.
- ZEBKER, H.A., ROSEN, P.A. and HENSLEY, S., 1997, Atmospheric effects in interferometric synthetic aperture radar surface deformation and topographic mapping. *Journal of Geophysical Research*, **102** (B4), 7547-7563.
- ZEBKER, H.A., ROSEN, P.A., GOLDSTEIN, R.M., GABRIEL, A. and WERNER, C.L., 1994a, On the derivation of coseismic displacement fields using differential radar interferometry: The Landers earthquake. *Journal of Geophysical Research*, **99** (B10), 19617-19634.
- ZEBKER, H.A., ROSEN, P.A., HENSLEY, S. and MOUGINIS-MARK, P.J., 1996, Analysis of active lava flows on Kilauea volcano, Hawaii, using SIR-C radar correlation measurements. *Geology*, **24**, 495-498.
- ZEBKER, H.A., WERNER, C.L., ROSEN, P.A. and HENSLEY, S., 1994b, Accuracy of topographic maps derived from ERS-1 interferometric radar. *IEEE Transactions on Geoscience and Remote Sensing*, **32**, 823-836.
- ZHANG, W. and MONTGOMERY, D.R., 1994, Digital elevation model grid size, landscape representation, and hydrologic simulations. *Water Resources Research*, **30**, 1019-1028.

# INDEX

---

- Accuracy, 50
- Across-track interferometry, 12
- Advanced SAR, 22
- Aerial photogrammetry, 41–42
- Airborne interferometry
  - Across-track interferometry, 12
  - Along-track interferometry, 13
  - Change detection, 21
  - First practical study, 5
  - Motion compensation, 14
  - Ocean currents, 20
- AIRSAR system, 29
- Along-track interferometry, 13
- Amplitude, 8, 27
- Applications
  - Change detection, 21
  - Coastal zones, 22
  - Digital elevation modelling, 19
  - Forestry, 21
  - Hydrology, 22
  - Ocean currents, 20
  - Polar research, 20
  - Potential applications, 6, 18
  - Seismic events, 20
  - Suitable baseline, 10–11
  - Surface movements, 20–21
  - Topographic mapping, 5, 6, 19
  - Volcanic hazards, 21
- Ascending orbit, 20, 28
- Atmospheric effects, 6, 11, 19, 24
- Attribute accuracy, 48
- Average fluctuation, 31
- Azimuth bandwidth, 58, 66–67
  
- B**ackscatter behaviour, 7, 8
- Bandwidth, 8
- Baseline
  - Critical length, 11
  - Definition, 10
  - Estimation, 10
  - Length, 10
  - Possible representations, 10
  - Sensitivity to height changes, 10
  - SRTM requirements, 23
- Baseline decorrelation, 24, 29
- Blunders, 47
- Branch cuts, 33
  
- Change detection, 20, 21
- Coarse co-registration, 30
- Coastal zones, 22
- Coherence
  - Ascending/Descending orbit, 28
  - Baseline decorrelation, 29
  - Coastal zones, 22
  - Co-registration, 31, 32
  - Critical baseline, 11
  - Forestry, 21
  - Interferometric product, 16
  - Multibaseline technique, 11
  - Multifrequency approach, 19
  - Ocean currents, 20
  - Temporal decorrelation, 24, 30
- Complex radar signal, 8, 27
- Contour lines, 40–41
- Convexity, 49, 52
- Co-registration
  - Average fluctuation, 31
  - Coherence, 31
  - Quality, 25
  - Signal-to-noise ratio, 28
- Coseismic displacements, 20
- Critical baseline, 11
- Cross-compatibility, 29
- Crossed orbits, 6
  
- D**ata acquisition, 12
- Data completeness, 48
- Data quality measures, 48
- Data quality
  - Atmospheric effects, 24
  - Bandwidth, 8
  - Baseline decorrelation, 24
  - Look angle, 7
  - Orbits, 23–24
  - Polarisation, 8
  - Processing, 24
  - Spatial resolution, 8
  - System noise, 7
  - System parameters, 7–8
  - Temporal decorrelation, 24
  - Wavelength, 7
- Data sets
  - DOSAR data, 30
  - Error propagation model, 80
  - ERS satellite data, 22

- Data sets (continued)
  - ERS tandem data, 28
  - ERS-1 data. *See* ERS-1 data
  - ERS-2 data, 6
  - Interferometric suitability, 28–30
  - JERS-1 data, 1, 21, 29, 43
  - MOMS, 44
  - RADARSAT data, 1, 21, 29, 43
  - SEASAT data, 6, 15, 19
  - Sensitivity study, 57
  - SIR-B data, 6
  - SIR-C data, 22
  - SPOT data, 43, 49, 50
  - TOPSAR data, 21, 29
  - X-SAR data, 22, 29
- Datum, 42
- Decorrelation
  - Baseline decorrelation, 11, 24, 29
  - Temporal decorrelation, 6, 21, 24, 29
- Deformations, 20
- DEM generation
  - Aerial photogrammetry, 41–42
  - Contour lines, 40–41
  - IRS-1C stereo imagery, 45
  - Laser scanning, 45–47
  - MOMS stereoscopic imagery, 44
  - Optical stereo imagery, 43–45
  - Radarclinometry, 43
  - Radargrammetry, 42
  - SPOT stereoscopic imagery, 43
- Descending orbit, 20, 28
- Differential interferometry, 6, 15, 17
- Digital elevation model
  - Applications, 19
  - Estimation of accuracy, 79–89
  - Quality control. *See* Quality control
- Doppler centroid frequency 59, 68–69
- DOSAR data, 30
- Dynamic height, 35
  
- E**llipsoid, 34
- ENVISAT mission, 20
- Error, 47
- Error propagation, 53
- Error propagation model
  - Advantages, 90
  - Data sets, 80–81
  - Empirical approach, 78–79
  - Estimation of DEM accuracy, 79–89
  - Limitations, 89
  - Monte Carlo simulation, 77
  - Schematic representation, 78
  
- Error propagation model (continued)
  - Theoretical background, 77–78
- ERS satellite data, 21
- ERS tandem data, 6, 28
- ERS-1 data
  - Change detection, 21
  - Differential interferometry, 15
  - Forestry, 21
  - Launch, 6
  - Radargrammetry, 43
  - Suitability, 1, 28
  - Topographic mapping, 19
- ERS-2 data, 6
  
- F**ine co-registration, 30
- Forestry, 21
- Fringe detection, 33
  
- G**eocoded products, 17
- Geocoding, 35
- Geoid, 34
- Geoid undulation, 34
- Geometry
  - Across-track interferometry, 12
  - Along-track interferometry, 13
  - General viewing geometry, 8–9
  - Repeat-pass interferometry, 14–15, 24
- Global positioning system
  - Aerial photogrammetry, 39, 41–42
  - Atmosphere, 24
  - Digital elevation model, 21
  - Ground control points, 50
  - Laser scanning, 45
  - Motion compensation, 15
  - SRTM mission, 23
  - Topographic mapping, 19
- Grid size, 50, 52
- Ground control points, 2, 49
  
- H**eight derivatives, 49
- Height profiles, 39
- Height systems, 34–35
- Hydrology, 22, 51
  
- I**ndian Remote Sensing satellites, 45
- Inertial navigation system
  - Airborne interferometry, 15, 19
  - Aerial photogrammetry, 39
  - Laser scanning, 39, 45
- Input parameters
  - Azimuth bandwidth, 58



- Input parameters (continued)  
 Doppler centroid frequency, 59  
 Orbit state vectors, 59  
 Pulse repetition frequency (PRF), 58  
 Range bandwidth, 58  
 Range sampling rate, 58  
 Interferogram, 15, 32  
 Interferometric phase, 9, 14  
 Interferometric products  
 Coherence, 16  
 Differential interferogram, 17  
 Digital elevation model, 17  
 Geocoded products, 17  
 Interferogram, 15  
 Quality assessment, 53  
 Simulated interferogram, 17  
 Interferometry. *See* SAR interferometry  
 Interpolation  
 Contour lines, 40
- J**  
 JERS-1 data, 1, 21, 29, 43
- K**  
 Kinematic GPS, 39, 42
- L**  
 Land subsidence, 22  
 Laser scanning, 45–47  
 Lava flows, 21  
 Least squares unwrapping, 33  
 Lineage, 48  
 Logical consistency, 49  
 Look angle, 7, 9–11, 21
- M**  
 Minimum cost network flow, 33  
 Missions  
 ENVISAT mission, 22  
 ERS tandem mission, 6  
 Shuttle imaging radar mission, 19, 29  
 Shuttle radar topography mission, 22  
 MOMS, 44  
 Monte Carlo simulation, 77  
 Motion compensation, 14, 19, 30  
 Multibaseline technique, 6, 11, 19  
 Multifrequency approach, 19  
 Multilook processing, 30
- N**  
 Normal height, 35
- O**  
 Ocean currents, 13, 20  
 Optical stereo imagery, 43–45  
 Orbits  
 Ascending orbit, 20, 28  
 Orbits (continued)  
 Co-registration, 30  
 Crossed orbits, 6  
 Descending orbit, 20, 28  
 Determination, 22–23  
 Precise orbit, 10  
 State vectors, 59, 70–71  
 Orthometric height, 35
- P**  
 Phase, 8, 27  
 Phase to height conversion, 34–35  
 Phase unwrapping, 12, 17, 32–33  
 Phasor, 27, 30  
 Pixel size, 8, 32  
 Pixel spacing, 32  
 Plan convexity, 49  
 Polar research, 20  
 Polarisation, 8  
 Positional accuracy, 48  
 Precise orbits, 10, 23  
 Processing  
 Co-registration, 30–32  
 Data quality, 24  
 Geocoding, 35  
 Interferogram generation, 32  
 Phase to height conversion, 34–35  
 Phase unwrapping, 32–33  
 Processing and archiving facilities, 28  
 Profile convexity, 49  
 Pulse repetition frequency (PRF), 58, 60–61
- Q**  
 Quality control  
 Ground control points, 49  
 Quality measures, 48–49  
 Reference DEM, 50  
 Theory, 47–48  
 User requirements, 50–53
- R**  
 Radarclinometry, 43  
 Radargrammetry, 42  
 RADARSAT data, 1, 21, 29, 43  
 Random errors, 47  
 Range bandwidth, 58, 64–65  
 Range sampling rate, 58, 62–63  
 Raster grid, 39  
 Reference DEMs, 2, 19, 50  
 Reference ellipsoid, 10  
 Reference surface  
 Ellipsoid, 34  
 Geoid, 34  
 Topography, 34  
 Repeat cycle, 29

- Repeat-pass interferometry, 14–15, 24
- Resampling, 32
- Resolution cell, 27
- Root mean square error
  - Contour lines, 40
  - Definition, 48
  - Vertical accuracy, 47
- SAR interferometry**
  - History, 6
  - Products, 17
- Satellite tracking, 29
- SEASAT data, 6, 15, 19
- Seismic events, 20
- Semantic accuracy, 49
- Sensitivity study
  - Azimuth bandwidth, 66–67
  - Combination of input parameters, 72–73
  - Data sets, 57
  - Doppler centroid frequency, 68–69
  - Orbit state vectors, 70–71
  - Processing scheme, 57
  - Pulse repetition frequency (PRF), 60–61
  - Range bandwidth, 64–65
  - Range sampling rate, 62–63
  - Shuttle imaging radar mission, 19, 29
- Shuttle radar topography mission, 22
- Signal-to-noise ratio, 11, 31
- Simulated interferogram, 17
- Single look complex data, 27
- SIR-B data, 6
- SIR-C data, 22
- Slope, 49, 52
- Slope aspect, 49
- Slope gradient, 49
- Software packages, 28, 36–37
- Spaceborne interferometry, 12, 14, 23
- Spatial resolution, 8
- Speckle, 8
- SPOT data, 43, 49, 50
- Surface movements, 20–21
- System noise, 7
- System parameters, 7–8
- Systematic errors, 47
- Temporal decorrelation**, 6, 21, 24, 29, 30
- Temporal information, 49
- Terrain height, 9, 12
- Tethered satellite system, 12
- Thermal noise, 7
- Topographic mapping, 5, 6, 19
- Topography, 34
- TOPSAR data, 21, 29
- Trends, 22–23
- Triangulated irregular networks, 39
- Vertical deflection**, 34
- Volcanic hazards, 21
- Wavelength**
  - Along-track interferometry, 13
  - Critical baseline, 11
  - Data quality, 7
  - Differential interferometry, 15
  - Multifrequency approach, 19
  - Phase difference, 9
- X-SAR data**, 22, 29

## GLOSSARY \*

---

**Accuracy.** The accuracy defines the quality of a measurement that is measured by the difference between the measurement and the value being estimated. The true value is seldom known, although it can be approximated in some instances. The accuracy is measured as root mean square (rms) error. See also *Precision*.

**Across-track direction.** see *Range direction*.

**Across-track interferometry.** The across-track method of interferometry is presently only employed on airborne systems as it requires two SAR antenna systems to be mounted simultaneously on the platform. The position of the two antennas mounted on an aircraft in this configuration is perpendicular to the flight direction. A problem in this geometry is the fact that the distinction between errors caused by the aircraft roll and the influence of the terrain slope is not possible.

**Along-track direction.** see *Azimuth direction*.

**Along-track interferometry.** The along-track method of interferometry is only applicable at present to airborne SAR systems, as both along-track and across-track methods require two antenna systems on the same platform. The yaw and pitch cause  $\rightarrow$  *baseline components* in y- and z-direction which produce additional phase differences. Before absolute velocity measurements are possible, a calibration of the phase difference is necessary.

**Amplitude.** The amplitude is a measure of the strength of the signal. In case of a complex signal it includes both the  $\rightarrow$  *magnitude* and the  $\rightarrow$  *phase*.

**Antenna.** The antenna is a device to radiate electromagnetic energy on transmission by a radar, and to collect such energy during reception. An antenna pattern is designed with spatial directivity, which concentrates the energy into a beam in both the vertical and the horizontal directions.

**Antenna footprint.** The antenna footprint covers the area on the ground hit by one transmitted pulse and from which the backscattered signal will be received.

**Ascending orbit.** The ascending orbit is a satellite orbit crossing south-north with a radar sensor looking to the east. The image is rotated towards west in this case.

**Azimuth direction.** The azimuth direction, often referred to as along-track direction, is defined as the flight direction of the satellite or airborne system.

**Backscatter coefficient.** The backscatter coefficient is defined as the  $\rightarrow$  *radar cross section* divided by the minimum resolved area illuminated on the target.

---

\* The terms given in this glossary were selected from various sources to ease the understanding of the text for readers not familiar in depth with the terminology in radar and SAR interferometry

**Bandwidth.** The bandwidth is a measure of the span of frequencies available in a signal or of the frequency limiting stages in the system. It is a fundamental parameter of any imaging system and determines the  $\rightarrow$  *resolution* available.

**Baseline.** The baseline is defined as the separation between the two antenna positions either mounted on an aircraft or realised by two repeating satellite orbits. The length of the baseline is taken as a measure for the  $\rightarrow$  *coherence* expected for SAR interferometric data. A precise knowledge of the length and the position of the baseline is a prerequisite for a good performance of the data processing. See also  $\rightarrow$  *critical baseline*.

**Baseline components.** The baseline geometry can be represented in three different ways. The parallel flight paths are separated by the baseline with an orientation angle  $\alpha$ . This baseline can also be divided into the horizontal and the vertical component as well as into the parallel and the perpendicular component of the baseline.

**Baseline decorrelation.** Since the two antennas are separated in the  $\rightarrow$  *across-track direction*, slightly different interference results are measured, even when the pixel derived from each antenna covers the same area. This results in a loss of  $\rightarrow$  *coherence* between the two antenna outputs, referred to as baseline decorrelation.

**Coherence.** The coherence is a measure for the correlation of the phase information of corresponding signals. It ranges from 0 to 1.

**Critical baseline.** The critical baseline is reached when the  $\rightarrow$  *baseline* becomes larger than half of the reflected beam width. In that case, the radar echoes have lost the  $\rightarrow$  *coherence*.

**Cycle slip.** A cycle slip occurs if a GPS receiver loses lock on one of more satellites which results in a number of simultaneously observed satellites of less than four. In this case a reinitialisation of the system becomes necessary in order to solve the ambiguities.

**Datum.** The datum describes the relationship between a particular local ellipsoid and a global geodetic reference system. It is defined by at least five parameters: the semi-major axis of the reference ellipsoid, the flattening, and the three datum shift parameters.

**Decorrelation.** The decorrelation is a measure of the degree of phase  $\rightarrow$  *coherence* in the complex radar returns from a target of interest acquired at different times. It has three uncorrelated components. The thermal component refers to the  $\rightarrow$  *thermal noise* introduced by the system. The spatial aspect is covered by effects related to the  $\rightarrow$  *baseline decorrelation*. Finally, there is a temporal component describing the  $\rightarrow$  *temporal decorrelation*.

**Deflection of the vertical.** The deflection of the vertical determines the angle between the directions of the ellipsoid normal and of the plumb line at a point.

**Depression angle.** The depression angle is the angle between a horizontal plane and the radar beam from the  $\rightarrow$  *antenna* to the ground surface.

**Descending orbit.** The descending orbit is a satellite orbit crossing north-south with a radar sensor looking to the west. The image is rotated towards east in this case.

**Dielectric constant.** For a given substance, the dielectric constant is defined as the ratio of the capacity of a condenser with that substance as dielectric to the capacity of that condenser with a vacuum as dielectric.

**Differential radar interferometry.** The differential use of SAR interferometry is adapted for the measurement of small-scale movements in the vertical direction, e.g. for change detection. This technique provides relative measures of the order of a few centimetres or even less. The displacement measured by differential interferometry is not vertical, but along the viewing direction.

**Doppler centroid.** The Doppler centroid is the centre Doppler frequency or zero of the Doppler spectrum as the radar beam sweeps past the target. It is found by correlating power spectra with some predefined weight functions. Since the Doppler centroid generally varies over range, estimation is performed at several range positions. The Doppler centroid estimate is required to maximise  $\rightarrow$  *signal-to-noise-ratio* and minimise azimuth ambiguities by matching the pass band of the azimuth compression filter to the spectral energy distribution of the SAR signal.

**Far range.** The far range refers to the portion of a radar image farthest from the flight path.

**Footprint.** see *Antenna footprint*.

**Foreshortening.** The time difference of two signals backscattered at the bottom and the top of a steep slope is shorter than in a flat area. Therefore, the distance between two points is mapped shorter in the image. This geometric effect called foreshortening compresses the backscattered signal energy, i.e. the affected area on the image appears brighter.

**Frame.** An  $\rightarrow$  *orbit* is split in several standard scenes called frames whose size and location depend on the satellite. The ERS satellite orbit, for example, consists of 7200 nodes and 400 of them are used to identify the SAR frames through the node closest to the frames' centre. The standard frame size of an ERS scene is 100 · 100 km.

**Frequency.** The frequency is the rate of oscillation of a wave. In the microwave range, the frequencies are on the order of 1 GHz to 100 GHz.

**Fringe.** A fringe represents the whole range of the phase in an interferogram from 0 to  $2\pi$  in a full colour cycle.

**Geoid.** The geoid is a gravitational equipotential surface near the mean sea level representing the surface of zero height. It is used as a  $\rightarrow$  *datum* for gravity survey and serves also as a reference surface for topographic heights.

**Geoid undulation.** The geoid undulation is defined as the vertical separation between the  $\rightarrow$  *geoid* and a particular reference ellipsoid, i.e. approximately the difference between the  $\rightarrow$  *normal height* and the  $\rightarrow$  *orthometric height*.

**Ground control point.** The ground control point (GCP) refers to a physical point on the ground whose ground positions are known with respect to some horizontal coordinate system and/or vertical → *datum*.

**Ground range.** The ground range is the distance from the → *nadir* to a given object.

**Incidence angle.** The incidence angle is the angle between the radar beam centre and the normal to the local topography.

**Inclination.** The inclination is the angle of the plane of a satellite orbit with respect to the equatorial plane of the earth.

**Intensity.** The intensity is a measure of the energy reflected or emitted by an object.

**Interferogram.** The interferogram is defined as the product of the complex SAR values of the second image with the complex conjugate of the reference image; i.e. the corresponding amplitudes have to be averaged and the corresponding phases have to be differenced at each point in the image. It contains the → *amplitude* as well as the → *phase* information of a SAR image pair.

**Interferometric processing.** The interferometric processing generally consists of the registration of the complex images, the formation of the → *interferogram*, the → *phase unwrapping* and the reconstruction of the digital elevation model.

**Layover.** The layover effect represents the extreme case of → *foreshortening*. The signal backscattered from the top of the mountain is received earlier than the signal from the bottom, i.e. the foreslope is reversed. The pixel information from various objects is superimposed which leads to a brighter appearance on the image.

**Line spacing.** The line spacing represents how much area each pixel covers in → *azimuth direction*.

**Look angle.** The look angle is defined as the angle between the direction the antenna is pointing when transmitting and receiving from a particular cell and the → *nadir*.

**Looks.** The frequency varies linearly with time so that the spectrum may be obtained by dividing the coherent integration time into sequential subintervals and computing the energy returned during each interval. These data segments represent the application of the pulse compression processing over only a part of the synthetic aperture and are referred to as looks.

**Magnitude.** The magnitude is the → *amplitude* of the wave irrespective of the → *phase*.

**Matched filtering.** see *SAR processing*.

**Motion compensation.** To provide topographic data with a precision of the order of one metre from interferometric airborne data, it is very important to measure and compensate for non-linear motion of the two antennas. Motion compensation is usually applied assuming that the terrain is flat at a certain reference level, which is often not valid. This leads to defocusing, peak misplacement, and phase errors in the compressed image.

**Nadir.** The nadir is defined as the direction towards the centre of the Earth.

**Near range.** The near range refers to the portion of a radar image closest to the flight path.

**Noise.** Noise is defined as random or regular interfering effects in the data which degrade its information-bearing quality. See also *speckle*.

**Normal height.** The normal height (elevation of a point on the Earth's surface) is the vertical distance above a certain reference ellipsoid and is measured along the ellipsoidal normal from the point to the ellipsoid. See also *orthometric height* and *geoid undulation*.

**Orbit.** The orbit is the curved path, usually elliptical, described by a satellite about the earth.

**Orthometric height.** The orthometric height (elevation of a point above mean sea level) is the vertical distance above the  $\rightarrow$  *geoid* and is measured along the curved plumb line from the point to the geoid. see also *normal height* and *geoid undulation*.

**Phase.** The phase is the angle of a complex number.

**Phase aliasing.** The phase aliasing is the folding of higher into lower frequency components in a discrete spectrum due to undersampling of the phase signal.

**Phase unwrapping.** The resultant  $\rightarrow$  *phase* of the  $\rightarrow$  *interferogram*, which is directly related to the topography, is only measured modulo  $2\pi$ . To calculate the elevation of each point it is necessary to add the correct integer number of phase cycles to each phase measurement. The problem of solving this  $2\pi$  ambiguity is called phase unwrapping.

**Phasor.** The phasor is the vector representing the resultant of all scattering objects within the  $\rightarrow$  *resolution cell*.

**Pixel.** Acronym for picture element. The pixels form the image in a regular grid and visualise the data. The size of the pixel can exceed the size of the  $\rightarrow$  *resolution cell* in order to obtain square pixels or to reduce the  $\rightarrow$  *noise*.

**Pixel spacing.** The pixel spacing represents how much area each pixel covers in  $\rightarrow$  *range direction*.

**Polarisation.** The polarisation defines the orientation of the electric (and magnetic) fields of an electromagnetic wave. Horizontal (H) / vertical (V) polarisation refers to the electric field (or magnetic field) vector being parallel to the surface of the medium that the wave is incident upon.

**Posting.** The posting is defined as the distance between the centres of the  $\rightarrow$  *resolution cell* and can be unequal to the size of the resolution cell.

**Precision.** The precision is a quality associated with a class of measurements and refers to the way in which repeated observations conform to themselves. The measure is given as standard deviation. See also *Accuracy*.

**Pulse repetition frequency.** The pulse repetition frequency (PRF) determines the number of pulses transmitted per second.

**Radar cross section.** The radar cross section is the area of a fictitious, perfect reflector of electromagnetic waves that would reflect the same amount of energy back to the radar as the actual target.

**Radar system.** The radar system consists of a transmitter (generates a high power pulse of light at radio wavelength), a switch (switches transmitted pulse to antenna, returns echoes to receiver), an  $\rightarrow$  *antenna* (directs transmitted pulse towards the area to be imaged, collects returned echoes), a receiver (converts returned echoes to digital numbers) and a data recorder (stores data values for later processing and display). Important radar system parameters are the  $\rightarrow$  *wavelength*,  $\rightarrow$  *polarisation*, pulse length,  $\rightarrow$  pulse *bandwidth*,  $\rightarrow$  *pulse repetition frequency*, transmit power, antenna size and operating rate.

**Radiometric resolution.** Radiometric resolution is a measure of how different two uniform (speckled) regions of different backscatter levels have to be in order to distinguish between them.

**Range.** The range is the distance from the radar to the target perpendicular the flight direction. It can be either represented as  $\rightarrow$  *slant range* or as  $\rightarrow$  *ground range*.

**Range direction.** The range direction, often referred to as across-track direction, is defined as the direction perpendicular to the flight direction of the satellite or airborne system.

**Reliability.** The reliability is the confidence that can be assigned to a conclusion of a probabilistic nature.

**Repeat cycle.** The repeat cycle is the time between one pass over a fixed location on earth and the subsequent pass over the same location. It is identified by the number of  $\rightarrow$  *orbits* between the two repeated passes. More practically, but less accurately it is identified by the number of days between repeat coverages.

**Repeat-pass interferometry.** Repeat-pass interferometry requires only one  $\rightarrow$  *antenna* and hence is the method most suited to spaceborne SAR sensors. This is also because for this method precise location of the flight path is required, and satellites typically have much more precise and stable orbital paths in the absence of the atmosphere, than do aircraft. The satellite has to pass nearly the same orbit to cover an area twice with a slightly different viewing geometry.

**Resolution.** The resolution is a measure for the minimum (spatial) separation between two measurements in order for a sensor to be able to discriminate between them. The range resolution depends on the pulse length whereas the azimuth resolution is determined by the angular beam width of the illuminated terrain strip. Spectral and radiometric resolutions refer to the resolving power of a system in wavelength and energy, respectively.



**Resolution cell.** The resolution cell is an element of a SAR image representing the physical properties. Besides the physical properties, the size of the resolution cell is also determined by the processing from raw data to → *single look complex* (SLC) data. See also *pixel*, *posting*.

**SAR correlation.** see *SAR processing*.

**SAR processing.** SAR processing, often referred to as SAR correlation, matched filtering or azimuth compression, consists of image focusing through matched filter integration, detection, and multi-look summation. The output files of a SAR processor usually are presented with unity aspect ratio (so that range and azimuth image scales are the same). Images may either be in → *slant range* or → *ground range* projection. Both of these spatial adjustments require resampling of the image file.

**Shadow.** The shadow effect in radar imagery is different from optical imagery. In the case of → *radar*, no information is received from the backslope which appear as black regions on the image. The length of the shadow depends on its position in range direction. Therefore, the shadow in → *far range* are longer than in → *near range*.

**Signal-to-noise-ratio.** The signal-to-noise-ratio (SNR) is the ratio of the level of the information-bearing signal to the level of the noise power. The maximum SNR of a device is called the “dynamic range”.

**Single look complex.** The single look complex (SLC) data contain signal information in a complex number, i.e. the → *intensity* and the → *phase* information is stored in a real and an imaginary part.

**Slant range.** The slant range represents the distance from radar sensor to the target.

**Speckle.** Speckle is a scattering phenomenon which arises because the resolution of the sensor is not sufficient to resolve individual scatterers. Physically speaking speckle is no → *noise*, since the same imaging configuration leads to the identical speckle pattern. Speckle can be reduced by multi-look processing and spatial averaging.

**Swath.** The swath is the strip of ground swept over by the moving radar beam.

**Synthetic aperture radar.** In a synthetic aperture radar (SAR) the azimuth resolution is achieved through computer operations on a set of (coherently recorded) signals such that the processor is able to function such as a large → *antenna* aperture in computer memory, thus realising azimuth improvement in proportion to aperture size.

**Temporal decorrelation.** The temporal decorrelation is caused by physical changes in the surface over the time period between observations.

**Track.** Each → *repeat cycle* has an internal number of → *orbits* called tracks which have the property of always covering the same area. For the ERS satellite the track numbers follow the orbit numbers.

**Wavelength.** The wavelength is defined as the velocity divided by the → *frequency* of a wave.

## APPENDIX A: INTERFEROMETRIC SOFTWARE

---

The institutes and companies who provided the following information about the software packages are listed in alphabetical order. This listing does not indicate the expression of any opinion of the author concerning the capabilities and performance of the mentioned software packages.

Product:	<b>InSAR software</b> <sup>3</sup>
Provider:	<b>Alaska SAR Facility (ASF)</b> Geophysical Institute University of Alaska Fairbanks Alaska 99775-0800 United States
Source of information	Rick Guritz
Platform	SUN, Silicon Graphics
Memory	256 Megabytes minimum, 512 Megabytes recommended
Software	No requirements
Programming language	C
Internal data format	Land Analysis System format for most products (line oriented binary files)
Supported sensors	ERS-1, ERS-2
Supported formats	ASF computer compatible signal data (CCSD) SLC (ASF SLC is a subframe of 30 x 40 km)
Processing facility	Alaska SAR Facility
Calculated products	Interferogram Coherence image Unwrapped phase Digital elevation model Simulated interferogram Geocoded products
Quality control	Ground control points comparison with reference DEMs

---

<sup>3</sup> has currently a restricted distribution to non-profit research and educational users of the United States

Product:	<b>EarthView InSAR 1.0.5/1.1.0</b>
Provider:	<b>Atlantis Scientific Inc.</b> 20 Colonnade Road, Suite 110 Nepean Ontario, K2E 7M6 Canada
Source of information	Internet ( <a href="http://www.atlsci.com/products/EarthView_InSAR.html">http://www.atlsci.com/products/EarthView_InSAR.html</a> )
Platform	SUN SparcStation SunOS 2.4 or higher
Memory	64 Megabyte
Software	EarthView
Programming language	C
Internal data format	MFF
Supported sensors	ERS-1, ERS-2, JERS-1, RADARSAT
Supported formats	RAW (processed by SLC
Processing facility	European PAFs, RADARSAT
Calculated products	Interferogram Coherence image Unwrapped phase Digital elevation model Differential interferogram Simulated interferogram Geocoded products
Quality control	Ground control points

Product:	<b>DIAPASON</b>
Provider:	<b>Centre National D'Etudes Spatiales (CNES) DGAT/SH/QTIS</b> 18 Avenue E. BELIN 31401 Toulouse CEDEX4 France 18 Avenue E. BELIN
Source of information	Didier Massonnet
Platform	DEC Alpha, SUN
Memory	64 Megabytes
Software	No requirements
Programming language	FORTRAN
Internal data format	Own
Supported sensors	ERS-1, ERS-2, SIR-C, X-SAR, RADARSAT
Supported formats	RAW, SLC
Processing facility	Any PAF
Calculated products	Interferogram Coherence image Simulated interferogram Differential interferogram
Quality control	Sequencing of lines in raw data Disparity (accuracy of co-registration through the measurement of the width of a histogram) Coherence image

Product:	<b>InSAR software</b>
Provider:	<b>Consorzio di Ricerca su Sistemi di Telesensori Avanzati (CO.RI.S.T.A.)</b> Piazzale Tecchio 80 80125 Napoli Italy
Source of information	Giovanni Alberti
Platform	IBM Risk 6000
Memory	196 Megabyte
Software	No requirements
Programming language	FORTRAN
Internal data format	Own format
Supported sensors	ERS-1, ERS-2, SIR-C, X-SAR, TOPSAR
Supported formats	RAW, SLC
Processing facility	Usually I-PAF
Calculated products	Interferogram Coherence image Unwrapped phase Digital elevation model Simulated interferogram
Quality control	Comparison to reference DEMs Ground control points

Product:	<b>GENESIS</b>
Provider:	<b>Deutsches Zentrum für Luft- und Raumfahrt (DLR)</b> Deutsches Fernerkundungsdatenzentrum Oberpfaffenhofen 82234 Weßling Germany
Source of information	Nico Adam
Platform	SUN
Memory	optimised by multi thread programming uses up to 500 Megabyte for a quarter scene
Software	No requirements
Programming language	Mainly C++, partly in IDL
Internal data format	SUN raster (extended to float and short int complex format)
Supported sensors	ERS-1, ERS-2, SIR-C, X-SAR
Supported formats	RAW, SLC
Processing facility	D-PAF, UK-PAF, I-PAF, C-PAF internal VMP
Calculated products	Interferogram Coherence image Unwrapped phase Differential interferogram Simulated interferogram Geocoded products Speed vector fields (for glaciers)
Quality control	Comparison with reference DEMs

Product:	<b>Interferometric SAR processor / Differential Interferometry and Geocoding Software</b>
Provider:	<b>Gamma Remote Sensing Research and Consulting AG</b> Thunstrasse 130 3074 Muri/Bern Switzerland
Source of information	Internet ( <a href="http://www.primenet.com/~gamma/gamma.html">http://www.primenet.com/~gamma/gamma.html</a> )
Platform	DEC, HP, SUN, Silicon Graphics
Memory	No requirements
Software	No requirements
Programming language	C
Internal data format	SUN raster
Supported sensors	ERS-1, ERS-2, SIR-C, X-SAR, JERS-1, RADARSAT, DOSAR
Supported formats	RAW (processed with Modular SAR Processor - MSP) SLC
Processing facility	European PAFs
Calculated products	Interferogram Coherence image Unwrapped phase Digital elevation model Differential interferogram Simulated interferogram Geocoded products
Quality control	

Product:	<b>InSAR software</b>
Provider:	<b>Institut für Navigation (INS)</b> Universität Stuttgart Geschwister-Scholl-Straße 24D 70174 Stuttgart
Source of information	Jürgen Schmidt
Platform	DEC, HP, SUN, IBM, Silicon Graphics, PC
Memory	32 Megabyte
Software	EASI/PACE
Programming language	C
Internal data format	PCIDSK Other formats supported by Generic Database Library
Supported sensors	ERS-1, ERS-2, SIR-C, X-SAR
Supported formats	SLC
Processing facility	European PAFs
Calculated products	Interferogram Coherence image Unwrapped phase Digital elevation model Differential interferogram Simulated interferogram Geocoded products
Quality control	Consistency checks Ground control points



Product:	<b>DIAPASON / SPOT3D</b>
Provider:	<b>ISTAR</b> Espace Beethoven Route Des Lucioles 6560 Valbonne France
Source of information	Stéphane Dupont
Platform	SUN
Memory	No requirements
Software	No requirements
Programming language	FORTRAN
Internal data format	Own
Supported sensors	ERS-1, ERS-2, RADARSAT
Supported formats	RAW, SLC
Processing facility	Any PAF
Calculated products	Interferogram Coherence image Unwrapped phase Digital elevation model Differential interferogram Simulated interferogram
Quality control	

Product:	<b>InSAR software</b>
Provider:	<b>Istituto di Ricerca per l'Elettromagnetismo e i Componenti Elettronici (IRECE-CNR)</b> Via Diocleziano 328 80124 Napoli Italy
Source of information	Gianfranco Fornaro
Platform	UNIX
Memory	128 Megabyte
Software	No requirements
Programming language	FORTRAN
Internal data format	Own
Supported sensors	ERS-1, ERS-2, SIR-C, X-SAR, E-SAR, TOPSAR
Supported formats	RAW, SLC
Processing facility	Usually I-PAF
Calculated products	Interferogram Coherence image Unwrapped phase Digital elevation model Differential interferogram Simulated interferogram Geocoded products
Quality control	Comparison with reference DEMs

Product:	<b>InSAR software</b>
Provider:	<b>Jet Propulsion Laboratory (JPL)</b> California Institute of Technology 4800 Oak Grove Drive Pasadena, California 91109 United States
Source of information	Eric Fielding
Platform	HP, SUN, SGI
Memory	256-512 Megabyte
Software	No requirements
Programming language	FORTRAN, C
Internal data format	Own
Supported sensors	ERS-1, ERS-2, SIR-C, X-SAR, JERS-1, TOPSAR, RADARSAT, SRTM
Supported formats	RAW, SLC
Processing facility	Any PAF
Calculated products	Interferogram Coherence image Unwrapped phase Digital elevation model Differential interferogram Simulated interferogram Geocoded products Height error maps
Quality control	Comparison with reference DEMs, Comparison with deformation measurements

Product:	<b>RSG - SAR Interferometry</b>
Provider:	<b>Joanneum Research</b> Forschungsgesellschaft mbH Steyrergasse 17 8010 Graz Austria
Source of information	Lado Kenyi
Platform	SUN
Memory	32 Megabyte
Software	Stand alone or ERDAS IMAGINE
Programming language	FORTRAN
Internal data format	Own
Supported sensors	ERS-1, ERS-2, RADARSAT
Supported formats	SLC
Processing facility	D-PAF, I-PAF, UK-PAF
Calculated products	Interferogram Coherence image Unwrapped phase Digital elevation model
Quality control	GCP residuals, DEM rms

Product:	<b>ISAR Version 3.0 (developed by POLIMI and ESA-ESRIN)</b>
Provider:	<b>Joint Research Centre (JRC)</b> Space Applications Institute Advanced Techniques Unit 21020 Ispra (Varese) Italy
Source of information	Flora Paganelli
Platform	SUN
Memory	32-64 Megabyte
Software	No requirements
Programming language	C
Internal data format	Own format
Supported sensors	ERS-1, ERS-2
Supported formats	SLC
Processing facility	I-PAF, D-PAF
Calculated products	Interferogram Coherence image Differential interferogram
Quality control	

Product:	<b>PACE IFSAR Interferometric SAR (Version 6.1 Beta)</b>
Provider:	<b>PCI Enterprises Inc.</b> 50 West Wilmot Street Richmond Hill Ontario L4B 1B5 Canada
Source of information	Internet ( <a href="http://www.pci.on.ca">http://www.pci.on.ca</a> )
Platform	PC, UNIX
Memory	No requirements
Software	EASI/PACE
Programming language	C
Internal data format	PCIDSK
Supported sensors	ERS-1, ERS-2
Supported formats	SLC
Processing facility	European PAFs
Calculated products	Interferogram Coherence image Unwrapped phase Simulated interferogram Digital elevation model Geocoded products
Quality control	

Product:	<b>Interferometric Quick-look Processor</b>
Provider:	<b>Politecnico di Milano (POLIMI)</b> Dipartimento di Elettronica e Informazione Piazza Leonardo da Vinci 32 20133 Milano Italy
Source of information	Fabio Gatelli
Platform	DEC, HP, Silicon Graphics
Memory	No requirements
Software	No requirements
Programming language	C
Internal data format	Own format
Supported sensors	ERS-1, ERS-2
Supported formats	RAW
Processing facility	European PAFs
Calculated products	Intensity multi-look image Multi-look interferogram Coherence image
Quality control	

Product:	<b>InSAR software</b> <b>Multibaseline software for phase unwrapping</b> <b>DEM generation and geocoding software</b>
Provider:	<b>Politecnico di Milano (POLIMI)</b> Dipartimento di Elettronica e Informazione Piazza Leonardo da Vinci 32 20133 Milano Italy
Source of information	Alessandro Ferretti
Platform	DEC, HP, Silicon Graphics
Memory	32 Megabyte
Software	No requirements
Programming language	C
Internal data format	Own format
Supported sensors	ERS-1, ERS-2
Supported formats	RAW
Processing facility	European PAFs
Calculated products	Interferogram Coherence image Unwrapped phase Digital elevation model
Quality control	



Product:	<b>Zürich Interferometry Processor (ZIP)</b>
Provider:	<b>Remote Sensing Laboratories (RSL)</b> University of Zurich Winterthurerstr. 190 8057 Zurich Switzerland
Source of information	David Small
Platform	SUN Solaris 2.x, previously SunOS 4.1.3
Memory	96 Megabyte
Software	IDL for some visualisations, ERS precise orbit input
Programming language	C, C++
Internal data format	RSL-modified SUN raster file (new types for float, double, float complex etc.)
Supported sensors	ERS-1, ERS-2, SIR-C, X-SAR, RADARSAT (data input, geocoding)
Supported formats	RAW (through RSL Modular SAR Processor - MSP) SLC (ESA CEOS, MDA ERS VMP)
Processing facility	ERS - Harmonised CEOS (D-PAF, ESA-ESRIN) ERS - tested on I-PAF, UK-PAF SLC SIR-C (JPL) X-SAR (D-PAF) ERS, SIR-C (RSL MSP)
Calculated products	Interferogram Coherence image Unwrapped phase Digital elevation model Differential interferogram Simulated interferogram Geocoded products
Quality control	DEM-flattened interferograms (using reference DEM) Backward geocoded slant-range DEM comparison with reference DEM Forward geocoded interferometric height, comparison with reference DEM

Product:	<b>matInSAR</b>
Provider:	<b>University of British Columbia (UBC)</b> Radar Remote Sensing Group Department of Electrical Engineering 2356 Main Mall Vancouver British Columbia V6T 1Z4 Canada
Source of information	Mike Seymour
Platform	must support Matlab
Memory	64 Megabytes
Software	Matlab Version 5.0
Programming language	Matlab
Internal data format	own (binary data file with associated ASCII text parameter file)
Supported sensors	ERS-1, ERS-2, RADARSAT
Supported formats	SLC
Processing facility	processing information available in header or parameter file
Calculated products	Interferogram Coherence image Unwrapped phase Digital elevation model
Quality control	Coherence image for data quality

Product:	<b>InSAR software</b>
Provider:	<b>University of Stanford</b> Department of Electrical Engineering 232 Durand, STARLAB Stanford California 94305-9515 United States
Source of information	Howard Zebker
Platform	UNIX
Memory	300 MB
Software	No requirements
Programming language	FORTRAN, C
Internal data format	Own
Supported sensors	ERS-1, ERS-2, SIR-C, JERS-1, TOPSAR, ERIM Lear jet
Supported formats	RAW
Processing facility	Any PAF
Calculated products	Interferogram Coherence image Unwrapped phase
Quality control	Coherence maps, Doppler analysis, autofocus

## APPENDIX B: CURRICULUM VITAE

---

### PERSONAL DATA

Name	Rüdiger Gens
Date and place of birth	13-October-1967 in Münster, Germany
Nationality	German
Marital status	Single
Present address	Cheruskerring 85, 48147 Münster, Germany Tel.: 0049-251-294867
Office	International Institute of Aerospace Surveys and Earth Sciences (ITC) P.O. Box 6, 7500 AA Enschede, the Netherlands Tel.: 0031-53-4874412, Fax: 0031-53-4874336 Email: gens@itc.nl Internet: <a href="http://www.itc.nl/~gens">http://www.itc.nl/~gens</a>

### PROFESSIONAL CAREER

October 1994 to 1998	Ph.D. researcher at the International Institute for Aerospace Survey and Earth Sciences (ITC), Enschede, the Netherlands; Title of the thesis: Quality assessment of SAR interferometric data Thesis defence: 27-May-1998
----------------------	--

### EDUCATION

October 1988 to September 1994	Geodesy at the University of Hannover, Germany specialising in Photogrammetry and Geodesy; Dipl.-Ing. degree: 26-September-1994
July 1987 to September 1988	Military Service
August 1978 to May 1987	Gymnasium Paulinum, Münster, Germany Graduation: Abitur, 29-May-1987

## APPENDIX C: PUBLICATIONS

---

- GENDEREN, J.L. VAN and GENS, R., 1996, SAR Interferometry: Principles and research trends. *Proceedings of the GEOINFORMATICS'96 Symposium*, Wuhan, China, Vol. I, pp. 99-106.
- GENDEREN, J.L. VAN, CASSELLS, C. AND GENS, R. (eds.), 1997, Synergy of remotely sensed data - A European scientific research network. Final report, Enschede, the Netherlands, ISBN 90-6164-151-9, 81 pages.
- GENDEREN, J.L. VAN, HUANG, Y., GENS, R., VEEN, B.S. VAN and HUURNEMAN, G., 1997, The ITC filter for improving ERS SAR interferograms. *3rd ERS Symposium*, Florence, Italy (<http://florence97.ers-symposium.org/data/vangendere/>), 7 pages.
- GENS, R. and GENDEREN, J.L. VAN, 1996, An approach to error propagation modelling of SAR interferometric data. *ESA Fringe'96 Workshop*, Zurich, Switzerland (<http://www.geo.unizh.ch/rsl/fringe96/papers/gens-genderen/>), 3 pages.
- GENS, R. and GENDEREN, J.L. VAN, 1996, Analysis of the geometric parameters of SAR interferometry for spaceborne systems. *International Archives of Photogrammetry and Remote Sensing*, **31** (B2), 107-110.
- GENS, R. and GENDEREN, J.L. VAN, 1996, SAR interferometry - issues, techniques, applications. *International Journal of Remote Sensing*, **17**, 1803-1835.
- GENS, R., GENDEREN, J.L. VAN and VEKERDY, Z., 1997, *A Tutorial on remote sensing image and data fusion*. Multimedia tutorial, Version 1.0 (Enschede: ITC).
- GENS, R., VEKERDY, Z. and POHL, C., 1998, Image and data fusion - concept and implementation of a multimedia tutorial. *Proceedings of the Second Conference on Fusion of Earth Data*, Sophia Antipolis, France, pp. 217-222.
- HUURNEMAN, G., GENS, R. and BROEKEMA, L., 1996, Thematic information extraction in a neural network classification of multi-sensor data including microwave phase information. *International Archives of Photogrammetry and Remote Sensing*, **31** (B2), 170-175.

# Wissenschaftliche Arbeiten der Fachrichtung Vermessungswesen der Universität Hannover

(Diese Arbeiten erschienen bis Nr. 86 unter "Wissenschaftliche Arbeiten des Lehrstuhle für Geodäsie, Photogrammetrie und Kartographie an der Technischen Universität Hannover".)

- Nr. 211 Fröhlich, M.: Zur Entwicklung eines Hochpräzisen Permanenten Positionierungsservice (HPPS). (Diss. 1995)
- Nr. 212 Grote, Th.: Regionale Quasigeoidmodellierung aus heterogenen Daten mit "cm"-Genauigkeit. (Diss. 1996)
- Nr. 213 Ardiansyah, M.: Auswertung von SPOT-Daten mit digitalen Bildverarbeitungsmethoden zur Untersuchung der Anwendungsmöglichkeit für das indonesische Kartenwerk. (Diss. 1996)
- Nr. 214 Pohl, Chr.: Geometric Aspects of Multisensor Image Fusion for Topographic Map Updating in the Humid Tropics. (Diss. 1996)
- Nr. 215 Goldan, H.-J.: Beiträge zur GPS-gestützten Höhenbestimmung im Küstenbereich. (Diss. 1996)
- Nr. 216 Krauter, E.,  
Pelzer, H.,  
Spellaue, R.: Ingenieurgeologische und ingenieurgeodätische Methoden zur Erfassung und Beschreibung von Hangrutschungen am Beispiel eines Großrutschareals nordöstlich von Quito. (Seminarbeiträge Quito, 1994)
- Nr. 217 Pelzer, H.: Proceedings of the 6th International FIG-Symposium on Deformation Measurements, 24-28 February, 1992.
- Nr. 218 Kuhlmann, H.: Ein Beitrag zur Überwachung von Brückenbauwerken mit kontinuierlich registrierten Messungen. (Diss.1996)
- Nr. 219 Knipp, K.: Untersuchungen zur Verwaltung und Verarbeitung von abbildenden Radardaten des Fernerkundungssatelliten ERS-1. (Diss.1996)
- Nr. 220 Lee, J.O.: Untersuchungen von Verfahren zur kombinierten Aero-triangulation mittels integriertem GPS/INS. (Diss. 1996)
- Nr. 221 Siebe, E.: Komponenten einer digitalen photogrammetrischen Stereo-Arbeitsstation und Auswertungen von Scanner-Daten. (Diss. 1997)
- Nr. 222 Schiewe, J.: Geo-Modellierungen mit Daten des Weltraumsensors MOMS-02. (Diss. 1997)
- Nr. 223 Willeke, U.: Zur Anwendung von Expertensystemen in der Grundstücksermittlung. (Diss. 1997)
- Nr. 224 Gülal, E.: Geodätische Überwachung einer Talsperre; eine Anwendung der KALMAN-Filtertechnik. (Diss. 1997)
- Nr. 225 Schmitz, M.: Untersuchungen zur strengen GPS Parametrisierung in der gemeinsamen Ausgleichung von kinematischem GPS und Aero-triangulation. (Diss. 1998)

Die "Wissenschaftliche Arbeiten ..." werden im Rahmen des wissenschaftlichen Schriftenaustausches verteilt und können über den Buchhandel nicht bezogen werden. Das Geodätische Institut der Universität Hannover (Nienburger Str. 1, 30167 Hannover) gibt Einzel Exemplare und das Gesamtverzeichnis der bisher erschienen Arbeiten an interessierte Wissenschaftler ab.